



Calhoun: The NPS Institutional Archive
DSpace Repository

Theses and Dissertations

1. Thesis and Dissertation Collection, all items

1986

A linear stability analysis of the rapid development of an extratropical cyclone.

Toll, Raymond F. Jr.

<http://hdl.handle.net/10945/21959>

Downloaded from NPS Archive: Calhoun



Calhoun is the Naval Postgraduate School's public access digital repository for research materials and institutional publications created by the NPS community. Calhoun is named for Professor of Mathematics Guy K. Calhoun, NPS's first appointed -- and published -- scholarly author.

Dudley Knox Library / Naval Postgraduate School
411 Dyer Road / 1 University Circle
Monterey, California USA 93943

<http://www.nps.edu/library>

DUDLEY KNOX LIBRARY
NAVAL POSTGRADUATE SCHOOL
MONTEREY, CALIFORNIA 93943

NAVAL POSTGRADUATE SCHOOL

Monterey, California



THESIS

A LINEAR STABILITY ANALYSIS
OF THE RAPID DEVELOPMENT OF
AN EXTRATROPICAL CYCLONE

by

Raymond F. Toll Jr.

March 1986

Thesis Advisor:

J. Chan

Co-Advisor:

C. Wash

Approved for public release; distribution unlimited.

T228080

REPORT DOCUMENTATION PAGE

| | | | |
|---|--------------------------------------|---|----------------------------|
| 1. REPORT SECURITY CLASSIFICATION | | 1b. RESTRICTIVE MARKINGS | |
| 2. SECURITY CLASSIFICATION AUTHORITY | | 3. DISTRIBUTION / AVAILABILITY OF REPORT | |
| 4. DECLASSIFICATION / DOWNGRADING SCHEDULE | | Approved for public release; distribution unlimited. | |
| 5. PERFORMING ORGANIZATION REPORT NUMBER(S) | | 5. MONITORING ORGANIZATION REPORT NUMBER(S) | |
| 6. NAME OF PERFORMING ORGANIZATION | 6b. OFFICE SYMBOL (If applicable) | 7a. NAME OF MONITORING ORGANIZATION | |
| Naval Postgraduate School | 63 | Naval Postgraduate School | |
| 7. ADDRESS (City, State, and ZIP Code) | | 7b. ADDRESS (City, State, and ZIP Code) | |
| Monterey, California 93943-5100 | | Monterey, California 93943-5100 | |
| 8. NAME OF FUNDING / SPONSORING ORGANIZATION | 8b. OFFICE SYMBOL (If applicable) | 9. PROCUREMENT INSTRUMENT IDENTIFICATION NUMBER | |
| 9. ADDRESS (City, State, and ZIP Code) | | 10. SOURCE OF FUNDING NUMBERS | |
| | | PROGRAM ELEMENT NO. | PROJECT NO. |
| | | TASK NO. | WORK UNIT ACCESSION NO. |
| 11. TITLE (Include Security Classification) | | | |
| A LINEAR STABILITY ANALYSIS OF THE RAPID DEVELOPMENT OF AN EXTRATROPICAL CYCLONE | | | |
| 12. PERSONAL AUTHOR(S) | | | |
| Toll, Raymond F. Jr. | | | |
| 13. TYPE OF REPORT | 13b. TIME COVERED | 14. DATE OF REPORT (Year, Month, Day) | 15. PAGE COUNT |
| Master's Thesis | FROM _____ TO _____ | 1986 March | 112 |
| 16. SUPPLEMENTARY NOTATION | | | |
| COSATI CODES | | 18. SUBJECT TERMS (Continue on reverse if necessary and identify by block number) | |
| FIELD | GROUP | SUB-GROUP | |
| | | | |
| | | | |
| | | | |
| 19. ABSTRACT (Continue on reverse if necessary and identify by block number) | | | |
| <p>The phenomenon of the rapid growth and development of an extratropical cyclone over the east coast of the United States (the Carolinas storm of March 1984) is studied through a linear stability analysis. Analyses of the cyclone structure suggest barotropic and baroclinic instabilities may be important. A linear stability model is used to investigate the roles and relative importance of shortwave baroclinic instability and barotropic instability in the growth and development of the storm. The growth rates, phase speeds and structure obtained from the linear model are consistent with those derived from observations. Energy budget results indicate that the vertical and horizontal barotropic terms are at least as important as the baroclinic term. It appears that the early growth and development of the cyclone can be explained through the contributions of barotropic and baroclinic instabilities without including convection.</p> | | | |
| 20. DISTRIBUTION / AVAILABILITY OF ABSTRACT | | 21. ABSTRACT SECURITY CLASSIFICATION | |
| <input checked="" type="checkbox"/> UNCLASSIFIED/UNLIMITED <input type="checkbox"/> SAME AS RPT. <input type="checkbox"/> DTIC USERS | | unclassified | |
| 22a. NAME OF RESPONSIBLE INDIVIDUAL | | 22b. TELEPHONE (Include Area Code) | 22c. OFFICE SYMBOL |
| J. Chan | | 408- 646-3107 | 63 Cd |

Approved for public release; distribution is unlimited.

A Linear Stability Analysis
of the Rapid Development of
an Extratropical Cyclone

by

Raymond F. Toll Jr.
Lieutenant, United States Navy
B.S., University of Utah, 1978

Submitted in partial fulfillment of the
requirements for the degree of

MASTER OF SCIENCE IN METEOROLOGY AND OCEANOGRAPHY

from the

NAVAL POSTGRADUATE SCHOOL
March 1986

ABSTRACT

The phenomenon of the rapid growth and development of an extratropical cyclone over the east coast of the United States (the Carolinas storm of March 1984) is studied through a linear stability analysis. Analyses of the cyclone structure suggest barotropic and baroclinic instabilities may be important. A linear stability model is used to investigate the roles and relative importance of short-wave baroclinic instability and barotropic instability in the growth and development of the storm. The growth rates, phase speeds and structure obtained from the linear model are consistent with those derived from observations. Energy budget results indicate that the vertical and horizontal barotropic terms are at least as important as the baroclinic term. It appears that the early growth and development of the cyclone can be explained through the contributions of barotropic and baroclinic instabilities without including convection.

TABLE OF CONTENTS

| | | |
|------|---|-----|
| I. | INTRODUCTION | 6 |
| II. | REVIEW OF THE MECHANISMS FOR GENESIS AND DEVELOPMENT OF EXTRATROPICAL CYCLONES | 9 |
| | A. BAROCLINIC INSTABILITY | 9 |
| | B. BAROTROPIC INSTABILITY | 11 |
| | C. JET STREAK DYNAMICS | 13 |
| | D. CONVECTION | 16 |
| | E. OTHER MECHANISMS | 17 |
| | F. DISCUSSION | 19 |
| III. | SYNOPTIC ANALYSIS AND DISCUSSION | 21 |
| | A. DATA AND METHODS OF ANALYSIS | 21 |
| | B. SYNOPTIC OVERVIEW | 22 |
| | C. DETAILED SURFACE ANALYSES OF THE GENESIS PERIOD | 28 |
| | D. VERTICAL CROSS-SECTIONS | 31 |
| | E. NUMERICAL MODEL PERFORMANCE | 34 |
| IV. | HYPOTHESIS | 60 |
| V. | LINEAR STABILITY ANALYSIS | 64 |
| | A. INTRODUCTION | 64 |
| | B. DESCRIPTION OF THE LINEAR STABILITY MODEL | 65 |
| | C. INITIALIZATION | 68 |
| | D. RESULTS | 73 |
| | 1. Growth Rates and Phase Speed | 73 |
| | 2. Structure | 75 |
| | 3. Energetics | 78 |
| VI. | CONCLUSIONS | 100 |
| | LIST OF REFERENCES | 102 |
| | INITIAL DISTRIBUTION LIST | 109 |

ACKNOWLEDGEMENTS

I wish to extend my sincere thanks to my advisors, Professors J. C. L. Chan and C. H. Wash. Without their guidance and timely critical review of this thesis as it evolved, this study could not have been completed. A special thanks to Professor Chan for all the extra undocumented time he spent helping me with the Fortran code, interpreting results, hours of valuable advice, and much needed words of encouragement. I am very grateful to Professor R. Gall for all of the time spent on the linear stability model, as well as the special trip he made to attend my presentation. His suggestions to use a linear stability analysis provides the very basis for this thesis. I also thank Ms. Stacey Heikkinen for her valuable programming assistance, LCDR Larry Warrenfeltz and LT Bob Rau for their help with the graphics and Dr. C. S. Liou for his assistance in reading the NORAPS fields. This thesis is dedicated to my wife, Kathy, and my son, Michael, whose support carried me through a very challenging period of my life.

I. INTRODUCTION

Extratropical cyclones have been the focus of extensive research for many years. Modern studies of genesis and development of cyclones began with the pioneering work of the Norwegian school that formulated the polar front theory (Bjerknes, 1919). Later, Charney (1947) proposed the instability theory to explain the cyclogenesis process. Petterssen (1956), Palmen and Newton (1969), Holton (1979) and others have provided textbook treatments of the structure and behavior of a typical cyclone.

A number of factors indicate that the east coast of the United States is a primary location for significant cyclone development (e.g., Sanders and Gyakum, 1980). These include land-sea temperature contrasts, the location and intensity of the Gulf Stream, air mass modification over the Atlantic Ocean, land-sea frictional effects, the shape of the coastline and the influence of the Appalachians (Kocin and Uccellini, 1985). Some of the cyclones that form along the east coast deepen rapidly and have presented major forecast problems. Operational as well as research numerical forecasts have only had marginal success in predicting the deepening process (Sanders and Gyakum, 1980; Bosart, 1981; Atlas, 1984). These cyclones exhibit deepening rates of at least 1 mb/h for 24 h in sea-level pressure. Observational studies such as that of Sanders and Gyakum (1980) have documented the climatological aspects of these explosively deepening cyclones. Deepening rates of these cyclones cannot be explained from quasi-geostrophy alone (Sanders, 1971; Sanders and Gyakum, 1980). Observations also have suggested that some of them initially form on the meso-alpha scale (200 - 2000 km). Therefore, it appears that other physical processes may contribute significantly to the growth and

development of this class of extratropical cyclones. It is important that these storms be studied and understood since public perception of forecast accuracy is particularly acute during these events. These cyclones have a large impact on centers of population and business as well as on naval operations.

An example of a rapidly developing cyclone along the east coast is the Carolinas storm of 28-30 March 1984. This cyclone formed along the North/ South Carolina border with a diameter of approximately 1000 km. From 0000GMT through 1500GMT on 29 March, the cyclone rapidly deepened while growing to a diameter of approximately 4000 km. The cyclone reached its lowest central pressure of 965 mb at 1500GMT while moving northeastward away from the coast. Its central pressure fell 15 mb in this 15 h period.

The operational numerical models (the Limited Fine Mesh Model (LFM) and the Navy Operational Global Atmospheric Prediction System (NOGAPS)) failed to predict the rapid development of this cyclone. However, the Navy Operational Regional Atmospheric Prediction System (NORAPS) and the Mesoscale Atmospheric Simulation System (MASS) did forecast the formation of the cyclone, although in both models the predicted low pressure center is southwestward of that analyzed by the National Meteorological Center (NMC).

The inaccurate forecasts of this and other rapidly developing cyclones suggest that certain dynamical features or processes associated with these cyclones may not be properly simulated or diagnosed. Bosart (1981), Uccellini et al. (1981, 1984) and Sanders and Gyakum (1980) have noted certain model deficiencies, including inadequate boundary layer and cumulus parameterizations, coarse vertical resolution and poor jet streak simulations. However, recent simulations of these storms using mesoscale models have produced some encouraging results (Kocin et al., 1984).

The objective of this thesis is to better understand the genesis and rapid development of maritime extratropical cyclones by studying the case of the Carolinas storm. Although over land, this storm exhibited many typical characteristics of a rapidly intensifying maritime cyclone. The abundance of land observations allows the synoptic as well as the sub-synoptic scale features to be better understood. A linear stability analysis will be performed to determine the roles and relative importance of shortwave baroclinic instability (Staley and Gall, 1977) and barotropic instability in the genesis and subsequent rapid development of this cyclone.

A literature survey will be presented first on the roles of baroclinic instability, barotropic instability, jet streak dynamics and convection on rapid cyclone development. Next, a detailed synopsis of the synoptic events that characterized the Carolinas storm will be summarized. The linear stability model developed by Gall (1976c) will be used to investigate the role of baroclinic and barotropic instabilities in the genesis of this storm. Finally, conclusions and possible avenues for future research will be suggested.

II. REVIEW OF THE MECHANISMS FOR GENESIS AND DEVELOPMENT OF EXTRATROPICAL CYCLONES

A. BAROCLINIC INSTABILITY

It is generally agreed that extratropical cyclones on the synoptic scale derive most of their energy from the release of the available potential energy inherent in air-mass contrasts. These disturbances depend on a pre-existing baroclinic structure of the basic current. However, the kinetic energy of the disturbance can also be obtained through the conversion of the kinetic energy of the basic current.

Baroclinic instability (BCI) is a mechanism that has been proposed to explain how potential energy of the basic current can be converted to kinetic energy of the disturbance. The principles of BCI were introduced by Charney (1947) and Eady (1949). Their studies show that the most baroclinically unstable waves have a wavelength of approximately 4000 km, which corresponds to that observed to have the largest amplitude in the extratropical cyclone at mid and upper levels (Holton, 1979).

Historically, the dynamics and thermodynamics of a developing baroclinic disturbance have been explained using quasi-geostrophic theory. This theory is based on mid-latitude, synoptic-scaled disturbances. Furthermore, the atmosphere is assumed to be frictionless and adiabatic. Also, the atmosphere can only undergo changes in such a way that geostrophic and hydrostatic balances are maintained. The theory greatly simplifies the system of equations that govern the dynamics and thermodynamics of the atmosphere, while preserving the fundamental physics which the original equations represent.

Extending the concepts of this theory, Petterssen (1956), Palmen and Newton (1969) and Holton (1979) have shown that when all other factors are held constant, the process of cyclone development can be accelerated if the static stability is reduced and/or diabatic heating (latent heat release, air-sea fluxes, radiation) is introduced. These other factors include warm air advection and the advection of positive vorticity at mid-tropospheric levels. As a result, the "self-limiting" process, in which the effect of temperature advection is partially offset by the adiabatic temperature changes caused by vertical motion, is reduced.

Other observational studies (Sanders and Gyakum, 1980) have documented the explosive development of certain cyclones. These incipient disturbances are relatively shallow and confined mostly to lower levels (Bosart, 1981). Several studies have attempted to explain this structure by modifying the early baroclinic theories which were based on quasi-geostrophy. Mansfield (1974) modified the Eady model to include a shallow baroclinic zone in the lowest 1.6 km. The results indicate that reducing the static stability in the lowest layers shortens the wavelength of maximum instability to 1000 km. Duncan (1977) and Staley and Gall (1977) found similar results.

Using a linearized general circulation model, Gall (1976a) demonstrated that disturbances with a zonal wavenumber of 15 exhibit the maximum growth rate. However, results from the nonlinear version of the model suggest waves with wavenumbers 5-7 to be the most unstable. Therefore, although shortwaves are the most baroclinically unstable, nonlinearity modifies the spectrum such that longer waves eventually dominate. Inclusion of wave-zonal flow interaction (Gall, 1976b) increases the low-level static stability because of the northward and upward eddy

transport of heat. This retards the growth rate of the shorter waves since they are primarily low-level disturbances. Gall (1976c) showed that although waves of wavenumber 15 are mostly confined near the surface, the vertical extent could be increased by including latent heat. In another numerical study, Gall et al. (1979) found the most unstable waves to be initially at wavenumber 13. However, friction, an increase in static stability and destruction of the north-south temperature gradient weakened these high wavenumber disturbances with time, so that wavenumber 7 became the most energetic.

These numerical studies as well as earlier case studies of extratropical cyclones (Bjerknes, from Godske et al., 1957; Palmen and Newton, 1969) have focussed on the evolution and the attendant structural changes of the cyclones on the synoptic scale. These findings suggest that BCI is a dominant mechanism in the genesis of a cyclone. However, once the cyclone has developed to the mature stage, the vertical tilt of the low pressure trough that was prevalent at the genesis stage becomes less apparent. This suggests that other processes besides BCI may have increased in importance. The next section will review studies which relate both baroclinic and barotropic instabilities to the genesis and development process.

B. BAROTROPIC INSTABILITY

As previously discussed, much of the current theory of eddies in the atmosphere is based upon the dynamic instability of zonal currents (Charney, 1947; Eady, 1949 and Kuo, 1949). These studies have shown that zonal flows with vertical or horizontal shears typical of the atmosphere were unstable to small perturbations. For mathematical reasons, these earlier studies involved essentially two-dimensional atmospheres in which the wind shears were either entirely baroclinic or barotropic. The previous section discussed

those studies that focussed on baroclinic instability. This section will address the effect of barotropic instability on the cyclogenetic process.

Textbook treatments of barotropic instability are contained in Holton (1979) and Pedlosky (1982). They both showed that the necessary condition for a region to be barotropically unstable is that the gradient of the absolute vorticity of the mean current must vanish somewhere in the region. Furthermore, a sufficiently large value of the beta term (which represents the change in the Coriolis force with respect to latitude) can barotropically stabilize the current. Pedlosky (1982) suggested that baroclinic instability is the favored mode for horizontally broad zonal currents, whereas very narrow currents would tend to be barotropically unstable. These authors further showed that barotropic instability converts kinetic energy from the basic current to the perturbation, in contrast to the energy flow description associated with baroclinic instability.

Studies using more realistic atmospheric flows with both horizontal and vertical shears were undertaken by Brown (1969) and Song (1971). Their results showed that baroclinic waves are barotropically damped. At longer wavelengths, they found that barotropic waves could exist. A later study by Gent (1974) found that waves with the largest meridional wavelength are the most barotropically unstable.

Most of these studies constructed mathematically simple wind fields, where the horizontal shear was invariant with height. A more realistic representation of a wind field was used by Gall (1976a). However, using a 40 m/s jet, he found that waves of all wavelengths receive most of their energy through baroclinic processes. For waves shorter than wavenumber 15, baroclinic instability is the most important contributor to the development of the perturbation. On the

other hand, the barotropic terms for the most part hamper wave growth.

Pedlosky (1982) suggested that in zonal currents where both baroclinic and barotropic instabilities are possible, the energy-transfer characteristics of the most unstable wave depend upon the detailed distribution of the zonal velocity and the potential vorticity of the basic state. Changing these parameters of the jet can profoundly affect whether baroclinic or barotropic mechanisms are favored for instability, as well as the wavelength of maximum instability.

These ideas were incorporated into a numerical study on polar lows conducted by Hodur (1984). He found the presence of both barotropic and baroclinic instabilities during the genesis of the polar low. In particular, by varying the intensity of the jet from 40 m/s to 60 m/s, he showed that for higher wavenumbers and a stronger jet, the perturbation can extract as much energy from eddy available potential energy as from zonal kinetic energy. For the weaker jet, the baroclinic term became the dominant contributor, which is consistent with the simulations of Gall (1976a). In Chapter 5, these ideas of how energy for the perturbation in the Carolinas storm is extracted from the mean flow through baroclinic and/or barotropic processes will be investigated further.

There have not been many studies on cyclone development through the mechanism of barotropic instability. This thesis will be the first to study this mechanism in conjunction with baroclinic instability in a real-case cyclone.

C. JET STREAK DYNAMICS

Palmen and Newton (1969) showed that appreciable upper-level divergence and vertical motion fields characterize synoptic-scaled disturbances in regions of the jet stream. Families of synoptic disturbances are typically found along

the polar front jet stream. From the study of many cases of cyclone life cycles, Petterssen (1956) formulated the rule that cyclone development occurs when and where a region of positive vorticity advection (PVA) at the upper levels becomes superimposed over a low-level baroclinic zone. This region of PVA is typically associated with the jet stream.

Other studies have attempted to test the hypothesis that when the static stability is weak, the superposition of frontal systems in the upper levels on the planetary boundary layer can result in favorable conditions necessary for rapid cyclone development. Palmen and Newton (1969), Kocin and Uccellini (1985) and others have suggested that jet streaks imbedded within upper-level trough/ridge systems enhance and focus upper-level divergence, energy exchange and momentum transport, all of which can play an important role in cyclone genesis and development. Shapiro (1982) suggested a way in which upper-level and lower-level fronts can be coupled via ageostrophic circulations associated with each feature. A pattern of intersecting upper and lower level jets has been shown by Uccellini and Johnson (1979) to be a classic configuration for triggering the release of convective and potential instabilities. The resultant latent heat release could then enhance the growth and development of the cyclone.

A case study by Calland (1983) of rapid cyclone development that occurred southeast of Japan in January, 1979 showed the importance of the jet streak. Specifically, his results suggested that upper-level forcing may play a greater role in the initiation of explosive development than was proposed by Petterssen (1956). They also point to the importance of boundary layer and convective processes during the explosive development phase.

From budget statistics, Conant (1982) illustrated the importance of the polar jet streak and an amplifying

mid-level trough when the Presidents' Day cyclone explosively deepened. In a study of a North Atlantic polar low, Wash and Cook (1985) found that the average horizontal advection of vorticity dominated the forcing terms and coincided with the intensification of the cyclone mass circulation, the large production of vorticity by the low-level convergence and the largest decrease in the sea-level pressure.

Uccellini et al. (1984) identified three jets that were deemed important in the development of the Presidents' Day cyclone. Diagnostic calculations revealed an increasingly unbalanced flow in the subtropical jet (STJ) associated with a super-geostrophic flow. The upper-level divergence associated with the STJ was linked to the intensification of the low-level jet along the east coast. Subsequent studies such as that by Uccellini et al. (1985) focussed on the amplifying polar jet. This latter study illustrated the role of dynamically-forced ageostrophic vertical circulations on the deformation of the tropopause. The dramatic tropopause fold which occurred during the trough amplification was consistent with the subsidence expected from geostrophic deformation patterns associated with the jet streak.

Using an analytic formulation, Hoskins and Bretherton (1972) were able to cause frontal formation near the tropopause and the associated tropopause folding through geostrophic confluence. It is apparent from arguments of Shapiro (1982) that a correct combination of stretching and shearing deformations can cause tropospheric folding. The resultant intrusion of stratospheric air, as characterized by high potential vorticity into the troposphere, could then spin up the lower levels and cause genesis. It seems reasonable that upper-level forcing would more strongly affect changes in the lower layers if the intermediate layers were convectively unstable. In this way, convective overturning

would efficiently transfer upper-level momentum to the surface. This apparent contribution to cyclogenesis through convective processes will be discussed further in the next section.

D. CONVECTION

It was observed by Petterssen (1956) that cases of moderate and heavy convection over a large area probably will not occur, even if surface heating is intense, unless the convection is associated with a cyclone. Palmen and Newton (1969) summarized from observations that although convective clouds cover very large regions of synoptic disturbances, areas occupied by clouds of considerable vertical development are small. However, since most of the rising motion associated with the cyclone takes place in the convective system, Palmen and Newton (1969) suggested that convection and the cyclone are dynamically linked. They further argued that the static stability, which measures the atmospheric susceptibility to convection, typically acts against cyclone development by lessening the effect of thermal advection. However, this damping term is considerably smaller for a given vertical motion when extensive condensation within the cyclone exists. If this condensation is convective in nature, development can proceed further and the cyclone can achieve a greater intensity.

The generation of available potential energy has been shown to be enhanced when precipitation occurs in the warm sector of a cyclone (Bullock and Johnson, 1971). Tracton (1973) stressed the importance of convection in enhancing cyclone development during the developing stage. Sanders and Gyakum (1980) noted that strong low-level baroclinity, a mobile 500 mb trough and intense convection are associated with rapid maritime cyclone development.

In a study of the Queen Elizabeth II (QEII) storm, Gyakum (1983a) found that the storm originated as a shallow

baroclinic disturbance, and then developed in response to low-level warm advection. He hypothesized that the mesoscale conditions during the incipient stages of the storm were linked to its subsequent explosive development on the synoptic scale through a significant increase in potential vorticity. This increase was proposed to be related to the deep convection, which appeared to be important in the explosive deepening phase. The storm formed on the anticyclonic side of the jet, suggesting that inertial instability might also have contributed to the development of the cyclone.

The second part of his study (Gyakum, 1983b) examined the dynamic and thermodynamic structure of the QEII storm. In this case, BCI appeared to be directly responsible for only a small part of the cyclone development. BCI was important in that it organized convective effects in such a way as to produce a positive feedback between convection and BCI. Gyakum was able to establish both observationally and numerically the critical importance of cumulus-induced heating effects in determining whether a cyclone explosively develops. However, key questions remain as to how the organization of the cumulus clouds are affected by the cyclone as well as the important aspects of the interaction between the cumulus clouds and the larger-scale features.

Liou and Elsberry (1985) from heat budget studies over the western North Pacific showed that increasing the heating rate (sensible and latent) reduces the sea-level pressure of a cyclone. This suggests that although diabatic processes might weaken horizontal temperature gradients and frontal zones, warming of the air column near the area of genesis aids in the process of cyclone formation.

E. OTHER MECHANISMS

Besides the four mechanisms described above, other possible hypotheses have been proposed to explain the

genesis and development of extratropical cyclones. For example, Petterssen (1956) showed the importance of orography by identifying distinct frequency maxima of episodes in both winter and summer of genesis to the east of the highest parts of the Rocky Mountains and the Alps. Palmen and Newton (1969) suggested that the overall process of genesis to the lee of mountains is one in which vorticity is first generated in a low-level trough, held fixed to the eastern slope and finally overtaken by the divergence region associated with an upper-level trough. The rapidity of development is at least partially due to the availability of significant amounts of vorticity at low levels.

Recent studies have also pointed to the importance of certain boundary layer processes in the genesis and development processes. Analyses of surface observations by Bosart (1981) of the Presidents' Day snowstorm suggested that the incipient cyclone originated as a shallow, baroclinic boundary layer disturbance along a coastal front in the Carolinas. Differential heating, moistening and roughness between land and sea in conjunction with cold air damming to the east of the Appalachians were proposed to be important physical mechanisms that contributed to the cyclone development. Rapid deepening of the cyclone occurred when it came under a favorable southwesterly flow ahead of a prominent, upper-level trough which had moved eastward from the Ohio valley. Energy, moisture and vorticity budgets analyzed by Bosart and Lin (1984) showed the importance of planetary boundary layer processes and cold air damming. However, a recent numerical study (Guo and Hoke, 1985) suggests that the latent heat release occurred in the Presidents' Day cyclone was more important than the sensible heat flux from the North Atlantic Ocean.

F. DISCUSSION

Many ideas resulting from various types of studies have been proposed to explain the behavior of a certain class of extratropical cyclones. These studies have primarily focussed on the mechanism of baroclinic instability, with the viewpoint that other processes can augment this mechanism and thereby explain the behavior of those cyclones that rapidly deepen.

Specifically, baroclinic instability has been used to explain the structural and developmental characteristics of the typical synoptic-scaled cyclone. However, studies by Gall (1976a) and Hodur (1984) suggested that barotropic instability also could be an important contributor to the rapid development of some of those cyclones. In addition, case studies have pointed to other processes that might be contributing to the genesis and developmental processes of these cyclones. These processes include (but are not limited to) convection, boundary layer processes and jet streak dynamics.

Each of these additional processes explain to a certain extent the behavior of a cyclone that rapidly develops. They also provide some physical insight as to why certain cyclones behave differently. The fact that the incipient cyclone can exist on the meso-alpha scale suggests that interaction with the mesoscale might be important. These ideas raise further questions about these cyclones. For example, why do some of these processes become important for a cyclone that rapidly develops as opposed to one that does not? Do these other processes also contribute to the genesis of the cyclone? If so, how does their combined effect modulate the developmental process? Does a strongly baroclinic atmosphere provide the background that is conducive to enhancing the effect of these other processes, or vice versa? What additional processes might be important at the genesis phase?

Sanders and Gyakum (1980) have shown that episodes of rapid cyclone development are not common events, suggesting that the atmosphere operates in a more subtle manner. Specifically, most cases of rapid cyclone development cannot be explained using quasi-geostrophy. Therefore, it is hypothesized that certain relationships between the aforementioned physical mechanisms at different spatial and temporal scales are crucial for the acceleration of cyclone growth and development. Development may also be accelerated if both sources of energy (eddy available potential energy and zonal kinetic energy) are available to the initial perturbation. In other words, a cyclone may develop rapidly through a combination of baroclinic and barotropic processes if the horizontal and vertical shears are of sufficient magnitude.

This thesis will focus on the processes of baroclinic and barotropic instabilities by studying the genesis, growth and behavior of the Carolinas storm of March 1984. Based upon the synoptic analysis and discussion of this cyclone (Chapter 3) it is hypothesized that both baroclinic and barotropic instabilities contributed to this particular cyclone event. Such a hypothesis will be tested in Chapter 5 using a linear stability analysis.

III. SYNOPTIC ANALYSIS AND DISCUSSION

A. DATA AND METHODS OF ANALYSIS

Operational height and temperature analyses at 850, 700, 500, 300 and 200 mb at the 0000 and 1200 GMT synoptic times and 3-hourly surface pressure analyses from NMC were used in this portion of the study. Height, temperature and wind analyses for the same levels from NORAPS were also used. Other data include hourly surface observations from the first-order stations and ship and buoy reports along coastal areas between 282100GMT through 290300GMT. Rawinsonde observations from stations throughout the central and eastern sections of the USA were also available.

The hourly observations were manually analyzed for temperatures, pressures and pressure tendencies. These analyses provide a more detailed depiction of the synoptic as well as the sub-synoptic events that occurred prior to and during genesis, as will be seen in section C of this Chapter.

To obtain information about the vertical structure of the atmosphere and the incipient cyclone, four cross-sections were chosen. The cross-sections were constructed using a technique similar to that described by Whittaker and Petersen (1975). Potential temperatures were first calculated from the pressure and temperature observations at each of the rawinsonde stations along the cross-section. Any static instability at each station is removed prior to the analysis. Temperatures and potential temperatures were then linearly interpolated onto 50 vertical levels and 50 horizontal grid points (all equally spaced).

The wind cross-section was constructed by first computing the wind component perpendicular to the cross-section. These normal components were then linearly

interpolated in the vertical for those levels in which wind observations were available. Otherwise, the thermal wind relation was used to provide an estimate of the winds in the following manner. The horizontal temperature gradient was first computed using the interpolated temperatures at the two grid points (one on each side) nearest to the station. The wind at a level above the highest level in which the wind observation was available can then be estimated with the assumption that the wind observation at the highest available level could be approximated by the geostrophic wind. This assumption was verified by geostrophic wind calculations (not shown) using the temperature field described above. This procedure is repeated for all the other levels above. After the winds have been computed to 100 mb, they are linearly interpolated in the horizontal to obtain a 50x50 grid of winds.

To gain further insight into the structure of the incipient low as well as possible physical processes, computations of static stability, absolute vorticity and Richardson numbers were made for each cross-section at 290000GMT. These are defined as follows:

$$\text{static stability (SS)} = -(\alpha/\theta)(\partial\theta/\partial P) \quad (3.1)$$

$$\text{Richardson number} = \text{SS}/|\partial U/\partial P|^2 \quad (3.2)$$

where α is the specific volume, θ the potential temperature, P the pressure and U the zonal wind.

B. SYNOPTIC OVERVIEW

The 28-30 March 1984 case of rapid cyclone development, which produced severe weather and heavy snowfall over the eastern portions of the United States, was one of the most

destructive on record. A series of tornadoes across South and North Carolina caused 57 deaths and 1,248 injuries, according to the 1984 Storm Data statistics (Kocin et al., 1984). Wind-driven tidal surges caused widespread damage along the middle Atlantic to the New England coastline. As much as 75 cm of snow fell across interior sections of Pennsylvania, New York and New England.

The following discussion will focus on the tracks and intensities of the individual low pressure systems that existed over a 48-h period between 280000GMT through 300000GMT. (All future references to time are with respect to GMT.) This section describes the synoptic background from which the Carolinas storm evolved. A more detailed analysis of the genesis period is contained in the next section.

At 280000, a mid- to upper-level synoptic-scaled trough extended through the central portions of the US. This trough was moving rapidly eastward with little change in amplitude until 281200, when it decelerated and began to deepen more rapidly (Fig. 3.1). A shortwave trough was also observed to the westnorthwest of the major 500 mb low center at 281200. The jet streak at 300 mb had winds of 100-140 kt and was located over central Texas.

Three separate low pressure centers can be identified from the NMC surface analyses between 280000 and 291200. The tracks and intensities of these systems are shown in Figs. 3.2 and 3.3 respectively. At 280000, low I was over east Texas with a pressure of 989 mb. This feature was imbedded in a large region of low sea-level pressure that encompassed most of the midwest sections of the US. Low I moved rapidly northeastward while slowly deepening to 984 mb. At 281200, low II formed over western Tennessee and moved slowly eastward to approximately 200 km west of the Appalachians. Low II continued to deepen slowly, with the central pressure reaching 982 mb 12 h later.

Between 281800 through 290000, surface pressure falls exceeded 6 mb over a 3-h interval across Georgia and Alabama concurrent with the formation and rapid movement of low III. Warm, humid air (dew-point depressions less than 3° C) at 281800 covered the southeastern US as far north as North Carolina. Moderate rain was also widespread across the eastern half of the US, with snow across New York and Pennsylvania. The widespread region of clouds that produced the moderate to heavy precipitation can be seen in Fig. 3.4.

A six-hourly sequence of surface analyses between 281800 and 290600 shown in Fig. 3.5 vividly depicts the large, intensifying cyclonic circulation that occupied the eastern half of the United States during this time. Imbedded within this large circulation are the three low pressure systems (lows I, II and III) described above. The unmarked low was a weak, shallow disturbance that had moved eastward across North Carolina.

Low III developed at 281800 over eastern Alabama along a cold front, and moved rapidly northeastward to a position over central Georgia by 282100. The available observations did not suggest low III originated in the Gulf of Mexico, which is consistent with the conclusion in related papers on this storm (Kocin et al., 1984; Hillger et al., 1985). A very large circular cloud mass southeast of the Appalachians can be observed at 282100 from infrared GOES imagery (Fig. 3.4). This feature was similar in shape and size to the mesoscale convective complex (MCC) described by Maddox (1980). At 282300, the satellite signature of this convective area appeared to change shape, perhaps due to a mid or upper-level wind maximum. The changes continued until by 290030 (not shown), a well-defined comma cloud was evident. The strong height gradient over this region on the 290000 NORAPS 500 mb analyses suggests that a wind maximum did exist over and to the southwest of the comma cloud

(Fig. 3.6). Satellite imageries at 282300 and 290100 show the area of severe weather near the South Carolina-Georgia border (Fig. 3.4). By 290000, the NMC 500 mb analysis (not shown) reveals that the shortwave had progressed to a position east of the longwave trough position at 500 mb, and lay southwest but in close proximity to an area of severe weather. Low I had become primarily a mid-level feature, and appeared to be associated with snowfall over Pennsylvania, New York and New England at this time. The rapid northeastward movement of low III on both Figs. 3.2 and 3.5 is apparent until 290000 when its translation speed was more consistent with that of a midlatitude synoptic-scaled cyclone.

The size of low III at this time was approximated by measuring the diameter of the 984 mb isobar (Fig. 3.5), which roughly coincides with the perimeter of the comma-shaped cloud (Fig. 3.4). Since the 984 mb isobar does not encircle low III, this approximation was only valid to the north, east and south of low III. (The extension of this isobar to the west of low III reflects the presence of low II.) The diameter was measured to be about 1000 km which at this latitude approximately corresponds to a disturbance of zonal wavenumber 15.

Between 290300 and 290600, low III deepened very rapidly. By 290600, low III became the dominant synoptic feature with respect to the other low pressure systems discussed above (Fig. 3.5). By noting the change in the distance of the 980 mb isobar from the center of low III at 290000 and 290600 (Fig. 3.5), it was estimated that the cyclone doubled in size within this time interval, which corresponds to a growth rate of approximately 3/day. The 980 mb isobar is used in estimating the size change because it better depicts the evolution of low III than does the 984 mb isobar (Fig. 3.5). This growth rate is further

substantiated by observing that at 290000, the surface pressure perturbation along a 2000 km north-south line centered in the middle of the low was approximately -6 mb. This pressure perturbation at 290600 became approximately -11 mb. These estimates of the growth rates will be discussed further in Chapter 5 when compared with the results of the linear stability model.

Between 290300 through 291500, the cyclone (low III) deepened from 982 to 965 mb (Fig. 3.3) and grew in size from approximately 1000 to 4000 km, while tracking to within approximately 100 km northeast of Norfolk, Va. at 290900. The most rapid development of the cyclone took place over land, although it reached its lowest pressure (at 291500) over water.

Satellite pictures (Fig. 3.4) show that as the cyclone developed, the associated convection that was located mostly northeastward of low III grew rapidly in horizontal extent. The 291200 operational analyses indicate that the cyclone extended from the surface through 500 mb. The cyclone was now situated completely in the cold air, and had become vertically stacked. No phase shift between the 500 mb thermal field and height field can be discerned, as had been evident at 290000 (Figs. 3.6 and 3.7). Subsequent satellite pictures after 291200 (not shown) indicate that the main areas of convection were 550 km to the north, east and southeast of the cyclone and had a north-south extent of approximately 2000 km. The low began to weaken at 292100, while moving northeastward parallel to the coastline.

The most noteworthy synoptic features at 290000 are the distinct westward vertical tilt of the pressure trough, as well as the phase difference between the thermal and height fields (Figs. 3.5, 3.6 and 3.7). These features imply the strong baroclinic nature of the atmosphere prior to and during genesis. The vertical structure also suggests that

the incipient cyclone was primarily a surface disturbance. The 850 mb height analysis (Fig. 3.7) further indicates the presence of a low-level jet over southeastern Georgia and South Carolina and the strong warm advection to the northeast of low III. This jet suggests that the low-level vertical and horizontal shears were greatly increased. Strong vertical shears could result in regions near the surface where low Richardson numbers might exist. These observations point to shortwave baroclinic instability as a possible contributor to the genesis of low III. The strong horizontal shears also suggest that barotropic instability may have played a role during the early stages of the development of the cyclone.

The 500 mb wind and temperature fields at 290000 (Fig. 3.8) indicate that cold advection is occurring at the exit region and warm advection at the entrance region of the jet. This suggests that rising motion would occur underneath and sinking motion to the south of the exit region of the 500 mb jet (Shapiro, 1982). In fact, most of the severe convection occurred underneath and to the north side of this region. Low III was also located almost directly under this area.

In summary, the Carolinas storm appeared to have formed in eastern Alabama at 281800 (low III in Fig. 3.2). The cyclone moved rapidly northeastward until 290000, when it began to decelerate quickly. The low continued to move at this slower speed until its demise. Furthermore, the cyclone began to deepen rapidly after 290000. Most of the severe convection occurred between 290000 and 290600. However, the convection was confined to a small region mostly to the northeast of the cyclone. The atmosphere appeared to be highly baroclinic at 290000 so that baroclinic processes could be important in the formation of low III and perhaps its subsequent rapid development. This idea

will be explored further using a linear stability model (Chapter 5). It is also apparent that to understand the behavior of this particular case of explosive cyclone development, a more detailed analysis of the environment near 290000 is warranted.

C.. DETAILED SURFACE ANALYSES OF THE GENESIS PERIOD

To provide a more coherent synopsis of the events that occurred around 290000, hourly surface observations in the eastern US for seven time periods (282100 to 290300) were analyzed. Each analysis includes the temperatures, pressures, pressure tendencies and frontal positions. These analyses augment Fig. 3.5 and were crucially aided by the information gleaned from satellite pictures.

The 282100 analysis (Fig. 3.9) shows a strong temperature gradient oriented along the lee slopes of the Appalachians. Low III was imbedded in this gradient over northeastern Alabama, with temperatures greater than 80° F to the southeast and less than 60° F to the northwest. The temperature analysis also suggests an extensive amount of cold air damming, which might have enhanced the temperature gradient. At this time, very little warm advection appears to be taking place ahead of the low.

Surface damming of cold air east of the Appalachians is particularly apparent north of the warm front. Richwien (1980) found that damming frequently occurs after a cold anticyclone becomes established over the northeastern US. The ridge axis typically extends southward between the Appalachians and the east coast. In this case, the surface analysis shows a weaker ridge across Virginia than Richwien observed, extending from a moderately strong anticyclone situated well to the north of the Great Lakes. This weak ridge over Virginia is coincident with colder air to the north of low III (Fig. 3.9). Consequently, it seems reasonable that damming may also have contributed to the rapid

development of low III. However, damming may also have played an important role in the formation, location and amount of snow to the north.

Between 282000 and 282100, rapid pressure falls (rises) ahead of (behind) low III can be readily observed (Fig. 3.10), which was largely related to the movement of this cyclone. In fact, the movement of low III is almost parallel to the isallobaric vector, which is directed north-eastward from north-central Georgia to northern South Carolina.

Major changes in the surface pressure and temperature fields appeared to have taken place between 282100 and 282200 (Fig. 3.11). Low III had moved very rapidly east-northeast to a position over central South Carolina. The central pressure fell to 978 mb and the strong baroclinic zone to the north of the low was perturbed. Also of particular interest in Fig. 3.11 is the warm air now prevalent ahead of the low. Large pressure falls are found to the northeast and south of low III (Fig. 3.12). The isallobaric vector is now directed east-northeast from northeastern Georgia towards the North/South Carolina border, which again is almost parallel to the movement of low III. The movement of low III appears to be towards the region of largest hourly surface pressure falls (Fig. 3.12).

By 282300, low III was located over northeastern South Carolina, continuing its rapid movement over the past hour (Fig. 3.13). Furthermore, the central pressure had decreased an additional 2 mb. Warm air advection had become much more prevalent ahead of the low, but the baroclinic zone was less perturbed than in the previous hour. One possible explanation for this is the apparent cold dome associated with the downdraft at Greensboro, North Carolina where moderate rain was reported at this time. The temperature has decreased by 2° F over the past hour at this

station. This drop in temperature had helped to strengthen the baroclinic zone to the north of the low. Pressure falls are again noted over a large area to the north, east and south of the low (Fig. 3.14) in conjunction with the movement and development of this feature. However, the isallobaric vector is not well-defined. The movement of low III is also not directly towards well-defined regions of pressure falls.

The 290000 surface analysis (Fig. 3.5) indicates that the low was situated at the North/South Carolina border, giving a forward speed of about 30 kt. Subsequent analyses show that low III moved at approximately this speed until its demise. Warm advection was still prevalent at 290000 ahead of the low, and colder air had begun to move southward toward the low from the north (not shown). The baroclinic zone also gradually weakened with time. The pressure analysis at 290000 (Fig. 3.5) suggests that the low filled slightly, but the surface pressure tendencies between 0000 and 0100 indicate large pressure falls northeast of the low (not shown), corresponding to the northeastward movement of the low.

These surface analyses in conjunction with Fig. 3.4 have shown that between 281800-282200, low III was primarily located underneath its associated cloud mass. At 282300, the low became removed from this cloud mass. Furthermore, the satellite signature at 282300 became more typical of a frontal wave, suggesting that baroclinic instability might be important. It appears that the baroclinity of the atmosphere in this region at this time is increased due to the presence of both the upper-level jet streak and the low-level jet. The horizontal and vertical shears associated with these jets together with the convectively unstable atmosphere appear to have created a favorable environment for the low to extract energy from this enhanced baroclinity.

D. VERTICAL CROSS-SECTIONS

To understand better the stability characteristics, structure of frontal zones and wind and temperature profiles associated with the 1984 Carolinas storm, four cross-sections (Fig. 3.15) were constructed prior to and following the genesis of low III. The first and second cross-sections were chosen perpendicular to the positions of the 500 mb jet at 281200 and 290000 respectively. The third cross-section is closely aligned with the upper-level trough, while the fourth goes through low III and the areas of severe convection at 290000.

The first cross-section is constructed at 281200 between Salem, Illinois and Brownsville, Texas to provide insights into the state of the atmosphere prior to genesis. However, analyses from this cross-section do not contribute significantly to the discussion at 290000, and therefore will not be presented. However it is noted that the upper-level jet streak was located over central Texas exhibiting a similar intensity to that observed at 290000. It is therefore concluded that the jet streak did not undergo any significant changes in intensity between 281200 and 290000.

The second cross-section (Fig. 3.16) from Peoria, Illinois (PIA) and West Palm Beach, Florida (PBI) shows an area of very strong vertical shear near the surface between PBI and Athens, Georgia (AHN). There is also the suggestion of a low-level jet at 750 mb between AYS and PBI. A well-defined jet is found near AHN at approximately 250 mb. The surface cold front can be seen north of Waycross, Georgia (AYS). This position is consistent with its analyzed position on Fig. 3.5 at 290000.

Low static stability values shown in Fig. 3.17 south of AHN correspond well with the areas of convection at this time. Note that areas of low static stability near the surface existed north and south of the cold front.

Richardson numbers (Ri) depicted in Fig. 3.18 show regions of low Ri at 800 mb over Athens and to the south near the surface in association with the low-level jet. Other areas of low Ri exist beneath the upper-level jet. These low values of Ri would therefore suggest that the environment was favorable for the genesis of a subsynoptic or meso-alpha scaled disturbance. The regions of lower Ri values near the surface should also favor baroclinic growth. In fact, low III was located approximately 250 km to the northeast of this cross-section between AHN and AYS at this time but was almost directly over Athens 2 hours previous. Absolute vorticity values over a large area south of AYS above 700 mb are small (Fig. 3.19). This area is on the anticyclonic side of the very strong jet over AHN. Inertial instability might therefore have been present.

The third cross-section (Fig. 3.20) was chosen to provide a better definition of the location of the jet streak over the southeast US by comparing it with profile II (Fig. 3.16). This cross-section from Dayton, Ohio (DAY) to Brownsville, Texas (BRO) shows a jet at Jackson, Mississippi (JAN) at around 250 mb. Note that in this profile the jet is weaker than the one found in profile II (Fig. 3.16) and located at a higher elevation. A lower-level jet (near 400 mb) appears over Lake Charles, Louisiana (LCH) at 290000. The strongest surface temperature gradient exists between LCH and BRO.

Low static stability values near the surface south of BNA (not shown) are indicative of the push of cold air southward behind the cold front. Near the surface south of JAN, values of Ri are relatively small (not shown). Areas of low Ri values are found at 400 mb near JAN. This is a result of vertical shear underneath and to the north of the jet. Absolute vorticity values south of LCH in Fig. 3.21 show that the jet at this location is more inertially stable

than that over AYS (Fig. 3.19). Therefore, the jet closer to the area where low III formed is more inertially unstable, providing further evidence that the jet streak was located in profile II.

The fourth cross-section (Fig. 3.22) extends from Appalachicola, Florida (AQQ) to Chatham, Massachusetts (CHH). In this profile, a jet is well-defined over Cape Hatteras (HAT) at about 200 mb, as well as a lower-level jet around 500 mb. A strong warm front can be seen between HAT and Wallops, Virginia (WAL). Low III existed between Cape Hatteras and Charleston, South Carolina (CHS), as can be seen from the isotach pattern.

Along this profile, regions of low static stability (Fig. 3.23) are evident near the surface. Severe convection was occurring around HAT at this time. Low Ri (not shown) prevailed over WAL. Absolute vorticity values were very small between HAT and CHS, particularly at 250 mb (Fig. 3.24), which corresponds with that area closest to the location of low III.

In summary, the atmosphere at 290000 was characterized by strong jets and associated baroclinic zones, areas of low Ri and two regions where inertial instability may have existed. In addition, the horizontal extent of the cyclone was approximately equivalent to that of a wave disturbance of zonal wavenumber 15 and was mostly confined to the low levels. Gall (1976a) has shown that for favorable linear growth of sub-synoptic scale baroclinic wave disturbances, the zonal Ri should be smaller near the surface than aloft. Mullen (1979) also found from 22 cases of polar lows that the mean center of the surface cyclone during genesis was characterized by Ri on the order of 1. Therefore, shortwave baroclinic instability may have played an important role in the genesis of this cyclone. The presence of the strong jet streak greatly increased the horizontal and vertical wind

shears near the location of the cyclone. As a result, barotropic instability may also have contributed to the genesis of low III. These ideas will be further tested in Chapter 5.

E. NUMERICAL MODEL PERFORMANCE

Previous studies have shown that numerical forecasts usually are not very successful in cases of rapid cyclone development (Sanders and Gyakum, 1980; and others). It is therefore of interest to evaluate the performance of the operational numerical models for this particular cyclone event.

The 36-h surface pressure forecasts from the NOGAPS (Rosmond, 1981), NORAPS (Hodur, 1982) and the NMC LFM were compared with those from the NMC surface analyses (Fig. 3.3). All of the models predicted a general decrease in surface pressure of the main low pressure system, but failed to deepen the low to the extent observed. The forecasts of the speed of movement were also slow (not shown). In addition, not all of these models predicted the genesis of low III. Only NORAPS and MASS (Kocin et al., 1984) correctly predicted such an event. Kocin et al. (1984) suggested that incorrect specification of the vertical latent heat distribution and wind fields may have been responsible for some of the forecast errors in these models. NOGAPS forecasts slightly overdeveloped low III when it had reached the mature stage over water, but was too weak when the incipient low was still over land (not shown). These results are consistent with those obtained by Toll and Clune (1985) who found that NOGAPS forecasts of the surface pressure of maritime low centers are too weak during the early stages of development, but are too strong during the mature and dissipating stages.

A more thorough examination of NOGAPS was conducted using a vortex tracking program developed by Williamson (1981) and modified by Brody et al. (1984) and Harr and

Tsui (1985). The cyclone positions forecast by NOGAPS are primarily to the left and behind the analyzed positions (Fig. 3.25). The slower-than-observed movement of the model cyclone is better depicted in Fig. 3.26. These results imply that NOGAPS was slow in predicting the forward movement of the storm.

These observations imply that the regional numerical models appear to be better capable of predicting the behavior of a cyclone prior to and during genesis than the global models. This might be anticipated in view of the fact that the incipient cyclone in this case was on the meso-alpha scale. In fact, NORAPS (Hodur, personal communication) produced more accurate forecasts of both the position and intensity of low III when the model was initialized with a high resolution analysis and its 12-h forecasts from the previous 12 h. (The NORAPS forecasts evaluated in this study were initialized by NOGAPS.) The more accurate NORAPS forecasts will be used in Chapter 5 as part of a linear stability study of this cyclone.

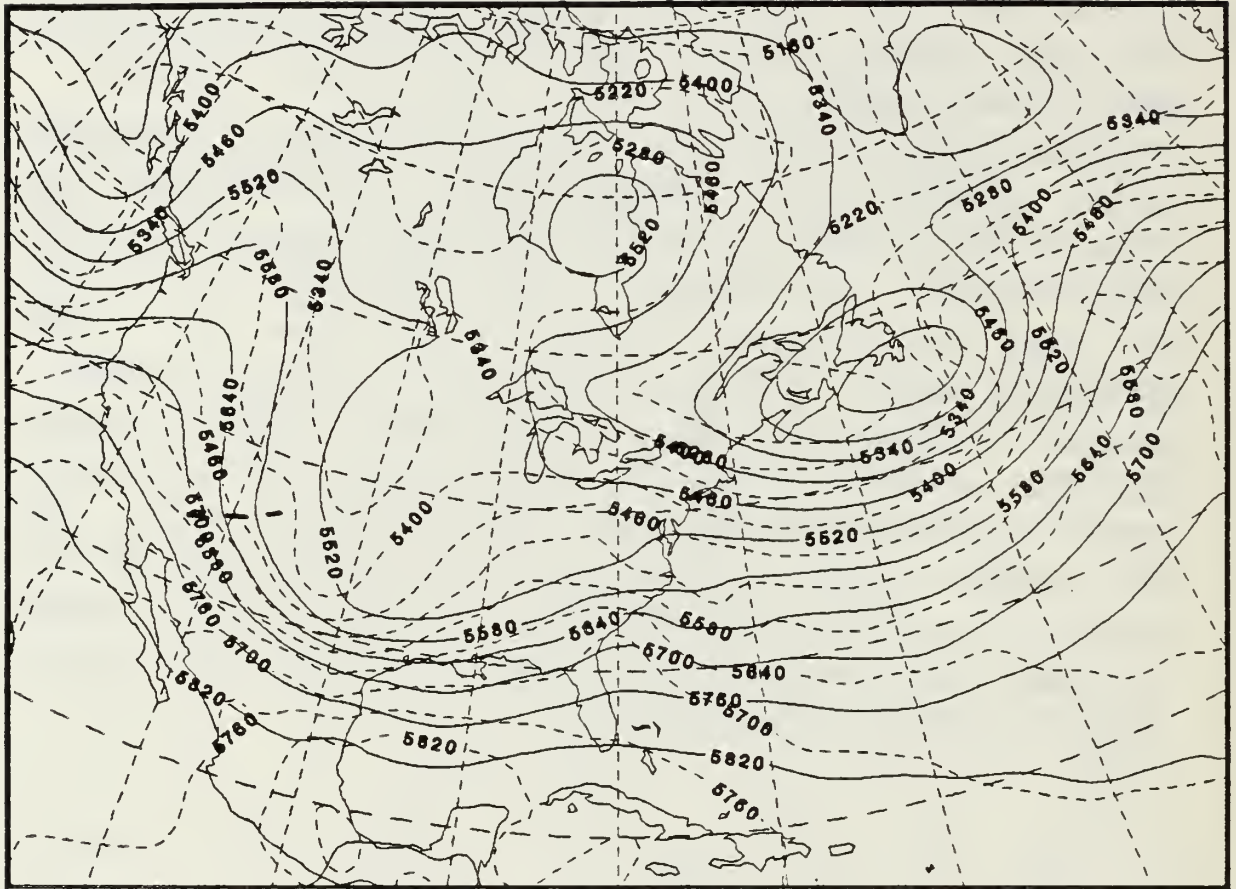


Fig. 3.1 281200 NORAPS 500 mb analysis of heights (solid, m) and 1000 - 500 mb thickness (dashed, m).

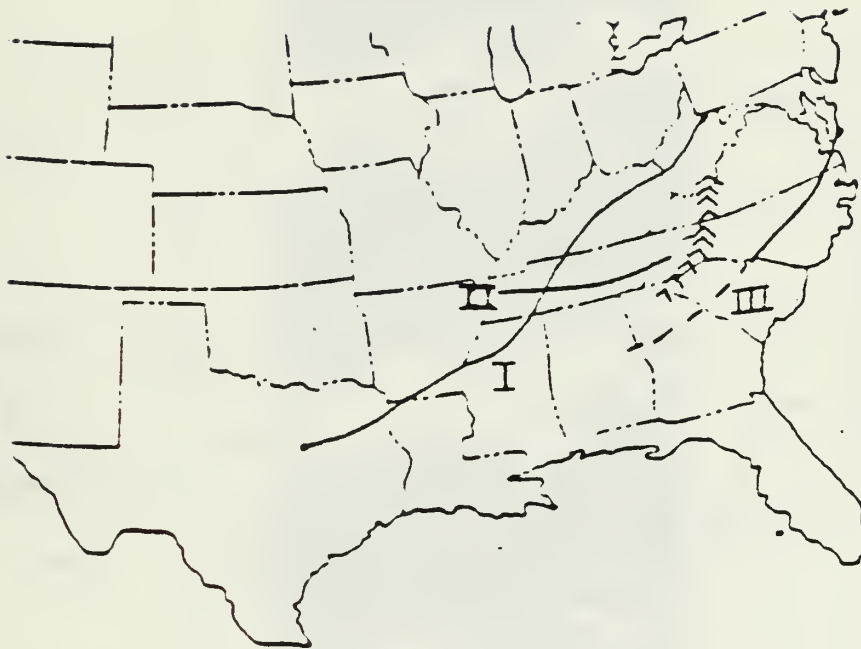


Fig. 3.2 Tracks of three different low pressure centers (I, II and III) as identified by NMC surface pressure analyses from 280000 through 291200.

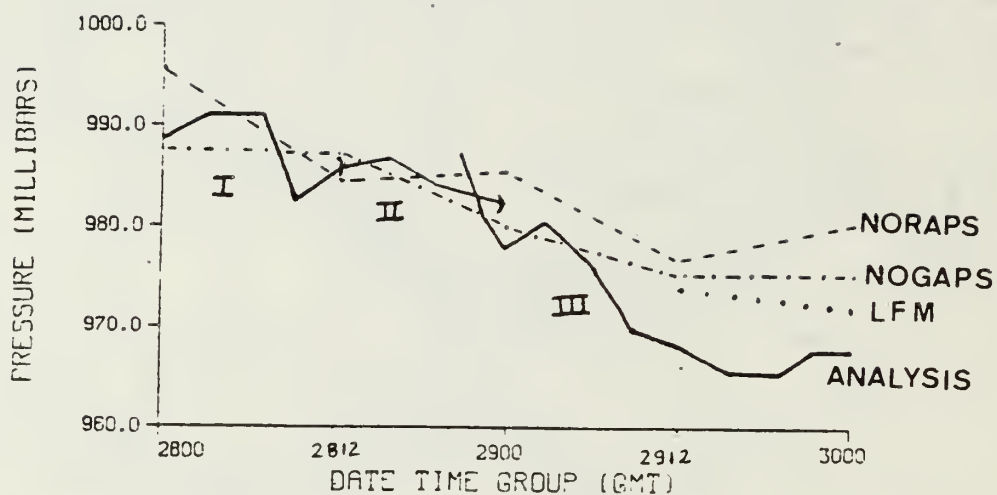


Fig. 3.3 Time variations of the central pressures of the three low pressure centers in Fig. 3.2, and the predicted central pressures of the main low system from NORAPS, NOGAPS and the LFM 36-h surface pressure forecasts.

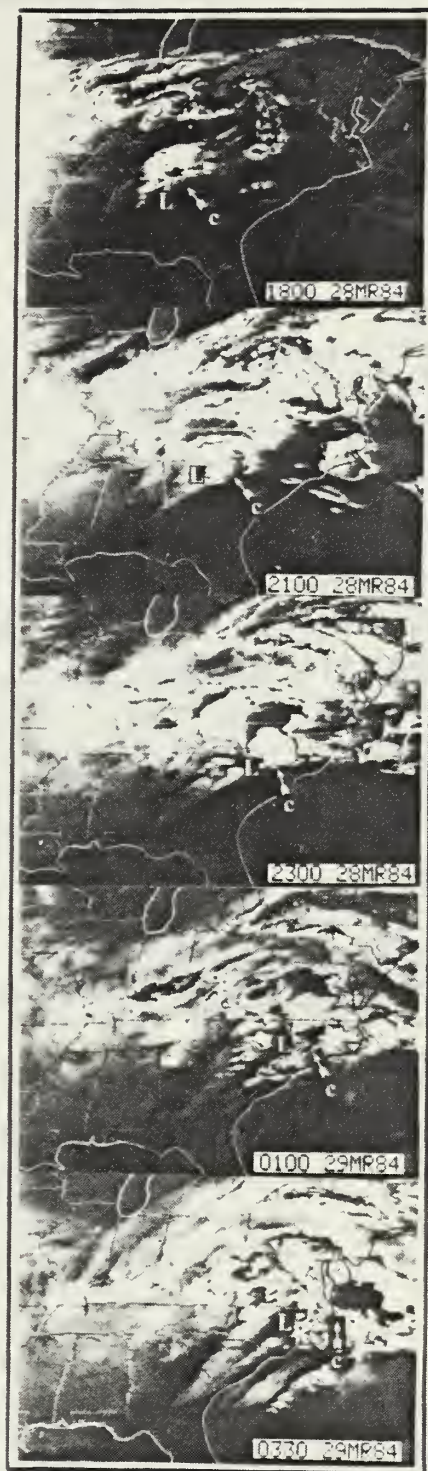


Fig. 3.4 Selected SMS-GOES infrared satellite imagery between 281800 and 290330. The surface low positions are indicated by L and c refers to the expanding region of lower cloud top temperatures. (Reproduced from Kocin et al., 1984).

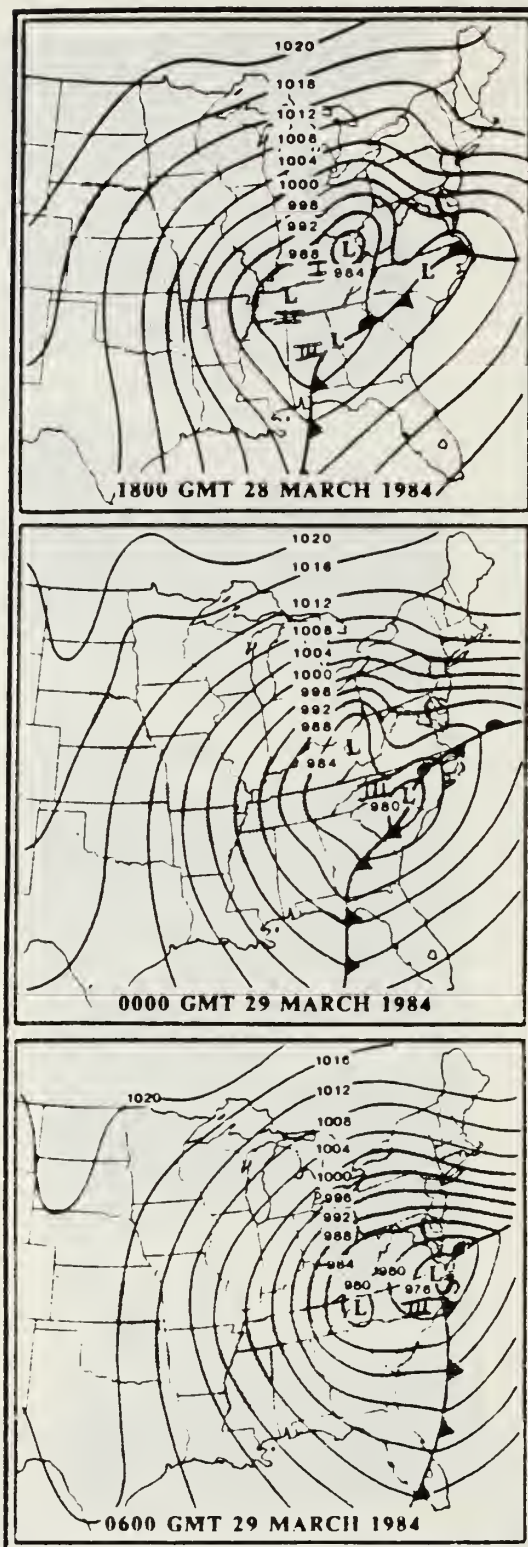


Fig. 3.5 Sea-level pressure (mb) and surface frontal analyses at 281800, 290000 and 290600. Three low pressure centers indicated on Fig. 3.2 are also labelled. (Reproduced from Kocin et al., 1984).

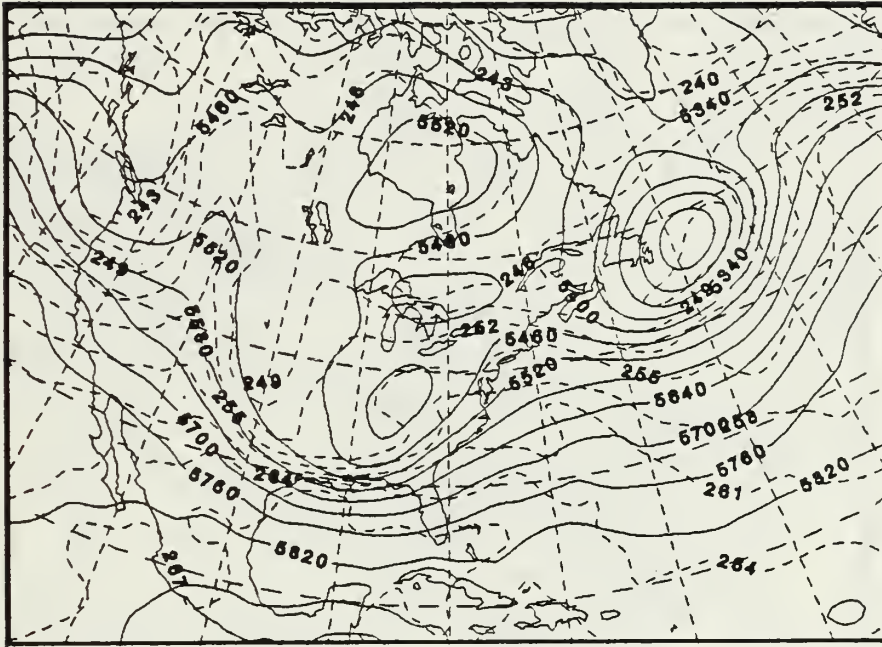


Fig. 3.6 290000 NORAPS 500 mb analysis of heights (solid, m) and 1000 - 500 mb thickness (dashed, m).

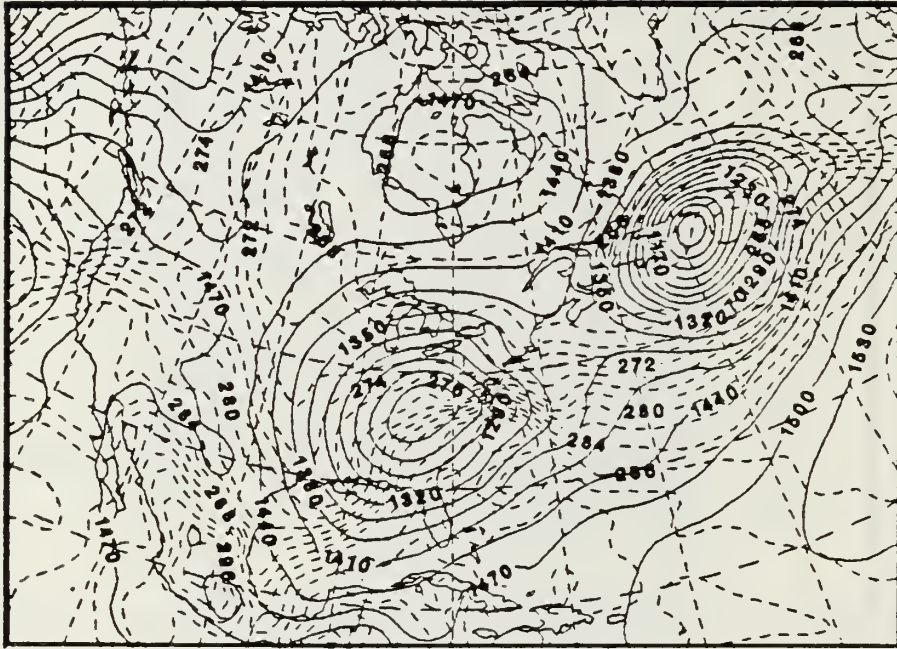


Fig. 3.7 NORAPS 290000 850 mb height analysis (solid) in gpm and temperature analysis (dashed) in °K.

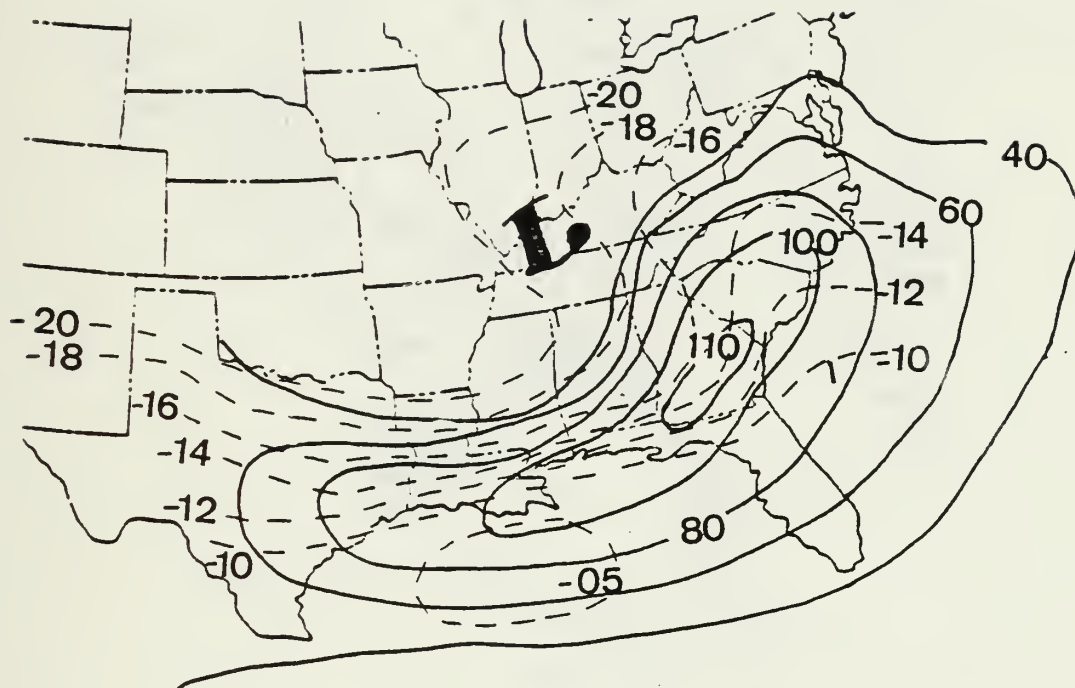


Fig. 3.8 Isotach (solid, kt) and temperature (dashed, °C) analyses at 500 mb at 290000. The letter L refers to the center of the 500 mb low center.

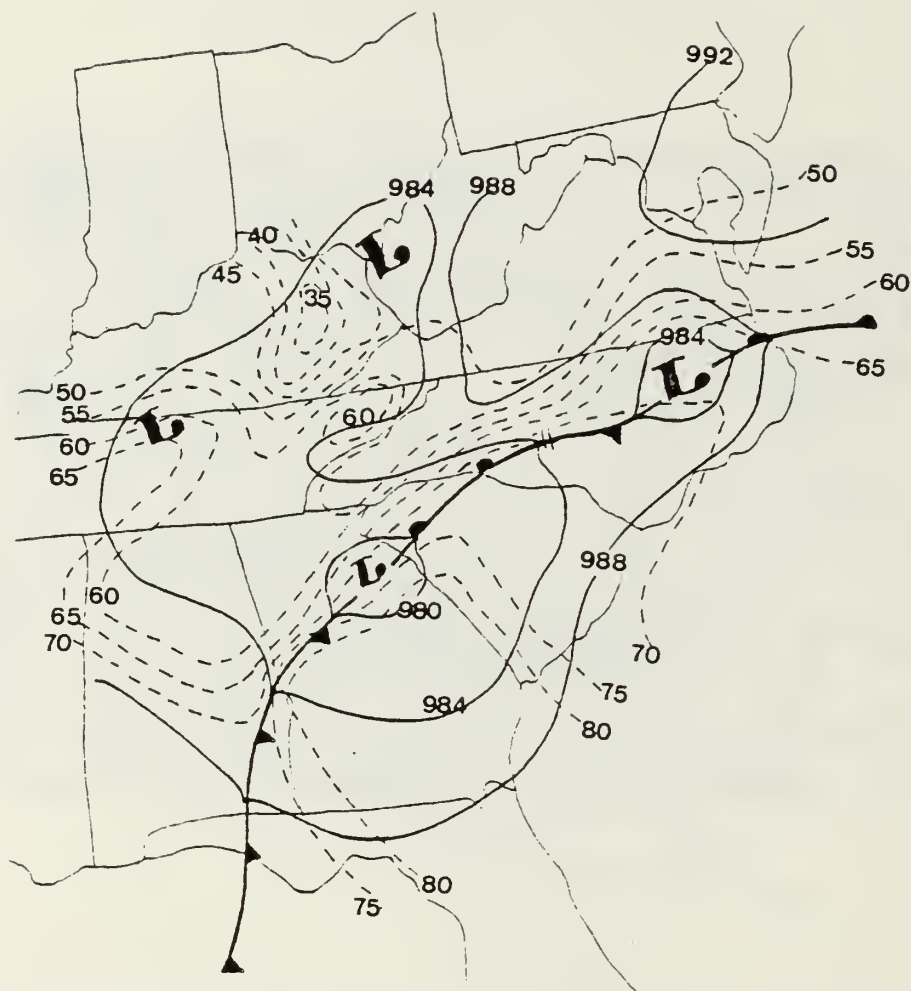


Fig. 3.9 Surface analysis for the southeastern United States at 282100. Solid lines are isobars (mb) and dashed lines are isotherms ($^{\circ}$ F).

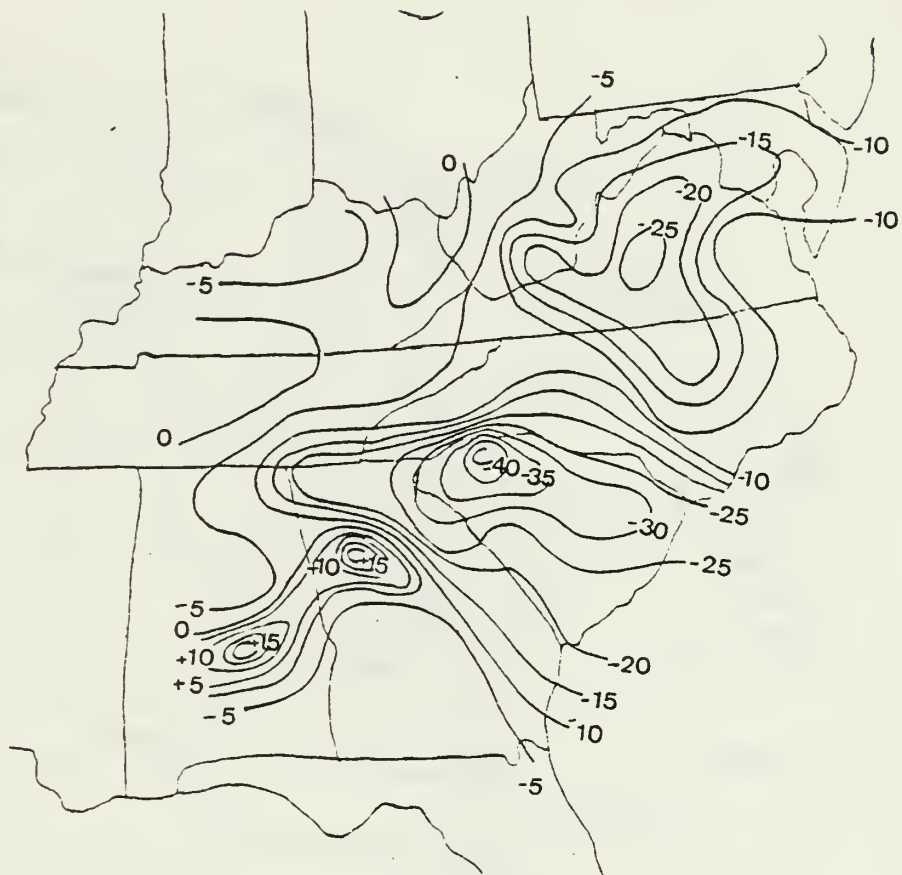


Fig. 3.10 Surface pressure tendencies from 282000 to 282100 in 0.1 mb/h.

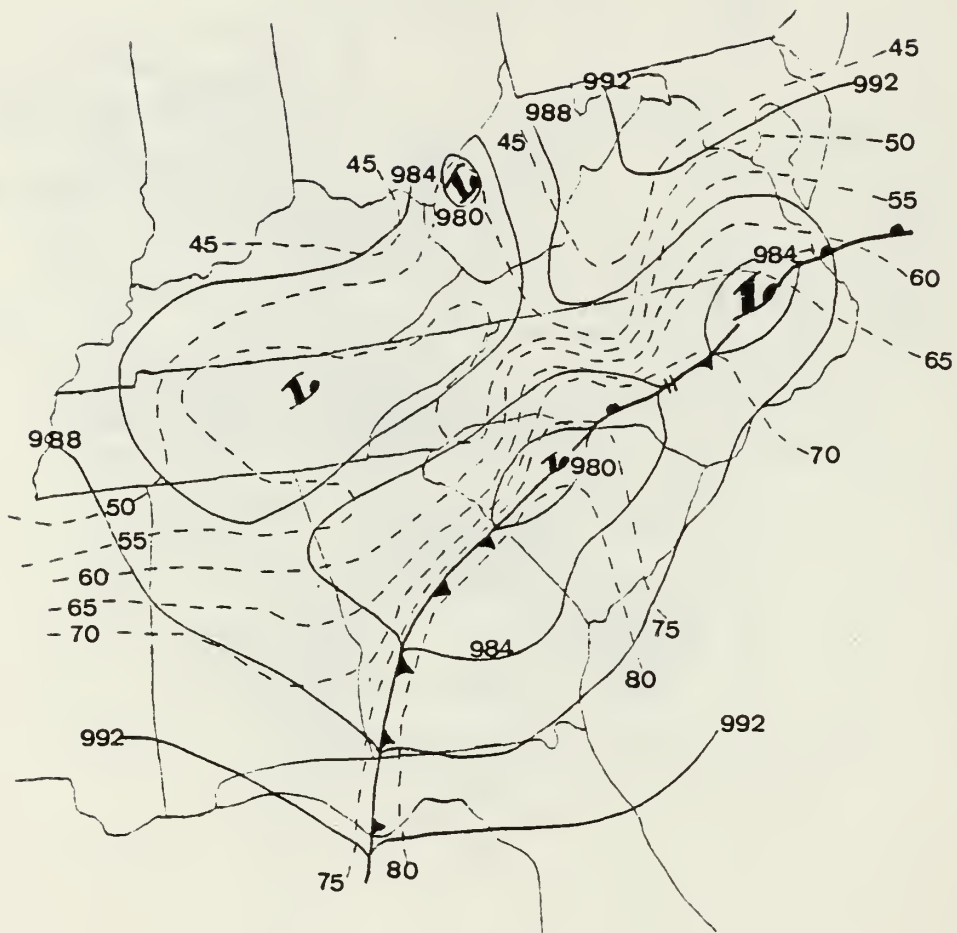


Fig. 3.11 As in Fig. 3.9 except for 282200.

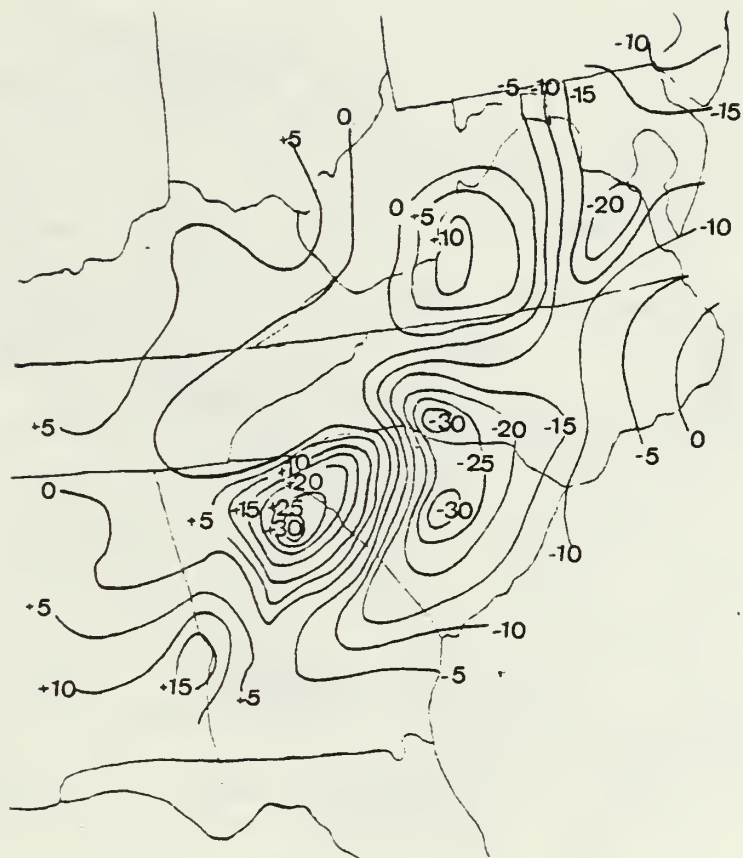


Fig. 3.12 As in Fig. 3.10 except for 282100 to 282200.

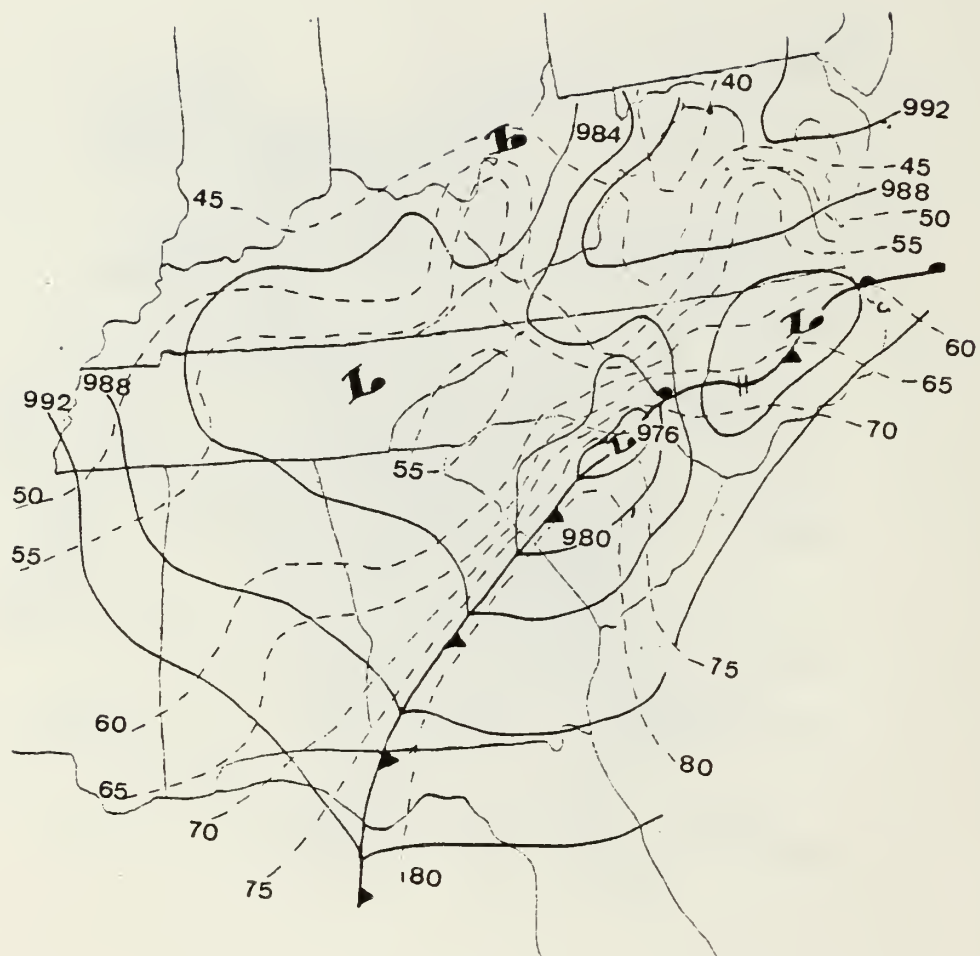


Fig. 3.13 As in Fig. 3.9 except for 282300.

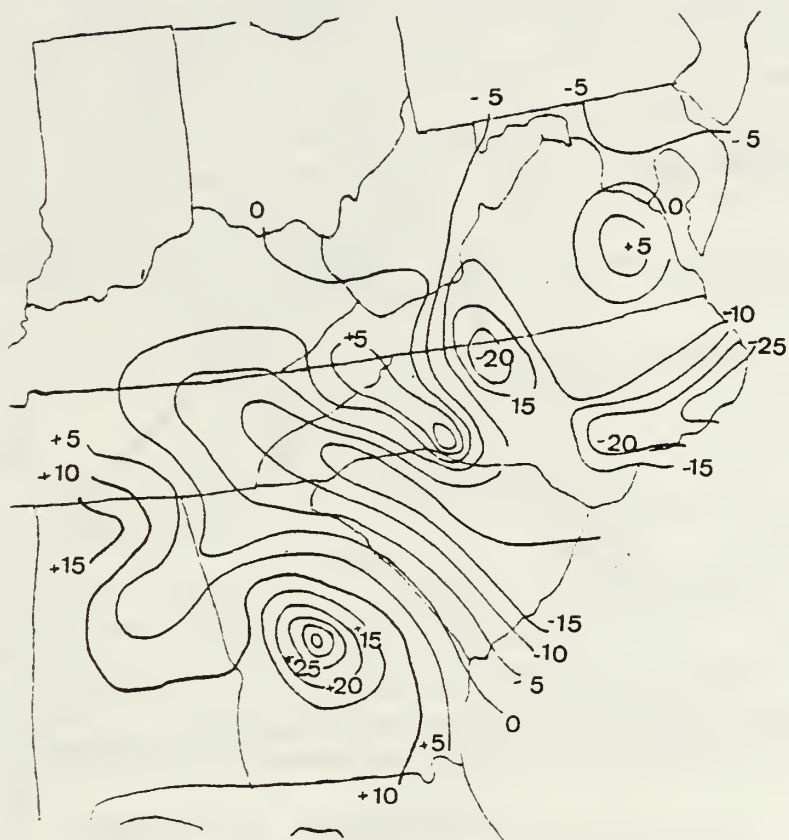


Fig. 3.14 As in Fig. 3.10 except for 282200 to 282300.

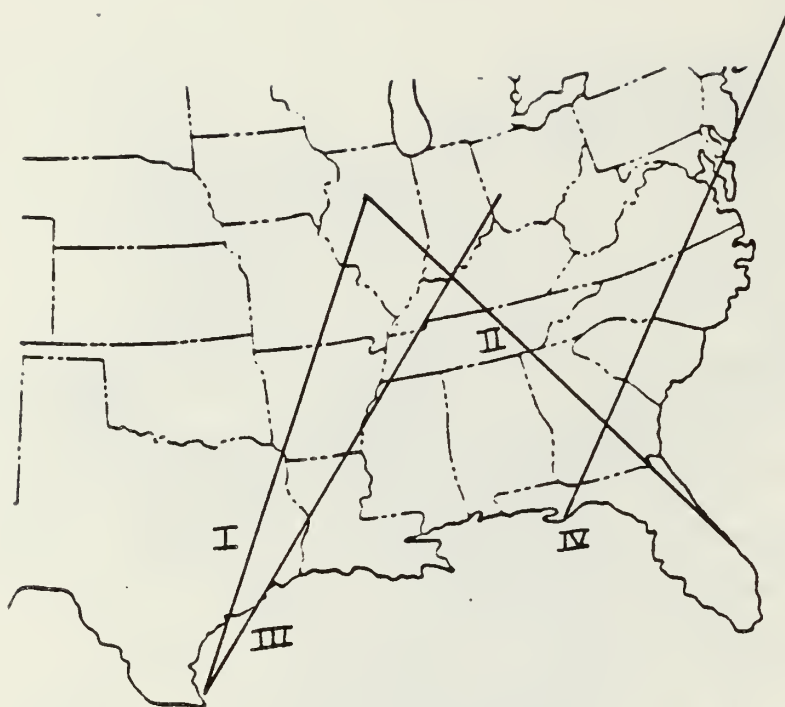


Fig. 3.15 Horizontal orientations and extent of the four cross-sections used in this study. Cross-section I includes rawinsonde data from Brownsville (Texas), Victoria (Texas), Longview (Texas), Little Rock (Arkansas) and Salem (Illinois) for 281200. Cross-section II includes rawinsonde data from West Palm Beach (Florida), Waycross (Georgia), Athens (Georgia), Nashville (Tennessee), Salem (Illinois) and Peoria (Illinois) for 290000. Cross-section III includes rawinsonde data from Brownsville (Texas), Lake Charles (Louisiana), Jackson (Mississippi), Nashville (Tennessee) and Dayton (Ohio) for 290000. Cross-section IV includes rawinsonde data from Appalachicola (Florida), Waycross (Georgia), Charleston (South Carolina), Cape Hatteras (North Carolina), Wallops Island (Virginia) and Chatham (Massachusetts) for 290000.

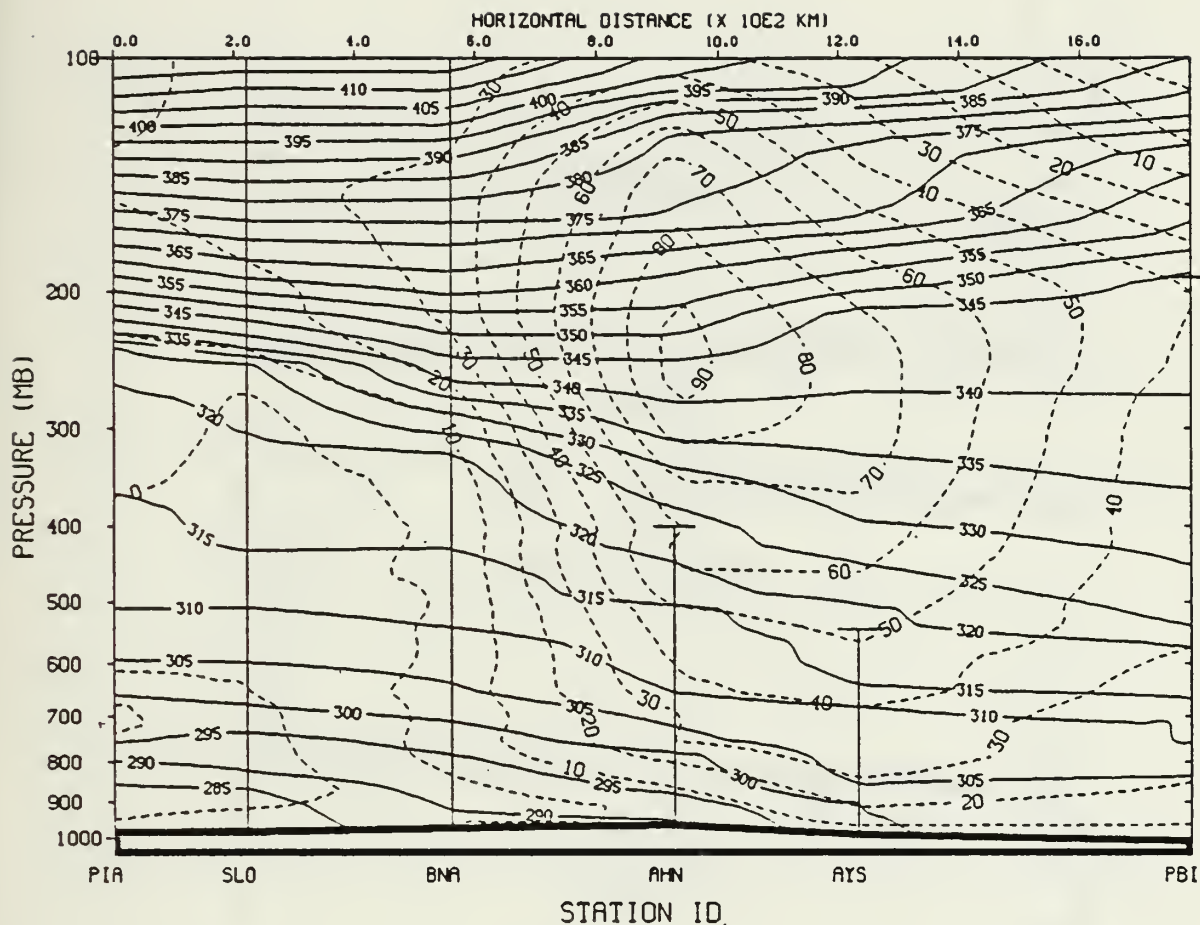


Fig. 3.16 Vertical cross-section through Peoria, Illinois (PIA), Salem, Illinois (SLO), Nashville, Tennessee (BNA), Athens, Georgia (AHN), Wavcross, Georgia (AYS) and West Palm Beach, Florida (PBI) at 290000. Isotachs (dashed, m/s) are the wind components normal to the cross-section. Solid lines are isentropes ($^{\circ}$ K).

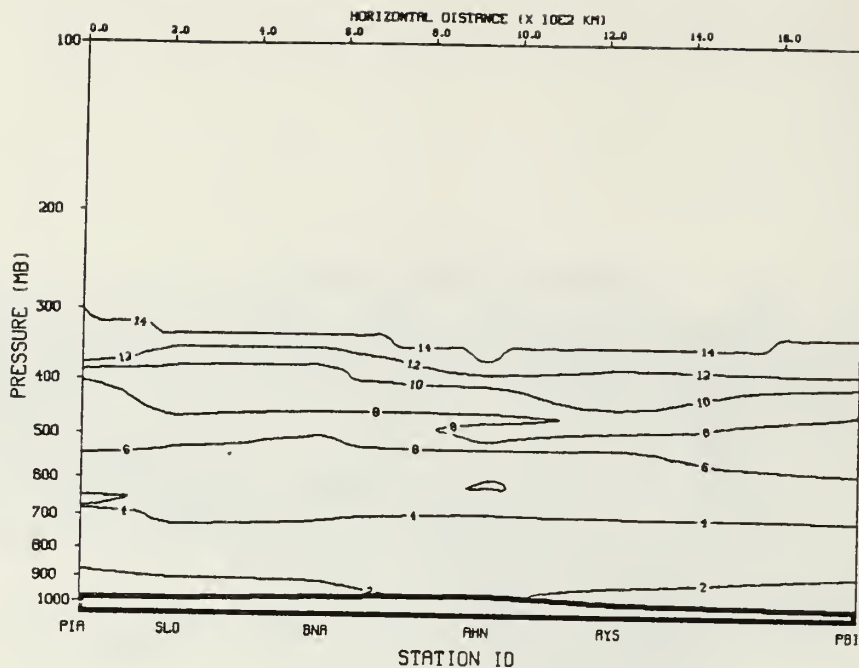


Fig. 3.17 Static Stability ($10^{-5} \text{ m}^3 \text{ kg}^{-1} \text{ Pa}^{-1}$) for the cross-section in Fig. 3.16.

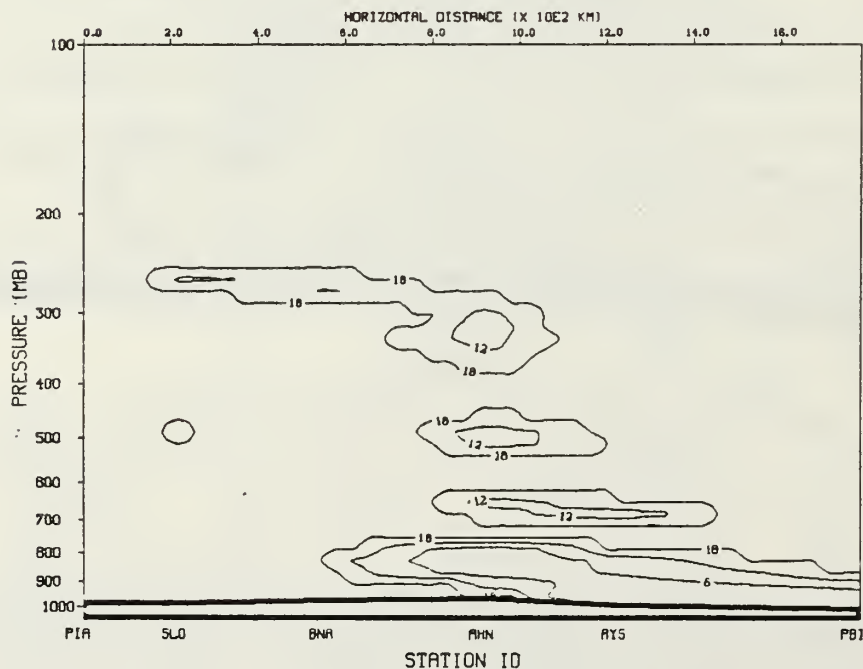
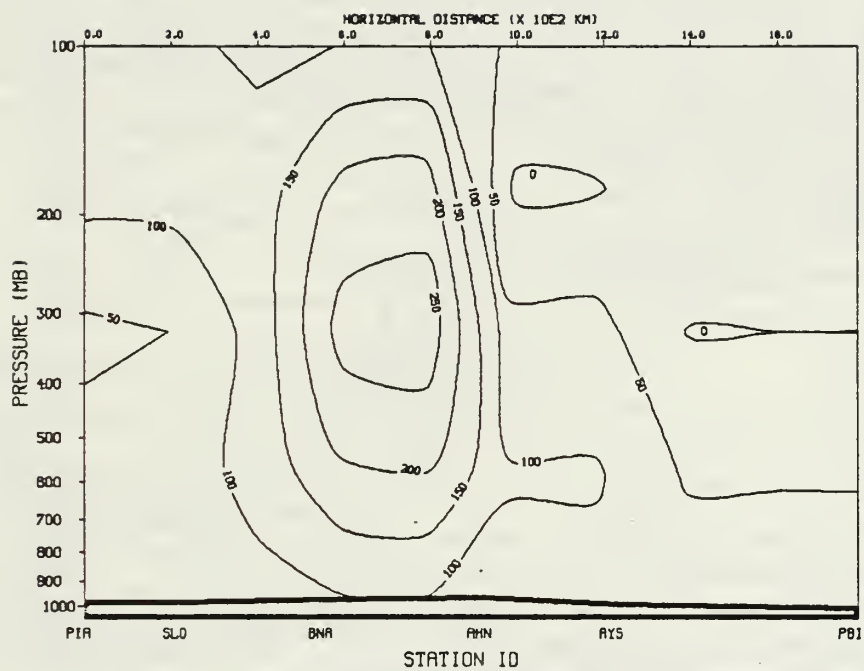


Fig. 3.18 Richardson numbers for the cross-section in Fig. 3.16. Only values less than or equal to 18 are plotted.



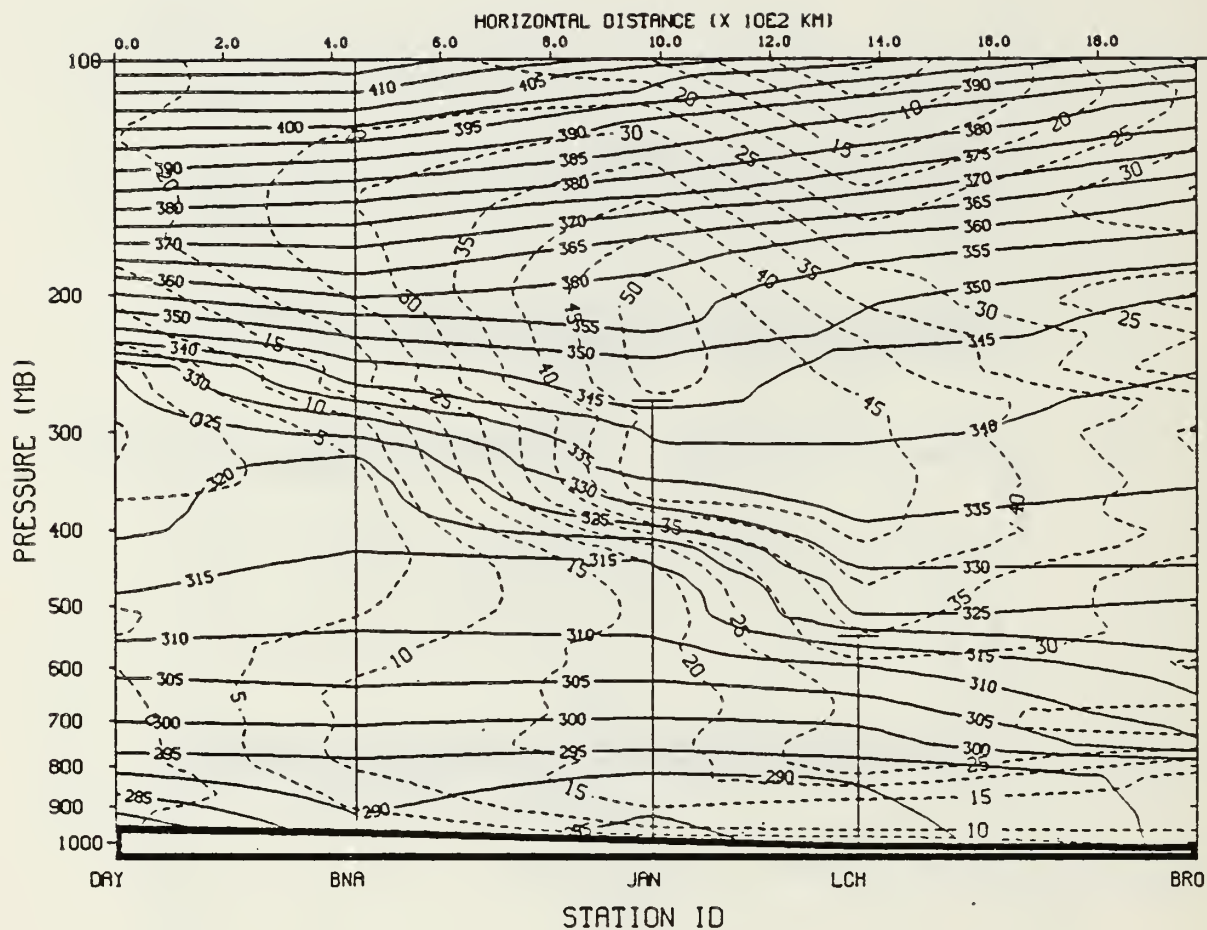


Fig. 3.20 As in Fig. 3.16 except for stations that include Dayton, Ohio (DAY), Nashville, Tennessee (BNA), Jackson, Mississippi (JAN), Lake Charles, Louisiana (LCH) and Brownsville, Texas (BRO).

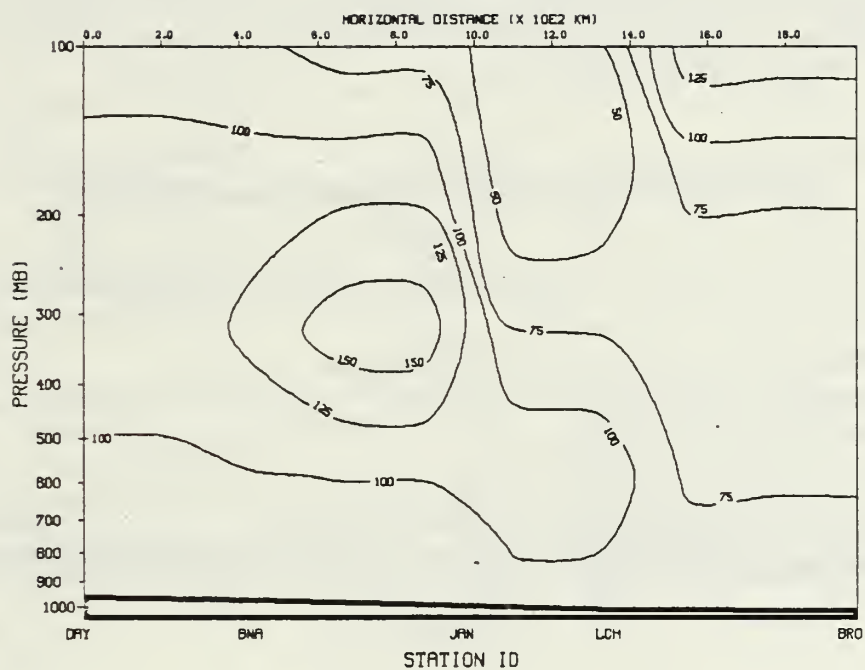


Fig. 3.21 Absolute vorticity (10^{-6} s^{-1}) for the cross-section in Fig. 3.20.

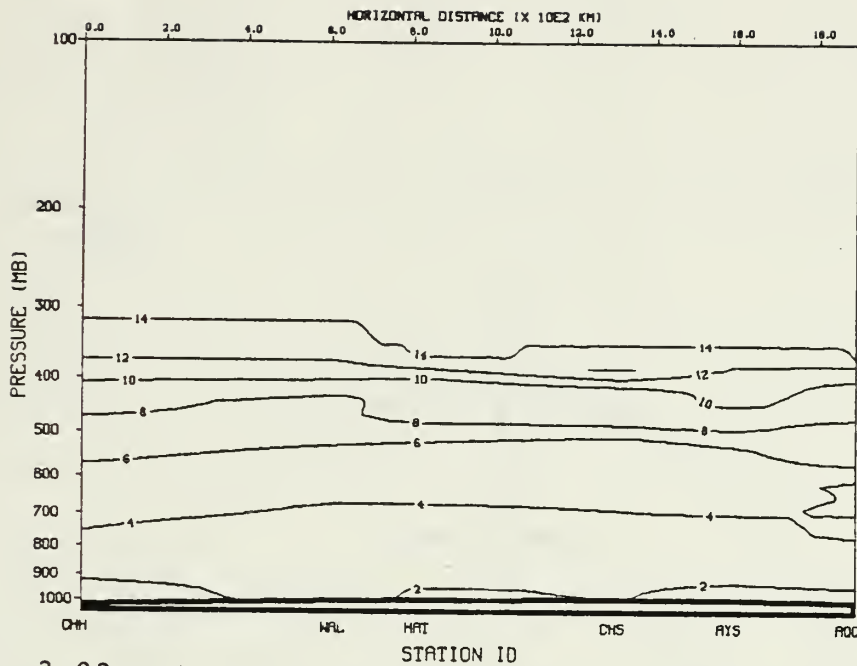


Fig. 3.23 Static Stability ($10^{-5} \text{ m}^3 \text{ kg}^{-1} \text{ Pa}^{-1}$) for the cross-section in Fig. 3.22.

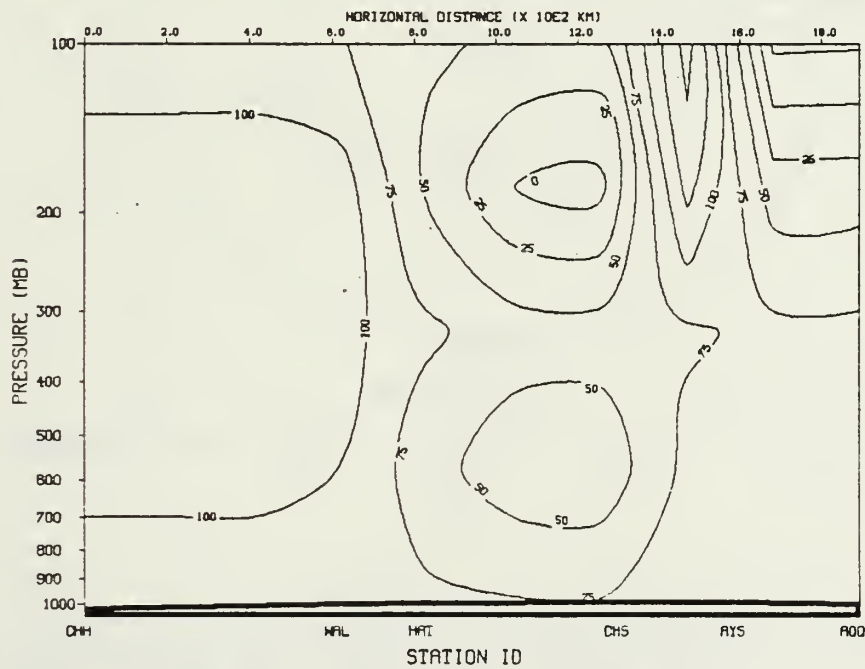


Fig. 3.24 Absolute vorticity (10^{-6} s^{-1}) for the cross-section in Fig. 3.22.

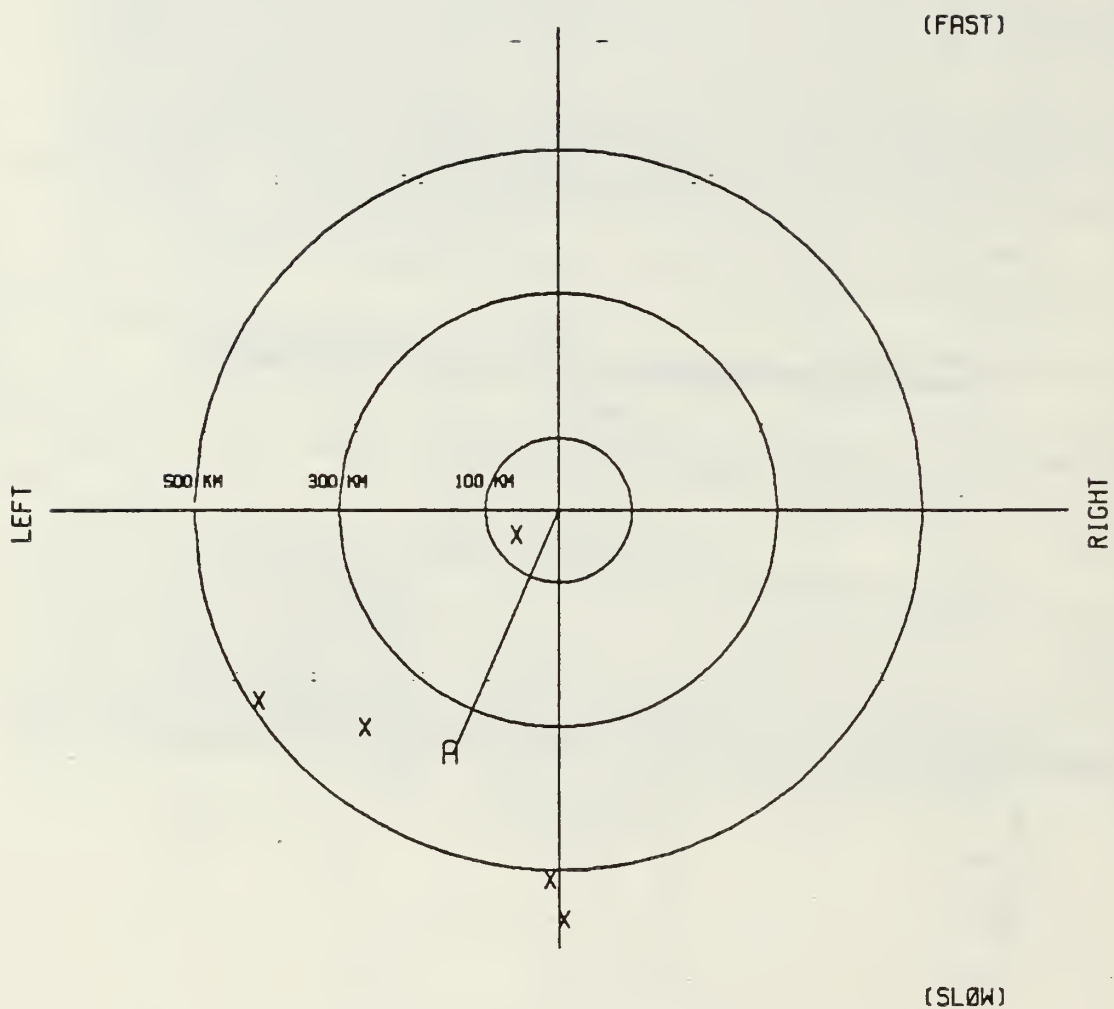


Fig. 3.25 NOGAPS forecast positions of the main low pressure system with respect to analyzed position at 290000, where the analyzed position is the center of the circle.

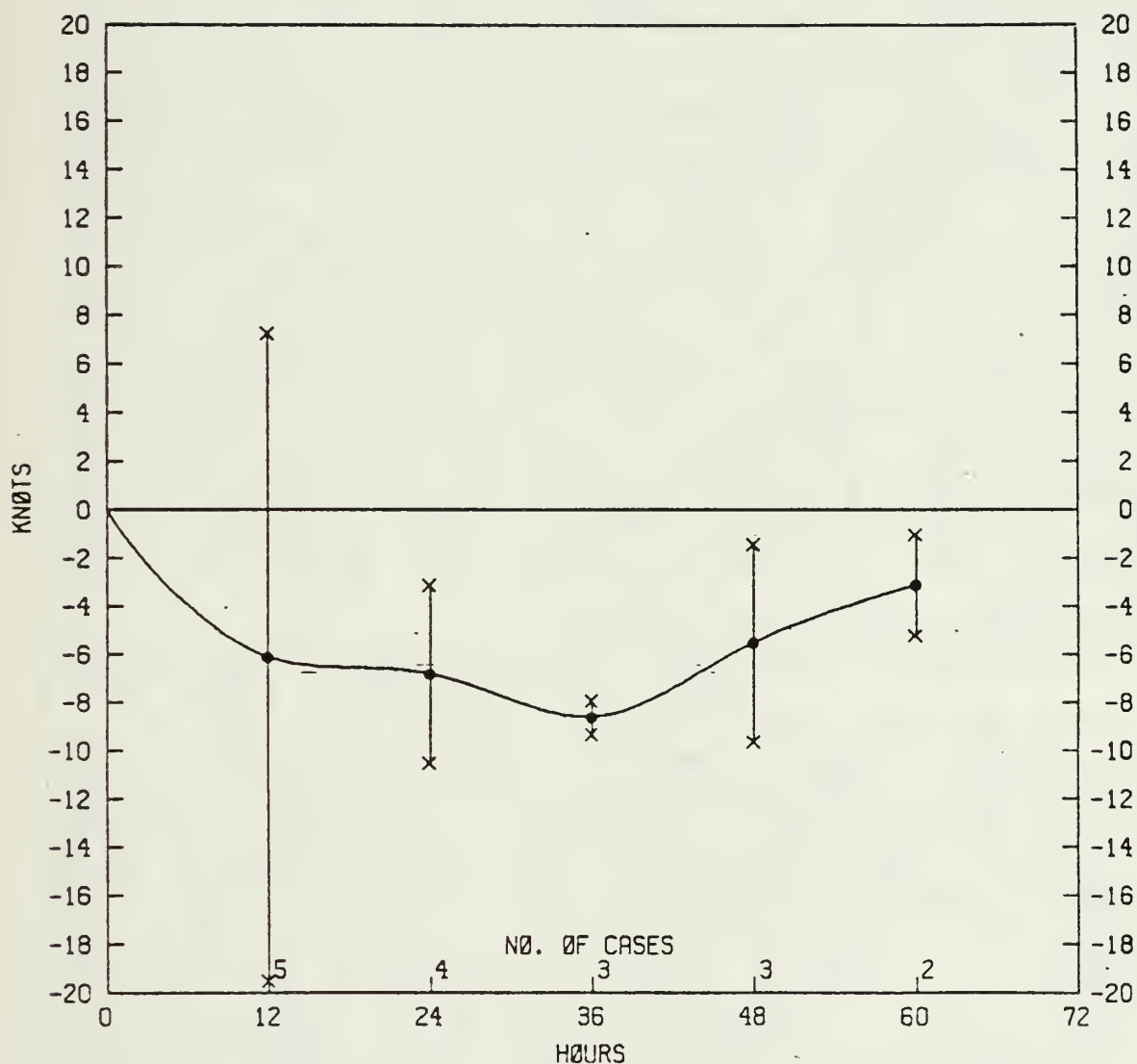


Fig. 3.26 Errors in forecasting the speed (kt) of the cyclone by NOGAPS at 12 to 60 h forecast intervals computed by the Vortex Tracking Program. Negative values indicate that the forecast cyclone is too slow. The crosses above and below the trend line (solid curve) indicate the standard deviation. All the forecasts were initialized at 280000.

IV. HYPOTHESIS

In this case of rapid cyclone development over the Carolinas, a strongly baroclinic environment was observed prior to genesis. Furthermore, an area of low static stability was present downstream of the polar front jet. The existence of the jet streak increased the horizontal and vertical shears. Therefore, both baroclinic and barotropic instabilities may have been important in the genesis of this cyclone. As the cyclone went through its life cycle, convective processes appeared to have played an increasingly important role in the development and maintenance process of the cyclone. Although the Carolinas storm was over land, it exhibited many characteristics of a rapidly deepening maritime cyclone. Therefore, it is reasonable that these mechanisms may also play similar roles for cyclones over water. Based on the analyses in Chapter 3, the following sequence of events is proposed to explain the genesis and rapid development of maritime cyclones.

An intense upper-level jet in thermal balance with a strong low-level baroclinic environment first moves into a convectively unstable region. Palmen and Newton (1969) showed that a strong divergence field is likely to be found at the left exit region of the jet. The movement of the jet also represents a rapid increase of kinetic energy in the region. As the jet streak moves to a position east of a synoptic scale trough, the strong divergence associated with the left front quadrant of the jet is augmented by the ambient divergence of the trough. The enhanced divergence pattern in this quadrant induces a surface cyclone. Concurrently, the import of kinetic energy invigorates the atmosphere in such a way as to initiate and maintain the convection, particularly if the atmosphere is convectively unstable. In other words, the atmosphere attempts to reduce the strong vertical wind shear associated with the jet via

convection. Strong vertical wind shear and low static stability reduce the Richardson number so that shortwave baroclinic instability can become an important contributor to the development process. The characteristic spatial scales of this mechanism suggest that the surface cyclone will form on the meso-alpha, rather than the synoptic, scale. On the meso-alpha scale, a strongly baroclinic environment is able to organize the convective processes more effectively. Furthermore, the baroclinic energy conversions can be better realized. As a result, convection is efficiently organized around the incipient cyclone. The strong shears associated with the jet streak can also create a barotropically unstable atmosphere in both the vertical and horizontal. Therefore, the growing perturbation can extract eddy available potential energy through baroclinic processes and zonal kinetic energy through barotropic mechanisms. The large amount of latent heat release near the incipient cyclone provides strong diabatic heating, which can partially offset the self-limiting process during the development phase (Palmen and Newton, 1969).

As the perturbation reaches its mature stage, the cyclone becomes more vertically aligned, which suggests that baroclinic instability has become a less dominant factor. Rapid development slows when convection decreases in intensity, or when the main areas of convection move far enough away from the cyclone as to weaken the effect of diabatic heating. The maturing cyclone is typically in the cold air with a mid-level trough situated above. Thus, according to the Petterssen development equation (Petterssen, 1956), the cyclone would quickly cease its development and begin to weaken. During convection, both the vertical and horizontal shears are weakened, thus reducing the possibility of barotropic instability.

In conclusion, genesis and rapid development is initiated by strong baroclinic instability. This instability favors the existence of a strong jet streak. However, a very intense jet streak can also produce barotropic instability through a transfer of momentum from the mean flow to the eddy in both the horizontal and vertical. Baroclinic and barotropic instabilities may therefore combine in such a way as to accelerate the growth process by providing the incipient cyclone with two energy sources. This hybrid perturbation can also be further assisted by moist processes.

In the particular case of the Carolinas storm, NORAPS analyses at 290000 show the incipient cyclone to be below 850 mb (Figs. 3.6 and 3.7). At 500 mb, a jet streak (110 kt) had moved around the base of the trough at this time, and was approximately 350 km southwest of the surface cyclone position. The 850 mb and 700 mb temperature and moisture analyses (not shown) as well as static stability calculations (Fig.3.17) reveal that the atmosphere over most of the area around the surface cyclone was convectively unstable. A low-level jet and strong warm air advection at 850 mb were found to extend to the east of the surface cyclone. The distinctive lag between the 500 mb isotherm and height pattern of approximately 45 degrees at 281200 had decreased to about 20-30 degrees by 290000. Furthermore, the 500 mb trough had significantly deepened over this same time interval. The cross-section analyses indicate that strong vertical shears below 850 mb existed near the area of genesis and rapid development, where low values of the Richardson number prevailed (Fig.3.18). Low values of absolute vorticity (Fig.3.19) were observed at mid and upper levels on the anticyclonic side of the jet.

Therefore, all of these conditions are consistent with the above proposal so that baroclinic and barotropic

instabilities appear to be responsible for the genesis of the Carolinas storm at 290000. The main purpose of this thesis is to examine such a hypothesis and to determine the role and relative importance of shortwave baroclinic and barotropic instabilities in the genesis and rapid development of this cyclone. Gall (1976a) has shown how these two instabilities can be diagnosed with a linear stability model. A version of this model will therefore be used to determine whether these mechanisms can help explain the behavior of this cyclone.

V. LINEAR STABILITY ANALYSIS

A. INTRODUCTION

The analyses in Chapter 3 led to the hypothesis in Chapter 4 that the processes of baroclinic and barotropic instabilities might explain the rapid growth and development of the Carolinas storm. Specifically, development was accelerated by two energy conversion processes operating in tandem from two different sources. These ideas will be tested using a linear stability model. Different versions of the model have been described and used by Gall (1976a,b,c), Blakeslee and Gall 1978) and Gall et al. (1979).

Linear theory considers the perturbations to be infinitesimally small, while observed eddies in the atmosphere are typically of large amplitude. Thus, it is assumed that disturbances, as they grow from small to observable size, do not appreciably change their structure. Hence, linear stability theory can be extended to those perturbations of finite amplitude. In fact, Gall (1976a) suggested that a linear model can produce perturbations with structures similar to those observed in the atmosphere. The linear stability analysis should provide a reasonable estimate of the growth rates, phase speeds, structure and energetics of a perturbation introduced to an unstable mean state that is representative of the atmosphere during the genesis of the Carolinas storm. As discussed by Gall (1976a), this technique also includes the effect of ageostrophic motions. Therefore, linear theory should be applicable to the Carolinas storm during the genesis and early stages of development. However, this linear analysis cannot provide an estimate of the location of the perturbation that would grow from the unstable initial state. Such an estimate can

be derived from vorticity advection arguments. On the other hand, the behavior and characteristics of the perturbation can be identified from the model. Therefore, a combination of these two approaches might provide better estimates of both the position and intensity of the incipient cyclone.

For the results from the linear analysis to be essentially valid, it is important to exclude any significant energy source that might be available from a nonlinear mechanism. For example, the initial conditions must be constructed along a cross-section that minimizes the nonlinear effects of moisture and convective processes. It is also possible that nonlinearities or unstable modes other than the desired Rossby modes would dominate the growth spectrum, and thus be of little use for the purposes of this study. Therefore, extra precautions become necessary to ensure that only the unstable baroclinic and barotropic modes emerge after the requisite number of integrations have been completed.

In the next section, the linear stability model to be used will be described. In section C, the cross-sections of zonal wind and temperature to be studied are presented. The results of the linear analysis, including the growth rates, energetics and structure of the perturbations, are shown in section D and compared with the observed fields.

B. DESCRIPTION OF THE LINEAR STABILITY MODEL

The linear stability model provided by Professor R. L. Gall¹ was first developed by him in 1976 (Gall, 1976a). The model is structured around the linearized primitive equations in pressure coordinates, which retain the effects of spherical geometry. The equations are written in "semi-spectral" form (Saltzman, 1957), in which the perturbations

¹1985 NAVAIRSYSCOM G. J. Haltiner Research Chair Professor in Meteorology, Naval Postgraduate School, Monterey, CA.

to the mean zonal flow are expressed as a Fourier series in zonal wavenumber. The meridional and vertical derivatives are evaluated by an energy-conserving centered difference scheme, while the zonal derivatives are evaluated analytically (consistent with the assumption that the atmosphere is invariant in the zonal direction). The time derivatives are replaced by centered differences with time-smoothing (Bleck, 1974) applied at each time step to reduce high frequency oscillations due to gravity waves, and to suppress the computational mode in time. The velocity components are staggered on the grid to reduce the spatial computational mode.

The model is confined to a channel in the meridional direction. No mass flux through the channel walls is allowed, and the frictional stresses and the turbulent transfer of heat and moisture across the walls are zero. No topography is included on the lower boundary. At the surface, only the vertical turbulent transfer of momentum is included, but none for heat or moisture. Thus, the total energy within the channel slowly diminishes during the course of the experiment.

The two dimensional (y, p) grid is oriented perpendicular to the zonal wind. To initiate the development of wave motion, a temperature perturbation of -0.1 to $+0.1^\circ$ Kelvin is added to the zonal mean temperature. After each timestep, the flow is modified by restoring the zonal flow to its original values and restricting the eddy portion of the flow to one zonal wavenumber. Therefore, the relative growth rates of different waves passing through the grid can be calculated. The growth rate of each wave then gives an estimate of the amount of the instability of the zonal flow.

The method for obtaining the linear solutions is the initial value technique. Specifically, an initial guess for the Fourier coefficients at each grid point of the

north-south cross-section is made, and the equations for these coefficients are numerically integrated in time until the most unstable mode dominates the flow, and the real and imaginary parts of the phase speed are the same at all grid points.

With the linear primitive equations, gravity-wave type solutions must be addressed. The introduction of a wave in the temperature field represents an imbalance to the geostrophic balance imposed on the mean zonal flow. As a result, gravity waves will be generated early in the experiment. These waves will remain in the solutions throughout the integration because of the absence of frictional forces or interactions with the zonal flow. The width of the jet determines the scale of the perturbation. Consequently, in other regions of the grid, the amplitude of the gravity waves may exceed that of the unstable wave. Thus, equality of the phase speeds and growth rates at all grid points cannot be expected. For these reasons, the integration must continue until the amplitude of the Rossby wave sufficiently exceeds that of the gravity waves and all other more slowly growing Rossby modes over most of the grid. Ideally, both growth rate and phase speed should become constant after development of the wave becomes exponential.

It should be noted that if two waves with the same zonal wavenumber have very similar growth rates, the initial value technique will be unable to discriminate between them. In this case, the mode with the most rapid growth rate will always be the larger of the two and will dominate the flow if given enough time. Thus, the model can only isolate the most unstable mode. In other words, other unstable modes cannot be identified by this technique even though they may exist. However, the emergence of this most unstable mode may not occur until the perturbation amplitude reaches unrealistically large values and the numerical assumptions

break down. For instance, the surface pressure perturbations could become large enough to give negative total pressure.

In this study, Gall's (1976a) model was modified such that integrations using various horizontal and vertical spatial resolutions can be made with minimal difficulty. Depending on the initial conditions, the model grid for these experiments consists of 10 or 11 grid points in both the horizontal and the vertical. This resolution was necessary to resolve a channel that extends from 26-40° N (approximately 1800 km). Thus, the horizontal grid length is approximately 180 km, compared with the 200 km used in Gall (1976c). Various horizontal and vertical grid lengths have been tested and no significant differences can be identified. Therefore, results using the above grid resolution for all experiments will be presented. The relatively narrow width of the channel used in this study compared with that of Gall (1976c) justified the f-plane approximation, with the value for the Coriolis force being valid at 33° N. Gall's calculations were based on a beta plane, with the channel extending from approximately 25-60° N. The more southward location of the present model channel for these experiments makes the flow more susceptible to inertial instability than that in Gall's experiments.

C. INITIALIZATION

Four different sets of initial conditions were used in this stability analysis. They include the real data, NORAPS analysis, NORAPS 24-h forecast and a data set generated from analytic functions. The first three sets of initial conditions were chosen so that the cross-section was oriented perpendicular to the jet streak, with the wind maximum located in the center of the profile. The cross-sections for both NORAPS cases closely approximated the location of the cross-section using the real data. It is also important

to emphasize that to be consistent with the design of this stability analysis model, the cross-sections do not include significant changes in terrain or major convective areas. The analytical conditions were chosen for sensitivity tests.

The real data case uses the information from the 50x50 grid of profile II described in Chapter 3 (Fig.3.16). The geostrophic winds were first calculated at each rawinsonde station from the horizontal temperature gradient across the station using the thermal wind equation. The winds were then linearly interpolated between stations. These geostrophic winds were then interpolated horizontally using a cubic spline onto the three staggered grids used by the model, with a maximum of 10 horizontal grid points and 10 vertical levels. The resulting horizontal grid length was approximately 178 km, with the horizontal width of the cross-section equal to approximately 1780 km. The vertical levels were placed at 1000, 909, 787, 715, 590, 511, 402, 301, 205 and 100 mb. These levels were chosen to eliminate interpolation in the vertical and to approximate the standard atmospheric levels. The temperature at each grid point was then calculated from these geostrophic winds. In this way, the winds and temperatures were kept in geostrophic balance.

To help isolate the Rossby mode, static and inertial stabilities were checked and adjusted as necessary such that the model atmosphere was both statically and inertially stable. A one-sided differencing scheme was used to calculate both the static stability and absolute vorticity at each grid point. If the static instability is found at a grid point, the potential temperature at the grid point one level below was changed such that stability prevailed with respect to the potential temperature at the grid point immediately above. When the absolute vorticity at a grid point is negative (that is, inertially unstable), the geostrophic

wind was changed at the grid point immediately to the south such that inertial stability existed with respect to the geostrophic wind at the original grid point. The wind and temperature fields were rebalanced geostrophically. Another stability check was then invoked, but no further instabilities were found.

The NORAPS analysis at 290000 provided another set of initial conditions for profile II in Fig. 3.15. To minimize the amount of interpolation necessary, the primary model grid points in both the horizontal and vertical were chosen to coincide with the NORAPS analyses. In this way, only one interpolation in the horizontal and one in the vertical was necessary. This results in a horizontal grid length of 179 km and 11 vertical levels (1000, 925, 850, 700, 500, 400, 300, 250, 200, 150, and 100 mb). To obtain the initial conditions, geostrophic winds were calculated from the NORAPS-analyzed temperatures. As in the real data case, a check for static and inertial instabilities was invoked for this cross-section. However, only changes to establish inertial stability were necessary as the NORAPS temperature analysis was statically stable. The resultant cross-section is shown in Fig. 5.1.

A third cross-section was produced using a NORAPS 24-h forecast initialized at 280000. This forecast is different from the one evaluated in Chapter 3. For the forecast used here, the first-guess fields consist of the 12-h NORAPS forecast from the previous 12 h. On the other hand, the operational NORAPS forecasts discussed in Chapter 3 used a 6-h NOGAPS forecast as the first-guess field. The former analysis also included more observations (Hodur, personal communication). The forecasts used in this present analysis provided a better prediction of the intensity of low III, but the location of the low center was to the southwest of the analyzed position. Nevertheless, this predicted

location of the cyclone was in better agreement with the analysis than that from operational forecasts. The grid points in this cross-section are identical to those for the NORAPS analysis case. Geostrophic winds were calculated from this temperature field (Fig. 5.2). Static and inertial stability checks were also invoked.

The temperature and wind fields in Figs. 5.1 and 5.2 are very similar, except that the maximum geostrophic winds for the NORAPS analysis case are 10-15 m/s stronger than those for the forecast. Stronger horizontal shear exists at the jet level for the analysis case, whereas the forecast shows stronger horizontal shears near the 700-850 mb levels. Strong vertical shear can also be seen near AHN (Athens, Georgia) in both cases. Note further that in both cases, the maximum winds are weaker than the observed zonal winds (Fig. 3.16). The positions of the jet in the analysis and the forecast are to the north of that observed. However, it must be pointed out that the winds in Figs. 5.1 and 5.2 were geostrophically computed. In fact, the geostrophic winds derived from the temperature field in Fig. 3.16 have similar magnitudes as those in the NORAPS analysis. The differences between the forecast and the analysis can be studied further by examining the surface charts (Figs 5.3 and 5.4). Note that the cross-section goes through the center of the incipient low in the forecast (Fig. 5.3), but is positioned to the southwest of the analyzed cyclone (Fig. 5.4). Therefore, the signature of the low-level perturbation is better defined in the forecast cross-section, as can be seen from the isotachs to the left (northwest) of AHN, where a cyclonic horizontal shear exists (Fig. 5.2).

The fourth set of initial conditions were analytically computed in a way similar to that in Gall (1976c). These conditions (Fig. 5.5) were used to test the sensitivity of the model for different jet intensities. The zonal mean

pressure field is independent of latitude, with the surface pressure set at 1013 mb. The horizontal grid is identical to that of the NORAPS cases. The ten vertical levels are from 1000 to 100 mb in increments of 100 mb. The winds are computed using the following equations:

$$U(y,p)=1/2(U_c(p)\cos(\pi x/L)) \quad (5.1)$$

$$U_c(p)=((1-p/p_o)/.775)UMAX \quad (p > 225 \text{ mb}) \quad (5.2)$$

$$U_c(p)=UMAX \quad (p < 225 \text{ mb}) \quad (5.3)$$

where UMAX is the maximum value of the zonal mean wind $U(y,p)$, L the width of the channel and p the surface pressure. In this study, three different values of UMAX (40, 60 and 80 m/s) were used. The latter wind maximum was chosen to correspond with that of the other initial conditions. The temperature field is computed from the zonal wind using the thermal wind equation. The boundary condition required to solve (5.3) is given by the zonal mean temperature $T(p)$ at the center of the channel:

$$T(p)=273.2(p/p_o) \quad (p > 225 \text{ mb}) \quad (5.4)$$

$$T(p)=205.8. \quad (p < 225 \text{ mb}) \quad (5.5)$$

The resultant vertical temperature profile at the center of the channel is a linear function of height, with a constant lapse rate to approximately 225 mb. Above 225 mb, the temperatures increase with height. The zonal wind is a

maximum close to the center of the channel above 225 mb. The zonal mean temperature and wind fields are in geostrophic balance.

In addition to the static and inertial stability checks already discussed, calculations of the absolute vorticity gradient were made to diagnose whether the initial conditions in each of the four data sets were barotropically unstable. The 80 m/s jet in the analytic case was inertially unstable, but barotropically stable. For the other three initial conditions, barotropic instability is prevalent to the south of the jet. The major difference is in the elevation at which barotropic instability existed. For the real data and NORAPS analysis case, this instability existed at the level of the 250 mb jet. However, in the NORAPS forecast case this instability was found mostly at the 850 mb level south of Athens. As will be discussed in the next section, these differences contributed to significant differences in the growth rate spectrum.

The model was integrated for each of the four initial conditions for a spectrum of wavenumbers to determine the most unstable wave. The structure and energetics of the most unstable mode will then be examined. The results from these experiments will be discussed in the next section.

D. RESULTS

1. Growth Rates and Phase Speed

The growth rates of the perturbations from the analytic case, NORAPS analysis and the NORAPS forecast are illustrated in Fig. 5.6. In the real data case, it appears that smaller scale instabilities contaminated the spectrum so that the growth rates of the most unstable Rossby modes became rather unrealistic. The results from the real data experiments will therefore not be shown, but will be qualitatively discussed.

The growth rate spectra for both NORAPS cases indicate that the wavelength of the most unstable perturbation occurs around wavenumbers 10-20, which is equivalent to a wavelength of approximately 2000 km at 33° N. For these wavenumbers, the growth rate is about 3.2-3.5 per day, which corresponds to a doubling time of approximately .23 days (5.5 h). Both of these growth rate curves exhibit similar tendencies, with lowest growth rates occurring at wavenumber 3. In the NORAPS analysis case, growth rates slowly decrease to wavenumber 30, compared to more constant growth rates in the NORAPS forecast case at higher wavenumbers. The growth rates for the analytic case with UMAX equal to 80 m/s are approximately constant between wavenumbers 3 and 15, but start to decrease at higher wavenumbers. The maximum growth rate (approximately 2/day) is also much less than that for the NORAPS cases. The curve for the analytic case changes dramatically for different jet intensities. For a 40 m/s jet, the growth rate spectrum is very similar to that of Gall (1976c) and Hodur (1984), with a sharp peak at wavenumber 15 and a secondary maxima at wavenumber 40. In the 60 m/s case, the growth rate curve is flatter, although a maximum is still at wavenumber 15. As will be seen later, these changes in the growth rate spectrum may be related to the energetics. In the weaker jet (40 and 60 m/s) cases, the waves shorter than wavenumber 5 are primarily baroclinic in nature, while the very long waves have combined baroclinic and barotropic properties. For the stronger (80 m/s) jet, the wave becomes more barotropic at all wavenumbers. In the real data case, the growth rate curve was approximately 4 per day, with similar tendencies to that of the NORAPS cases. One possible explanation could be the fact that the real data case was the most barotropically unstable in the horizontal, and the NORAPS forecast case the least.

As discussed in Chapter III, the size of the cyclone (low III in Fig. 3.5) was approximately 1000 km at 290000. In less than 6 h between 290000 and 290600, the cyclone doubled in size as well as intensity. A perturbation with a wavelength of 2000 km at the latitude of the cyclone has a wavenumber of about 15. These observations are therefore consistent with the growth rate associated with the most unstable wavenumber.

The phase speed (Fig. 5.7) for wavenumbers 7 - 30 for the NORAPS forecast case closely approximate the speed of the cyclone. The phase speeds depicted are those for the maximum surface pressure perturbation. In general, all the phase speeds for the three initial conditions are higher than what was observed. This could be related to the fact that the model has no friction, which would have retarded the speed of movement of the perturbation. The phase speeds also decrease with increasing wavenumber (with the exception of wavenumber 35), consistent with the results of Gall (1976c).

2. Structure

The NORAPS forecast case will be used to examine the structure of the perturbation more closely because the cross-section in this case is oriented through the middle of the cyclone (Fig. 5.3). In the NORAPS analysis case, the cyclone was northeast of the cross-section (Fig. 5.4). As discussed before, the cyclone size corresponds approximately to a zonal wavenumber 15, which has the maximum growth rate for the NORAPS forecast case. This growth rate as well as the phase speed also agree very well with observations. Therefore, the structure of the perturbation for wavenumber 15 in the NORAPS forecast case will be presented, although it should be pointed out that the structures for wavenumbers 10 through 20 are very similar.

The variations of the geopotential amplitude perturbation along the cross-section are depicted in Fig. 5.8. Two maxima can be identified, one near the surface between stations AHN and AYS and another at approximately 500 mb between BNA and AHN. The positions of these two maxima indicate a northward tilt with height. These maxima occur in the regions where the Richardson number (Ri) is the lowest (not shown) and the vertical and horizontal shears are the strongest.

The maximum temperature perturbation is found near AHN, with a similar northward tilt with height (Fig. 5.9). This maximum occurs near the surface and coincides with the strongest baroclinic zone (Fig. 5.2). The perturbation is confined to the lowest layers.

The maximum perturbation in vertical motion (Fig. 5.10) occurs at approximately the 700 mb level, primarily over AHN and southward. The sign of the vertical barotropic term (discussed in the next sub-section) calculated from the model indicates that this maximum perturbation corresponds to an area of rising motion. This area also coincides with a region of low Ri (not shown) and strong horizontal and vertical wind shears (Fig. 5.2).

In contrast to pure baroclinic disturbances, these temperature and vertical motion perturbations are not coincident everywhere, with the temperature perturbation to the north and at a lower level than the vertical motion perturbation. These patterns suggest that warm air is rising, and cold air is sinking beneath 700 mb (vertical motion values increasing with maximum temperature perturbation values). A reversal above this level occurs as the temperature perturbation values decrease with constant vertical motion values. This suggests that baroclinic conversion contributes to the development of the cyclone at lower levels, but inhibits growth at mid-levels. This result is consistent with that

of Hodur (1984). These ideas will be discussed further in the next sub-section.

For wavenumbers 10-20 in the NORAPS analysis case, the maximum height, temperature and vertical motion perturbations were located near the anticyclonic side of the jet level (coincident with the strong horizontal shear region depicted on Fig. 5.1). In these experiments, the barotropic mode appears to dominate over the baroclinic mode, resulting in the maximum perturbation growth being at higher levels. The relative contributions from the barotropic and baroclinic processes will be discussed further in the next subsection. At higher wavenumbers (greater than 25), the maximum height and temperature perturbations were found near the surface, similar to that found for wavenumbers 10-20 in the NORAPS forecast case. (Similar results were also found for the higher wavenumbers in the forecast case). Furthermore, in the forecast case, the strongest horizontal and vertical shears were located below 800 mb. The strength and position of both the horizontal and vertical shears appear to dictate the location and amount of perturbation growth. Therefore, the emergence of the most unstable baroclinic or barotropic mode seems to depend on the relative magnitudes of the vertical and horizontal shears.

The horizontal variations of the geopotential amplitude perturbations for wavenumber 15 for the NORAPS forecast case are depicted in Figs. 5.11 and 5.12. These figures are constructed from the profile of the height perturbations in Fig. 5.8, using the following equation:

$$H(x,y,p)=H_0(y,p)\sin(2\pi x/L + \Phi) \quad (5.6)$$

where L is the wavelength corresponding to a particular zonal wavenumber, Φ the phase angle and $H_0(y,p)$ the maximum amplitude of the height perturbation. The vertical profile

depicted in Fig. 5.8 is placed at the middle of the plot for convenience. Since this is a linear model, the phase angles are all relative.

The maximum surface height perturbation (Fig 5.11) is found underneath but somewhat southward of the jet, as might be expected. A distinct westward tilt with height of the geopotential perturbation can be seen by comparing Figs. 5.11 and 5.12. The height perturbations at 500 mb are oriented in a northwest-southeast direction south of the jet (Fig. 5.2), which indicates that the horizontal tilt of the 500 mb heights is opposite to the horizontal wind shear south of the jet and parallel to that north of the jet. These observations suggest that baroclinic instability exists underneath the jet, and barotropic instability prevails to the south of the jet. On the other hand, barotropic stability is suggested to the north of the jet.

In summary, for the NORAPS forecast case, the horizontal and vertical structure of the perturbation identified by the linear stability model to have the highest growth rate bears close resemblance to the cyclone. As will be discussed further in the next subsection, the barotropic modes in the NORAPS analysis case dominated the growth rate spectrum (except for the higher wavenumbers) since the maximum perturbations were located near the jet level. Although baroclinic instability may also have existed and contributed to the growth of the cyclone in a different region, this model is not capable of identifying this "secondary" instability mode. On the other hand, the strongest horizontal and vertical shears in the NORAPS forecast case were present at lower levels and may therefore have allowed the baroclinic mode to become dominant at the wavenumbers close to those observed.

3. Energetics

a. Energy Budget Wavenumber Distribution

Since the zonal flow within the linear model consists of a zonal flow and a single zonal wave, the kinetic energy equation of the wave can be written as;

$$\frac{\partial K_e}{\partial t} = - \overline{u'v'} \frac{\partial \bar{u}}{\partial \phi} - \frac{\tan \phi}{a} (\bar{u} \cdot \overline{u'v'}) - \overline{u'w'} \frac{\partial \bar{u}}{\partial p} - \overline{w'\alpha'} \quad (5.7)$$

where K_e is the total kinetic energy of the wave, R the radius of the earth, ϕ is the latitude and U is the zonal wind. The primed variables represent the eddies. The first two terms on the right-hand-side of the equation are referred to as the horizontal barotropic conversion term. The third term is referred to as vertical barotropic conversion. This term is neglected in quasi-geostrophic models, and therefore represents a nongeostrophic effect (Gall, 1976a). Hodur (1984) considered this term as a baroclinic term because of its relation to the horizontal temperature gradient via the thermal wind equation. Orlanski (1968) noted that this term may become important for shorter waves when the Richardson number is small. The last term represents the baroclinic conversion.

Previous studies by Gall and others have shown that waves derive most of their energy by baroclinic processes. Shorter waves (wavenumbers greater than 5) are barotropically damped in the horizontal. However, the vertical barotropic conversion contributes to wave growth especially for short waves (wavenumbers greater than 10). Therefore, perturbations with higher wavenumbers can extract energy from the zonal flow through both baroclinic and barotropic processes. Hodur (1984) found that for stronger jets, the vertical barotropic term increased in importance relative to the baroclinic term. On the other hand, Brown

(1969) and others found that the horizontal term contributes only for the very long waves, and thus have identified the planetary waves as being barotropic.

For the analytic initial conditions with values of UMAX set at 40 m/s, the energetics resemble those found by Gall (1976a,c). With a 60 m/s jet, the results of Hodur (1984) were essentially reproduced. Specifically, the baroclinic conversion provides the largest contribution to the wave growth, but the vertical barotropic term is more important for higher wavenumbers in the 60 m/s case than in the 40 m/s case. Except for low wavenumbers, the horizontal barotropic term provides a damping effect on wave growth.

The results for the 80 m/s jet are shown in Fig.5.13. The horizontal term exhibits similar tendencies to the experiments with weaker jets, although this term is the most dominant at lower wavenumbers. However, the baroclinic and vertical barotropic conversions dominate for the higher wavenumbers. For all wavenumbers the vertical barotropic term contributes to wave development. The baroclinic conversion inhibits wave growth for lower wavenumbers but enhances shortwave development. With a 67 m/s jet, Hodur (1984) found the baroclinic and vertical barotropic conversions to be of equal magnitude. He therefore labeled his perturbation a mixed baroclinic wave.

In the set of experiments using the NORAPS analysis as initial conditions, the horizontal barotropic term is the most dominant term for all waves with wavenumbers less than 25 (Fig. 5.14). The baroclinic term damps wave growth for this same range of waves but becomes an important contributor beyond wavenumber 25. The vertical barotropic term contributes for all waves, especially for higher wavenumbers. The large contribution from the horizontal barotropic term is a result of the barotropically unstable initial profile (Fig 5.1).

It appears that between wavenumbers 25-30, a transition from the horizontal barotropic to the vertical barotropic and baroclinic modes exists (Fig. 5.14). This is consistent with height perturbations calculated from the NORAPS analysis case (not shown), where perturbations greater than 25 were very similar to those from the NORAPS forecast case between wavenumbers 10-20. This transition at higher wavenumbers apparently results from the increasingly important contribution from the vertical motion term for disturbances of smaller spatial scales.

For the less barotropically unstable initial conditions (the NORAPS forecast case), all terms contribute to wave growth, with the vertical barotropic term contributing the most to the wave (Fig. 5.15). Furthermore, the contribution from the vertical barotropic term increases until wavenumber 30 and then decreases. However, the baroclinic term increases and the horizontal barotropic term decreases at higher wavenumbers.

Therefore, it appears that the structure of the perturbation is dependent upon which mode is dominant at a particular wavenumber. At those wavenumbers where the vertical barotropic and baroclinic terms are dominant, the perturbation is confined to lower levels. On the other hand, the wave will be evident at higher levels if the horizontal barotropic mode is the strongest. For example, in the NORAPS analysis case, the baroclinic mode emerges beyond wavenumber 25 when both the vertical barotropic and baroclinic terms become more important. The baroclinic mode probably also exists at lower wavenumbers. However, the model is unable to identify this mode because of the much larger instability from the horizontal barotropic mode.

b. Vertical Distribution

The NORAPS 24-h forecast case will be used to examine the vertical distribution of the kinetic energy

budget terms since the structure of the most unstable mode resembles the closest to that observed. In contrast to Gall (1976a,c), the eddy kinetic energy (Fig. 5.16) is found to be a maximum at 850 mb for wavenumbers 10, 15, 20 and 30 with a slow increase at the surface for successively higher wavenumbers. The fact that the maximum is not found at the surface could be attributed to the friction inherent with the initial profile. (The maximum occur at the surface in all analytic cases where no friction was present.) Note that the maximum eddy kinetic energy is found at the level of maximum vertical wind shear.

The vertical distribution of the eddy kinetic energy budget terms for wavenumber 15 in the NORAPS 24-h forecast case is depicted in Fig. 5.17. The vertical barotropic term is the largest contributor to wave growth. The maximum contributions from the baroclinic and vertical barotropic terms are largest at 850 mb, whereas the horizontal term contributes most at 700 mb. On the other hand, baroclinic damping occurs below 900 mb and above 600 mb, consistent with the temperature and vertical motion perturbations discussed in the previous section.

Thus, the perturbation can be largely explained by the vertical barotropic process at lower levels, with baroclinic instability playing a less significant role. The baroclinic term actually inhibits growth above the mid-levels and at the lowest levels. This finding is similar with Hodur (1984) who noted that baroclinic damping occurred at mid-levels for waves with wavenumber 40. The shallow nature of these waves is also similar with the vertical extent of the cyclone in this case study.

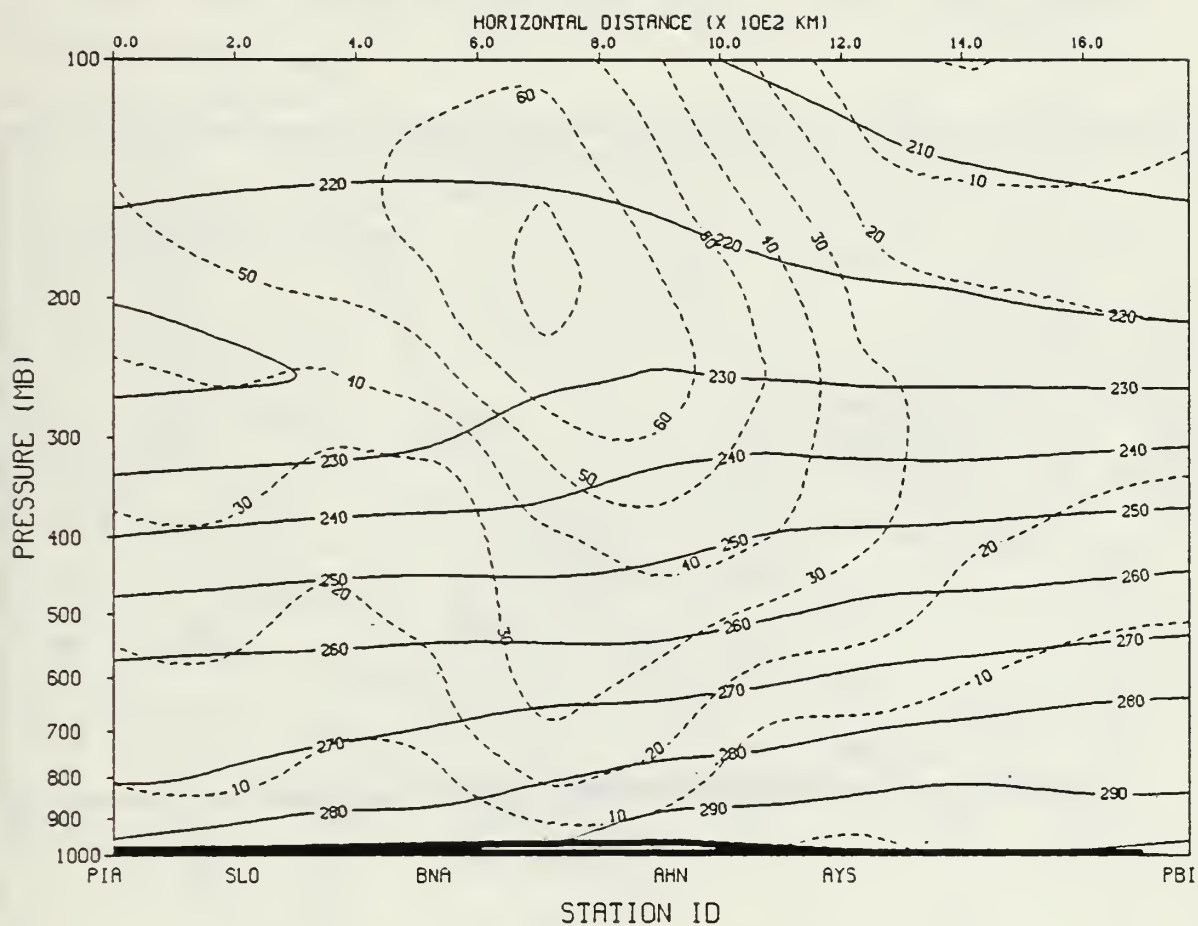


Fig. 5.1 North-south cross-section of the initial zonal flow from the NORAPS 290000 analysis. Dashed lines denote isotachs (m/s) and solid lines denote isotherms ($^{\circ}$ K).

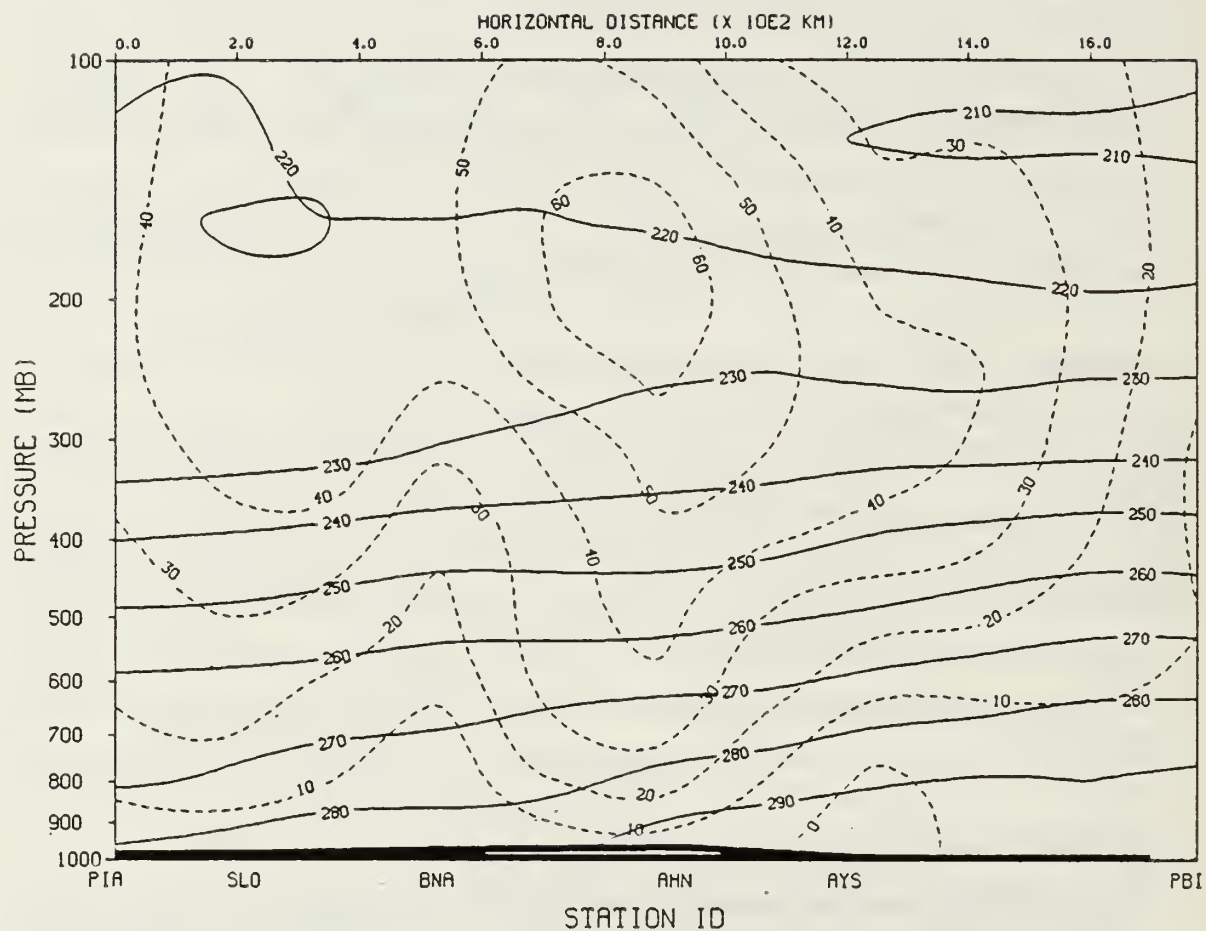


Fig. 5.2 As in Fig. 5.1, except the data are from the NORAPS 24-h forecast valid at 290000.

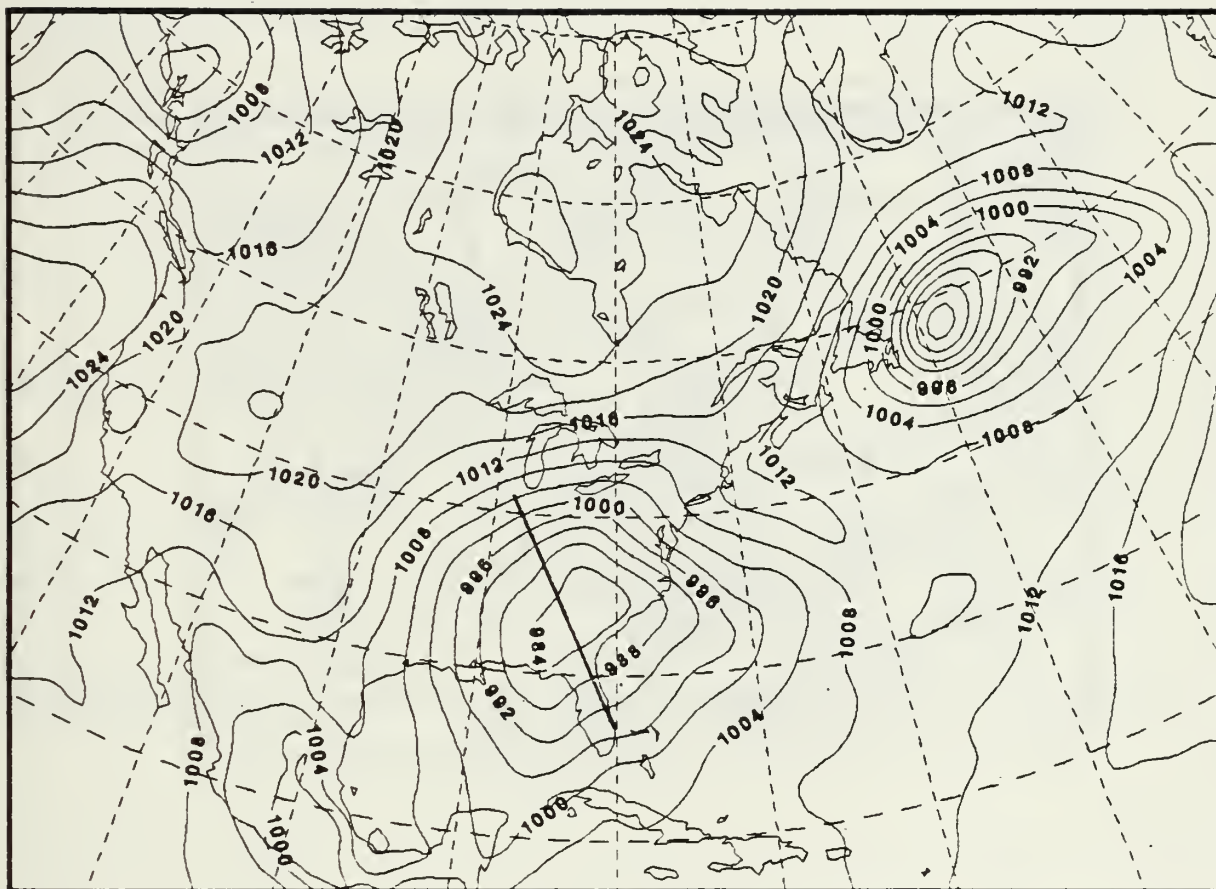


Fig. 5.3 NORAPS 24-h forecast of surface pressure (solid, mb) and 1000 - 500 mb thickness (dashed, m) valid at 290000. The thick solid line indicates the position of a vertical cross-section used in the stability analysis.

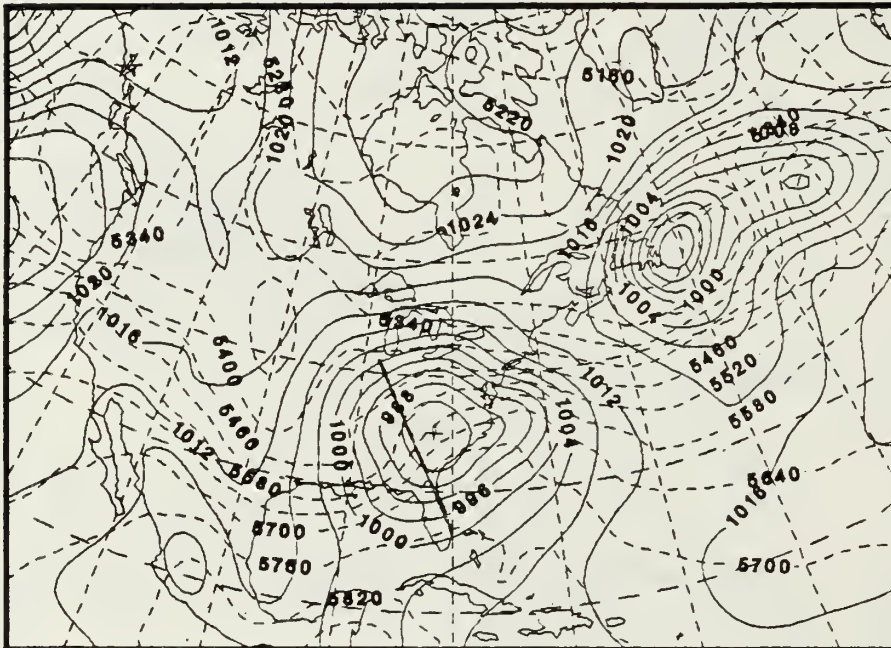


Fig. 5.4 As in Fig. 5.3 except for NORAPS analysis.

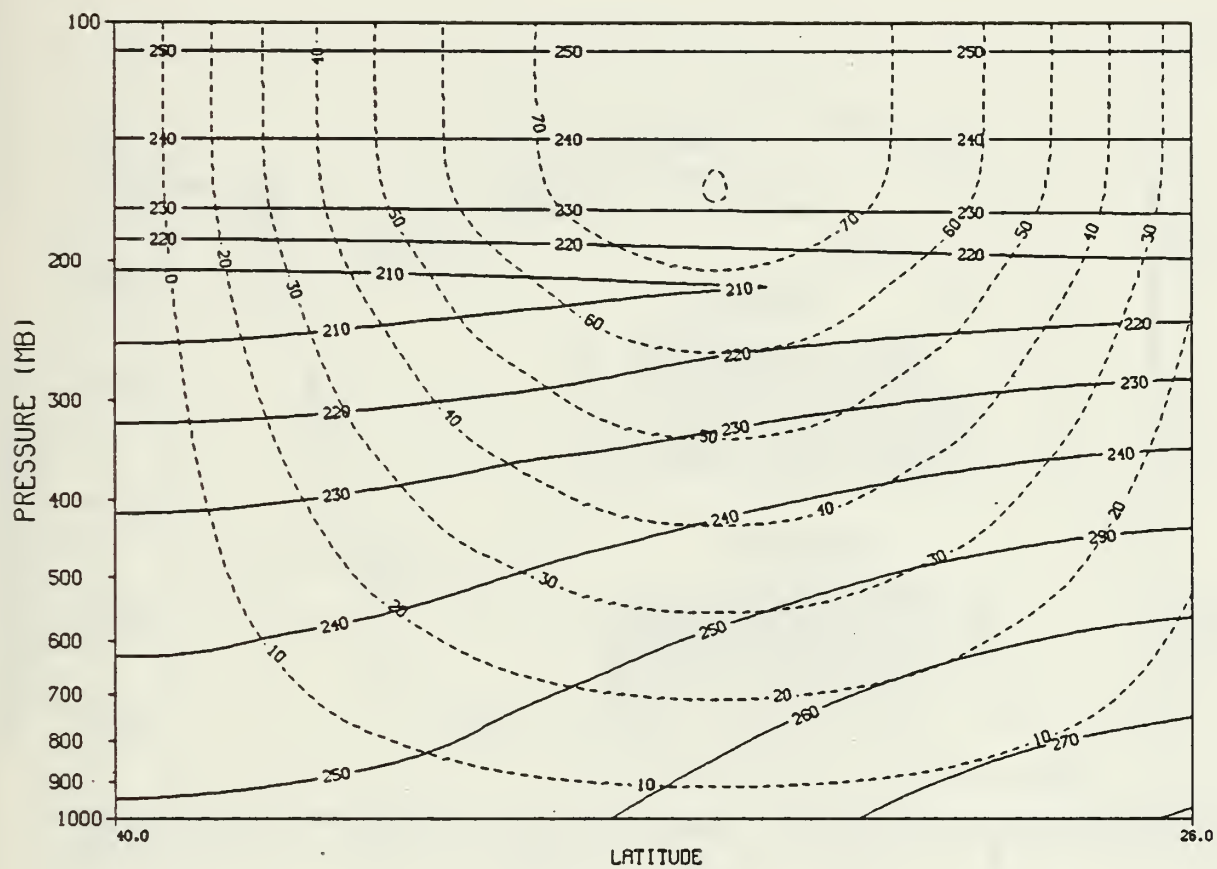


Fig. 5.5 As in Fig. 5.1 except the profile is generated analytically. See text for further description.

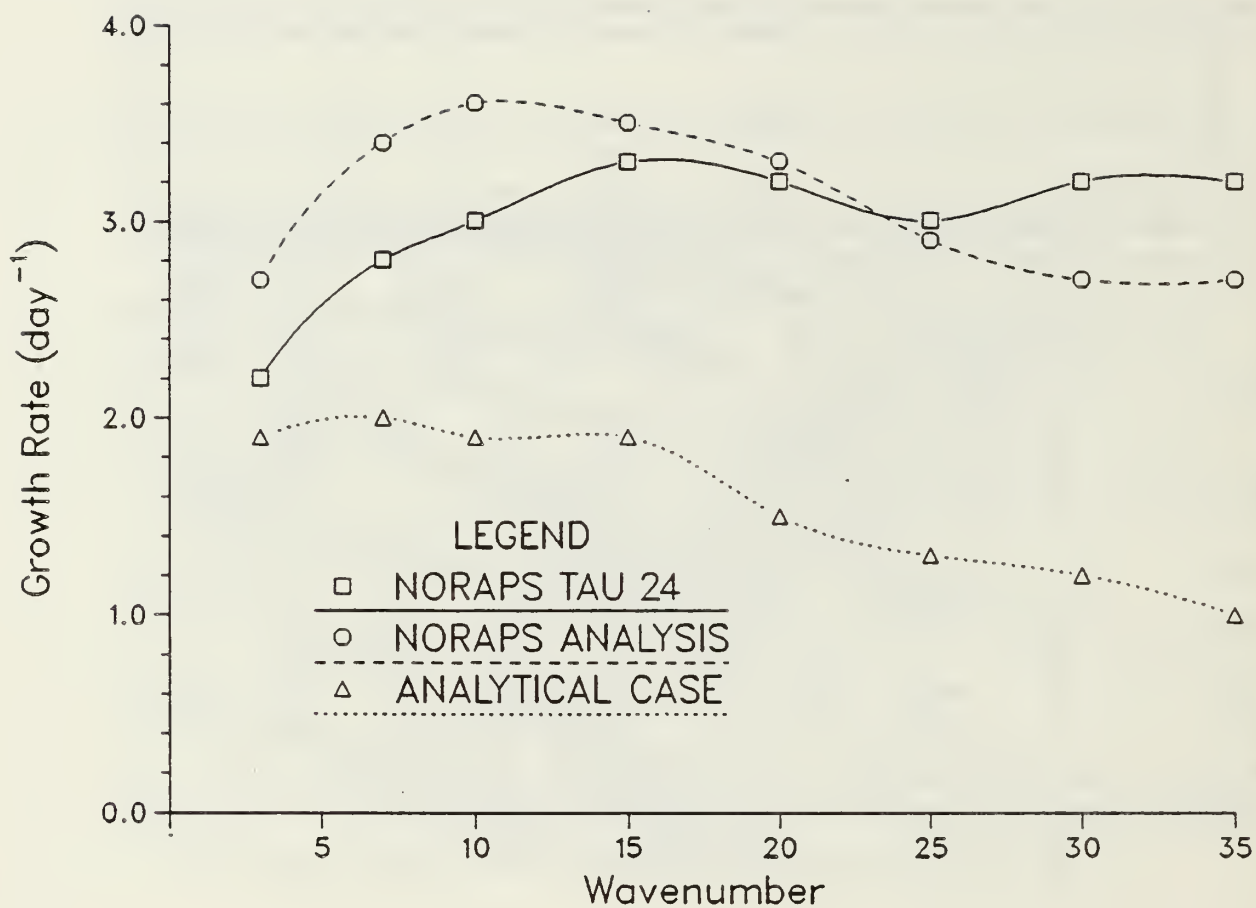


Fig. 5.6 Spectral distribution of growth rates from the stability model. Tau-24 indicates the 24-h NORAPS forecast. The analytical case is for UMAX = 80 m/s.

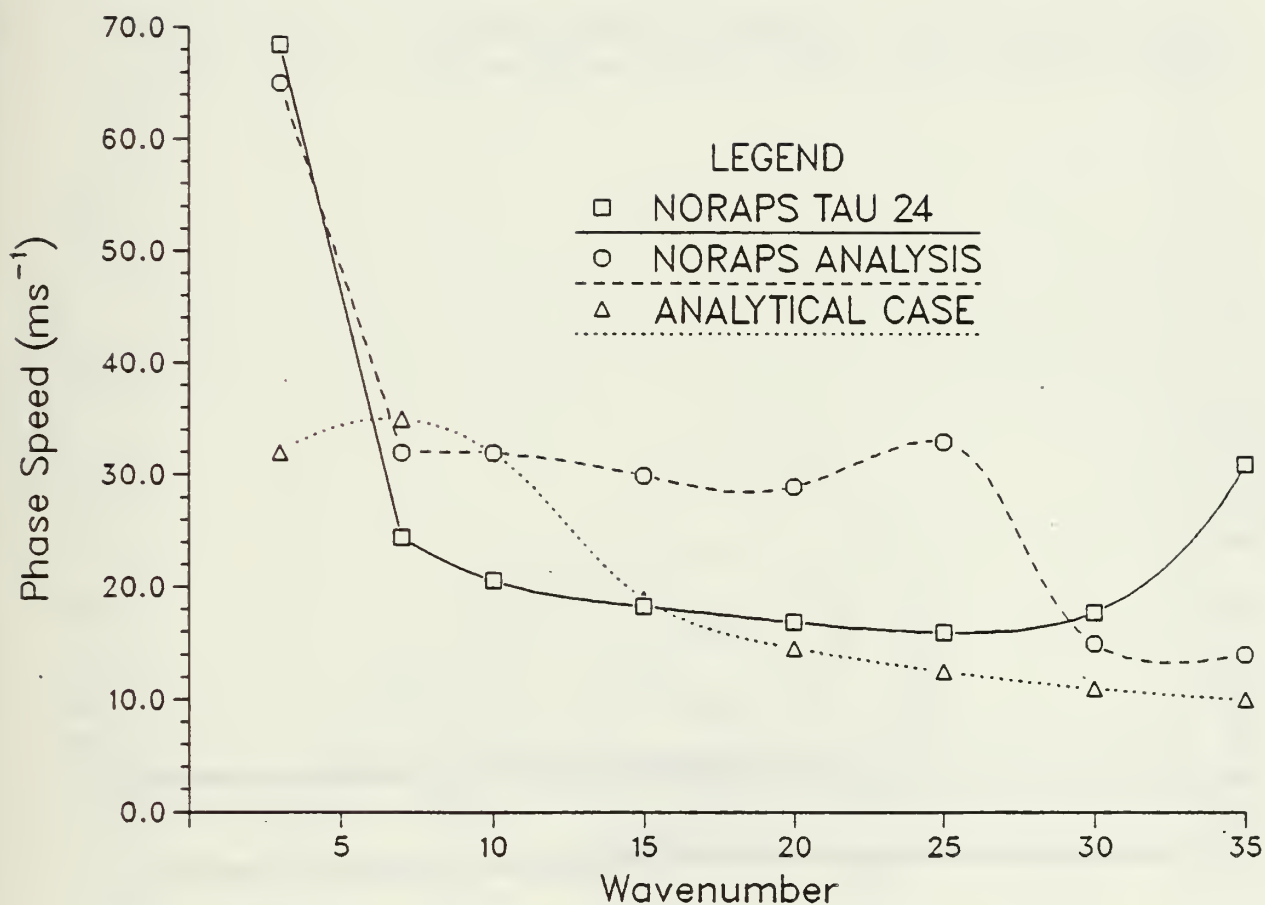


Fig. 5.7 As in Fig. 5.6 except for the phase speed which was computed for the wavelength of the wave at 33° N .

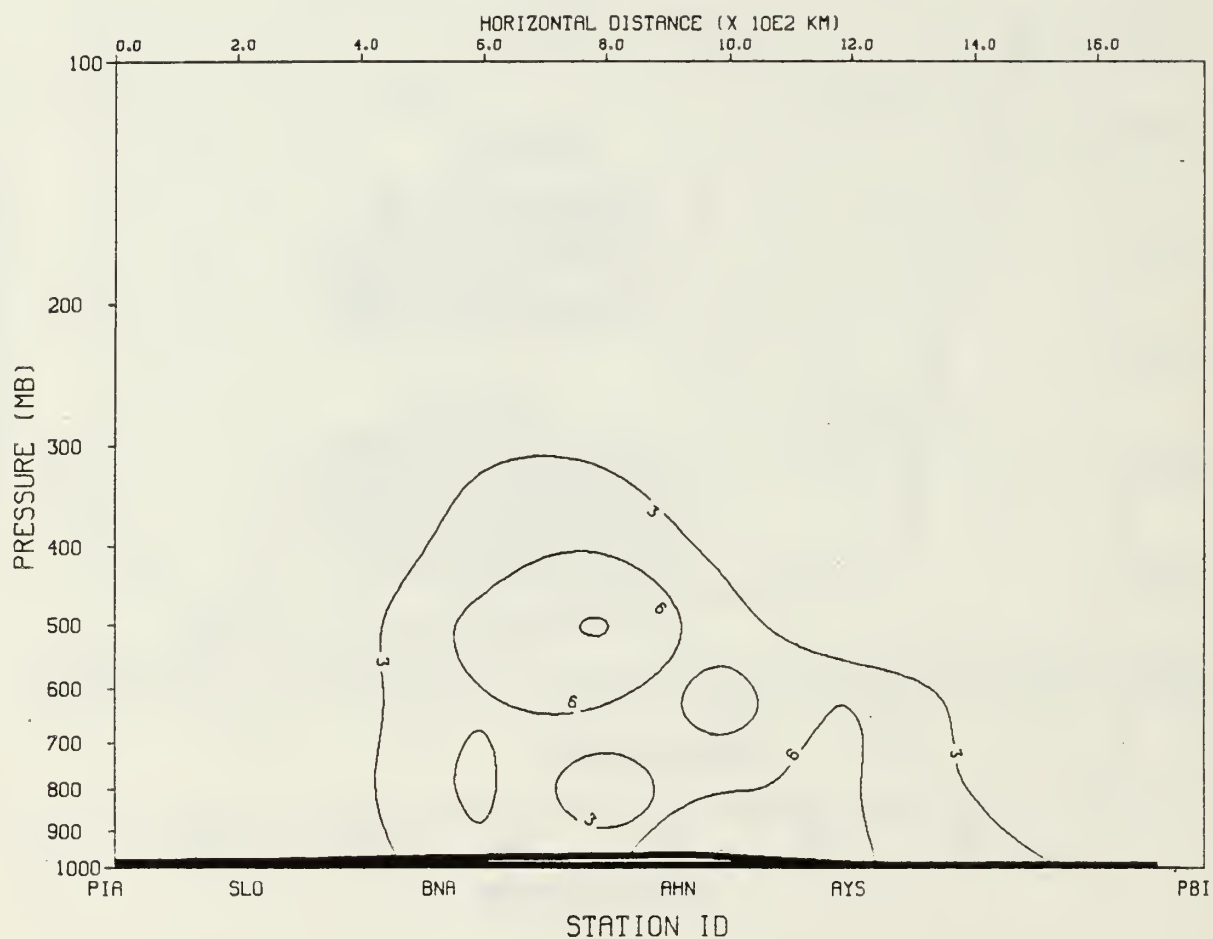


Fig. 5.8 Geopotential height perturbation computed from the linear model for wavenumber 15 for the NORAPS 24-h forecast case. The data have been normalized so that the largest value is 10.

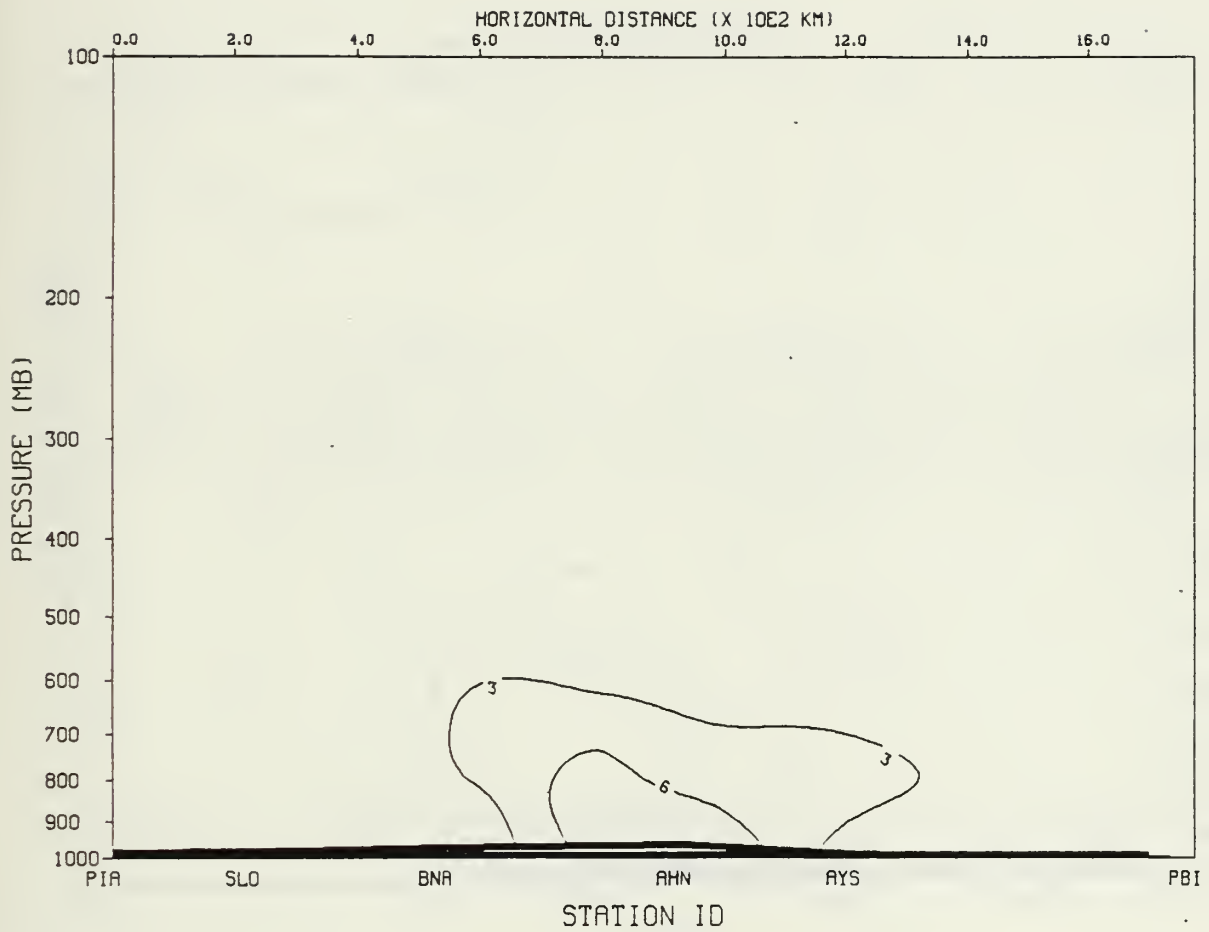


Fig. 5.9 As in Fig. 5.8 except for the temperature perturbation ($^{\circ}\text{C}$).

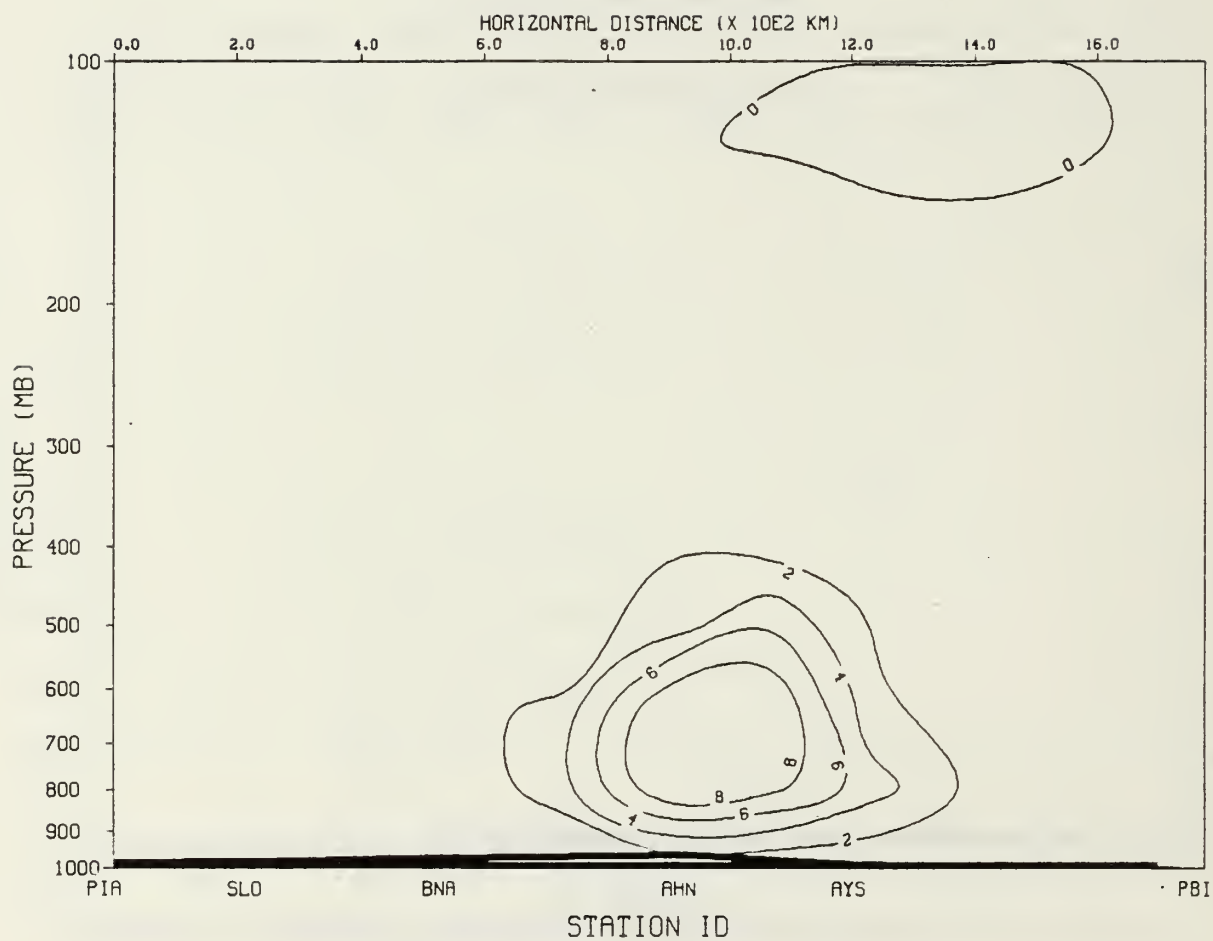


Fig. 5.10 As in Fig. 5.8 except for the vertical velocity perturbation in Pa/s.

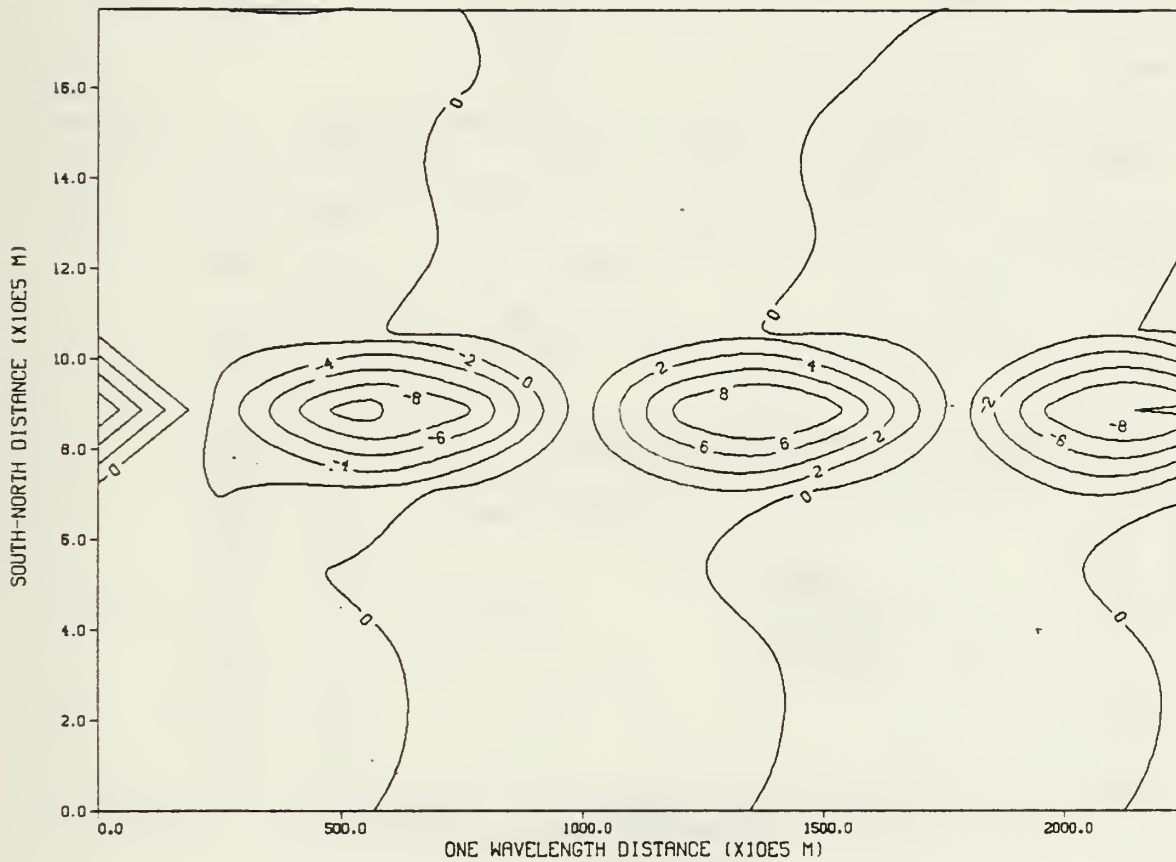


Fig. 5.11 Surface geopotential height perturbation in the horizontal for wavenumber 15 for the NORAPS 24-h forecast case. The data has been normalized so that the largest value is 10. The vertical cross-section is centered in the middle of the channel in the north-south direction for convenience. Distances along both axes are labelled in meters.

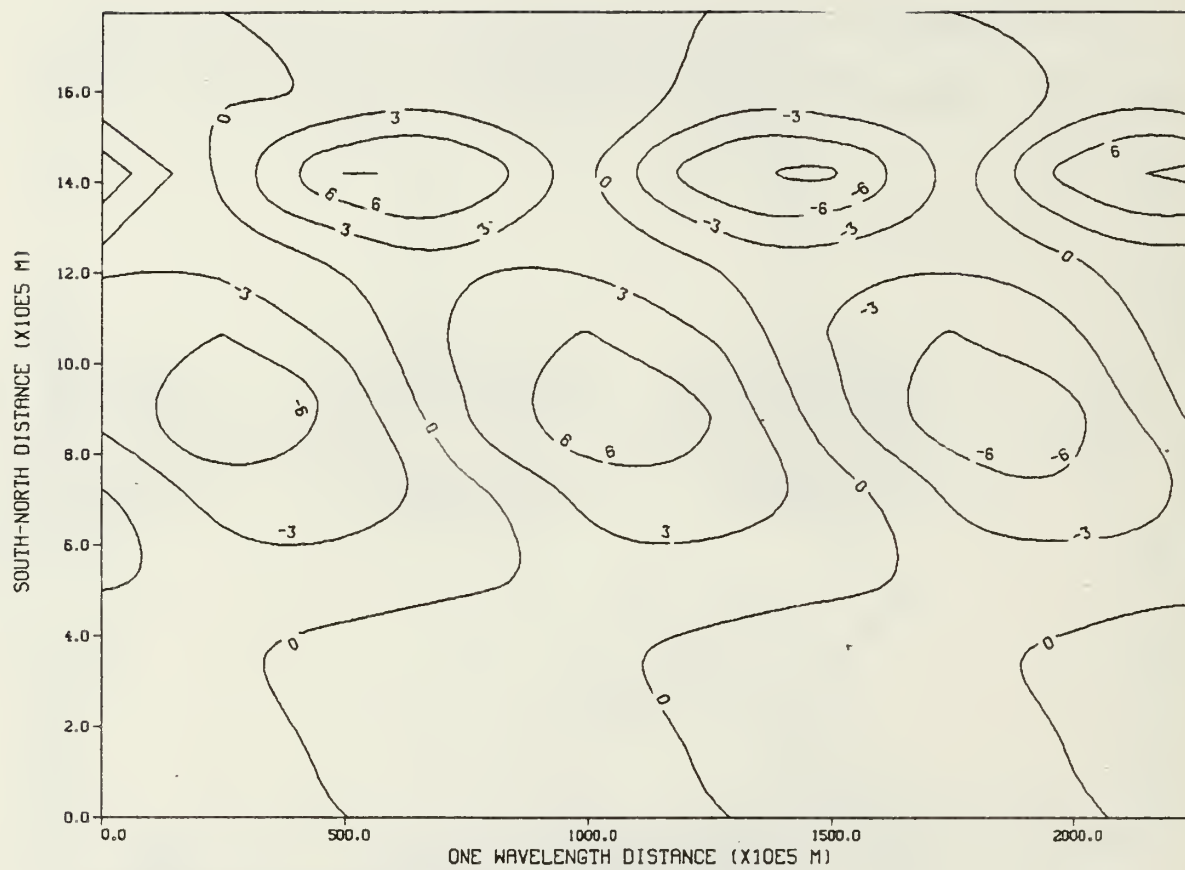


Fig. 5.12 As in Fig. 5.11 except for 500 mb.

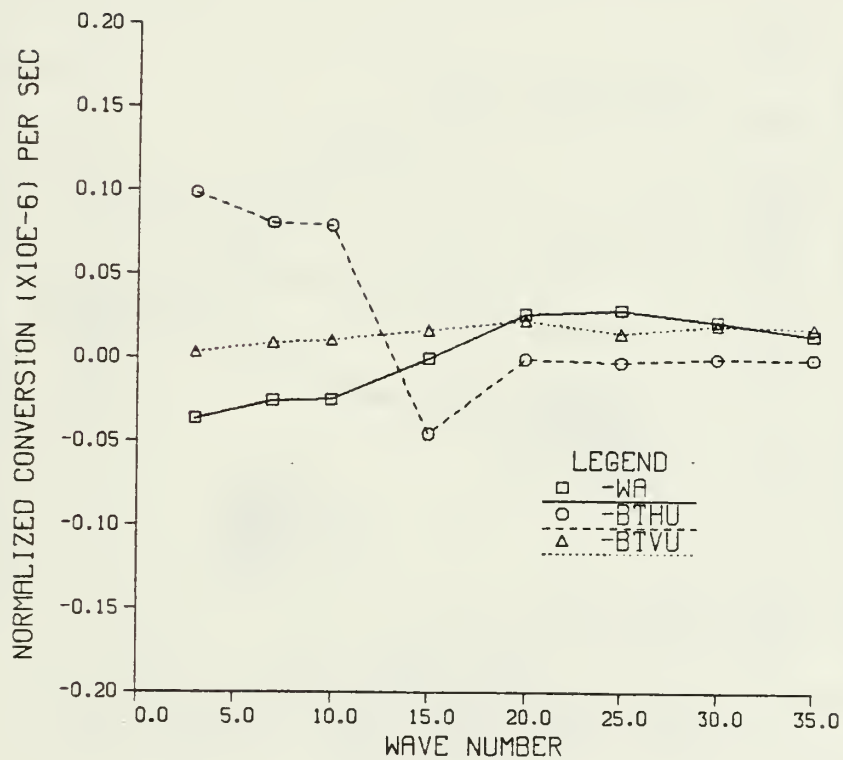


Fig. 5.13 Spectral distributions of the vertically integrated values of the baroclinic term (WA), the vertical barotropic (BTVU) and the horizontal barotropic terms (BTHU), calculated by the linear model for the analytic zonal mean flow.

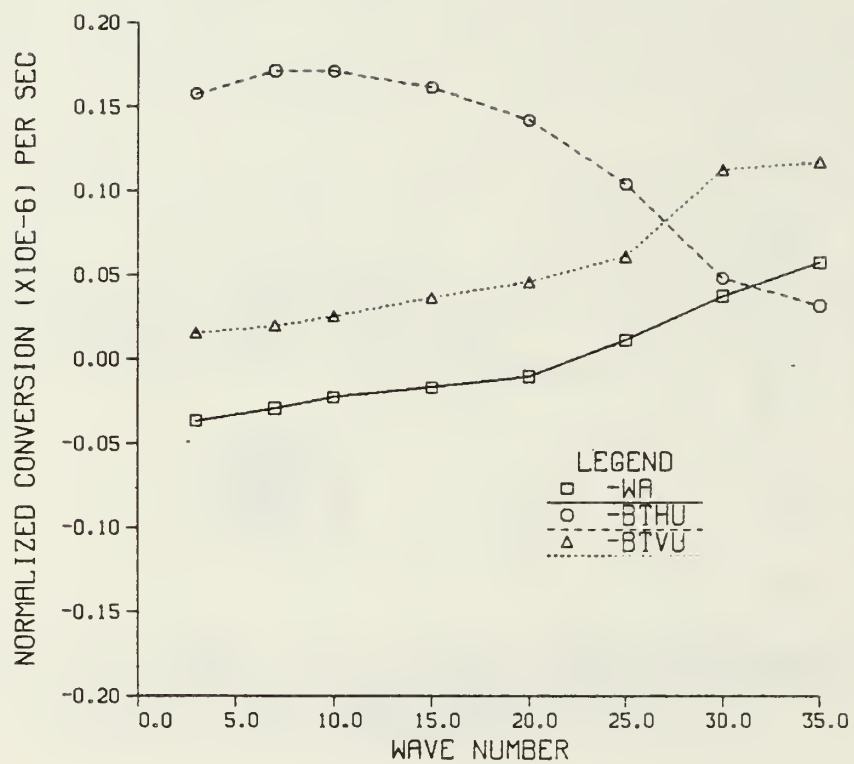


Fig. 5.14 As in Fig. 5.13 except for NORAPS analysis case.

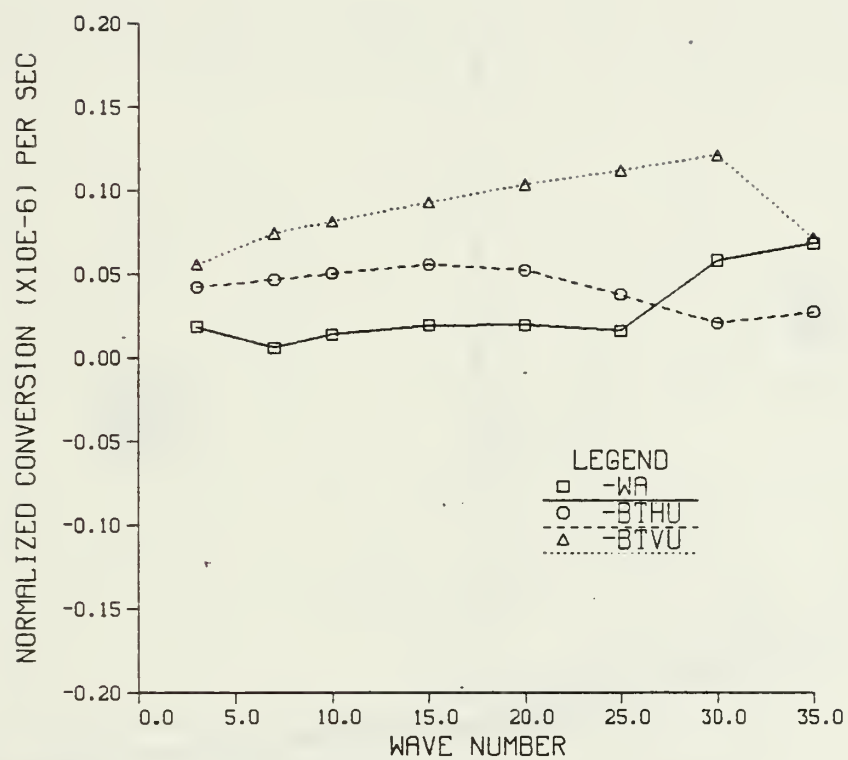


Fig. 5.15 As in Fig. 5.14 except for NORAPS Tau 24 case.

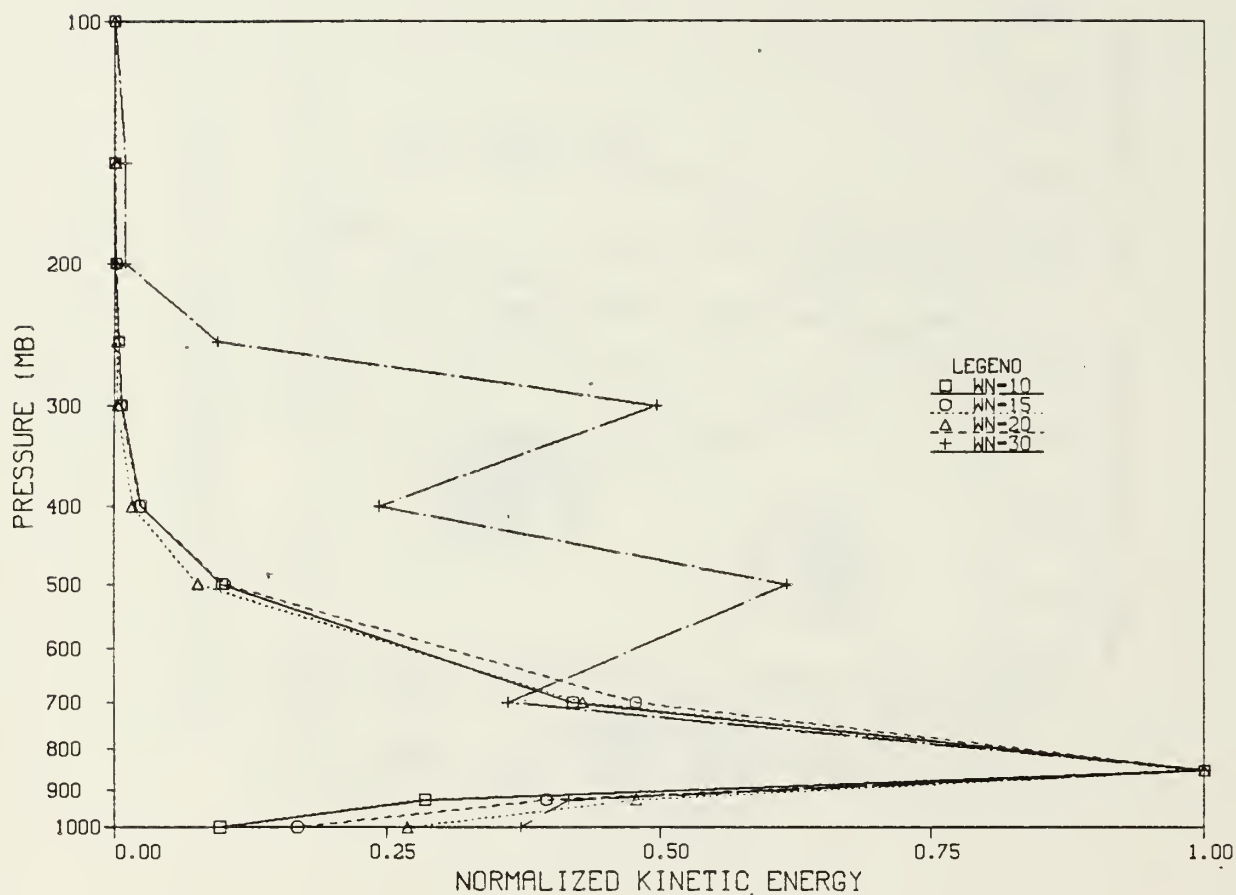


Fig. 5.16 Vertical distribution of the eddy kinetic energy (m^2/s^2) of wavenumbers (WN) 10, 15, 20 and 30 for the zonal mean flow from the NORAPS 24-h forecast.

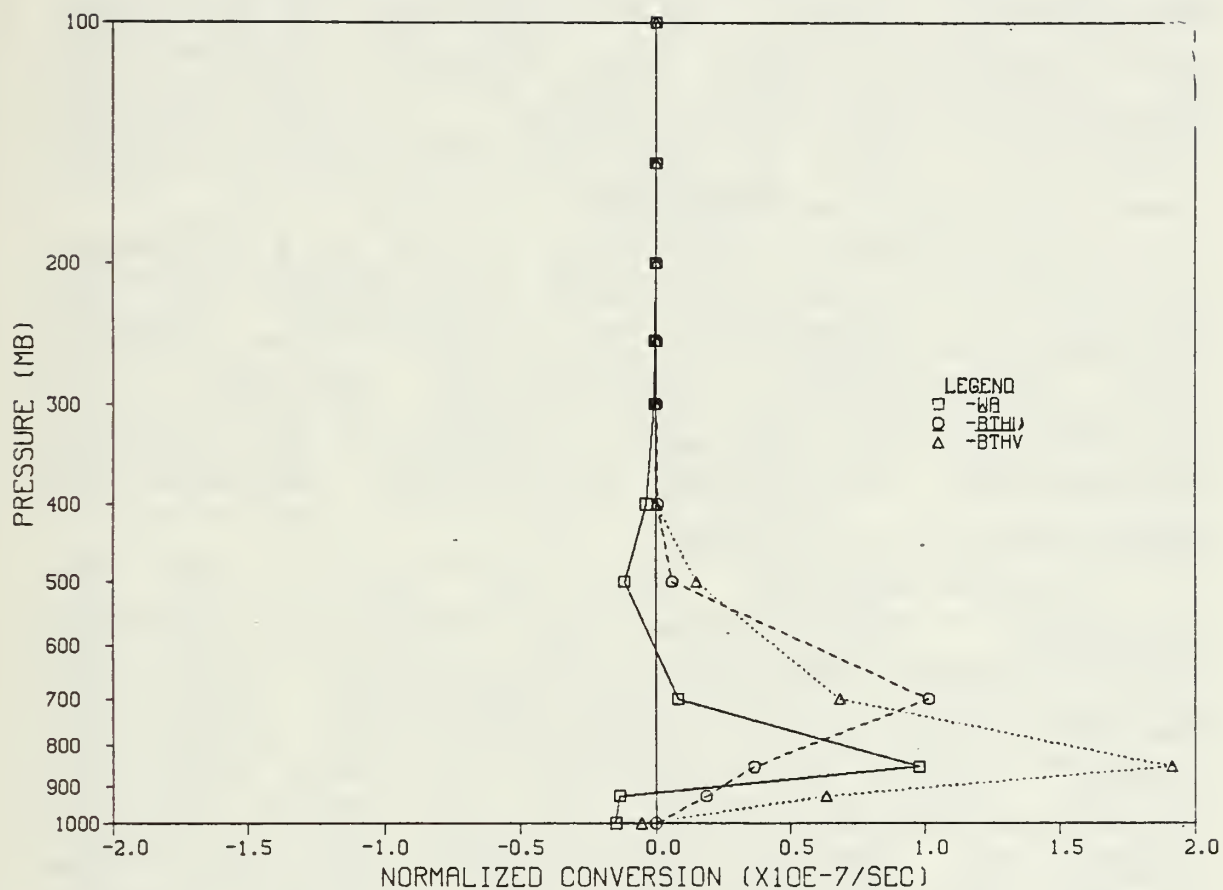


Fig. 5.17 Vertical distribution of the meridionally averaged normalized energy conversion ($\text{Pa m}^3 \text{ s}^{-1} \text{ kg}^{-1}$) from the baroclinic term (WA), vertical barotropic term (BTVU) and horizontal barotropic term (BTHU) for wavenumber 15 for the NORAPS 24-h forecast zonal flow.

VI. CONCLUSIONS

Previous studies have suggested a variety of mechanisms and processes to explain the rapid development of some extratropical cyclones. It is reasonable that some favorable interaction between these different processes could accelerate the developmental process. This study has identified two of these processes as being important for one case of rapid cyclone development.

A detailed synoptic evaluation of the rapid development of the Carolinas storm of March, 1985 suggests that the atmosphere was probably both baroclinically and barotropically unstable during the genesis stage. Therefore, it is hypothesized that a combination of baroclinic and barotropic instabilities could explain the behavior, structure and growth rate of this cyclone.

A linear stability model was used to test this hypothesis. Three different sets of initial conditions along a vertical cross-section perpendicular to the jet were employed. These include a temperature analysis using rawinsondes, a NORAPS temperature analysis, and a NORAPS 24-h temperature forecast. Geostrophic winds were calculated for each of these three temperature fields. The growth rates and phase speeds of the most unstable modes were consistent with observations. However, the structure of the perturbation depends on whether the most unstable mode is primarily baroclinic or barotropic. The horizontal barotropic mode was most evident at upper levels, whereas the baroclinic and vertical barotropic modes were found near the surface. The unstable mode that best explains the Carolinas storm appears to be a mixed baroclinic/vertical barotropic mode.

This case study of rapid cyclone growth and development has shown that the general behavior, structure and

energetics of the cyclone is consistent with the results from a linear stability analysis. Thus, it appears that linear theory can be used to explain the genesis and initial growth of the Carolinas storm. Furthermore, baroclinic instability alone cannot explain the growth and development of the cyclone. In fact, the growth of the cyclone has been found to be the result of barotropic and baroclinic instabilities. These instabilities can account for the initial growth and development of the cyclone without including the effects from convection.

Research should be continued to further our understanding and prediction capabilities of rapid cyclone development. Specifically, our understanding of barotropic instability from both theoretical and applications standpoints must be improved. How baroclinic and barotropic instabilities interact with each other as well as other processes need to be better understood. A more coherent picture of how convective and boundary layer processes, topographic influences and jet streak dynamics interact and contribute to rapid cyclone development should also be addressed. The variety of physical processes that are present in the rapid development of maritime extratropical cyclones suggests that the interaction between different scales of motion could be very important. For example, Thorpe and Emanuel (1985) have proposed that moist symmetric instability, which operates on scales of 100 km and has been used to explain frontal structures, can contribute to cyclone growth from potential vorticity arguments. These ideas need to be explored through observational studies using a dense data network that can spatially and temporally resolve motions on the mesoscale. Numerical and theoretical studies are also necessary to provide further physical insights into the problem.

LIST OF REFERENCES

- Atlas, R., 1984: The effect of physical parameterizations and initial data on the numerical prediction of the Presidents' Day cyclone. Preprints, Tenth Conf. on Wea. Forecasting/Analysis., Tampa, FL, 580-587.
- Bjerknes, J., 1919: On the structure of moving cyclones. Geofys. Publikasjoner, Norske Videnskaps-Akad, Oslo 1, No.1, 1-8.
- Blakeslee, R., and R. L. Gall, 1978: The effect of the meridional circulation on the baroclinic instability of the winter zonal flow. J. Atmos. Sci., 35, 2368-2372.
- Bleck, R., 1974: Short range prediction in isentropic coordinates with filtered and unfiltered numerical models. Mon. Wea. Rev., 102, 813-829.
- Bosart, L. F., 1981: The Presidents' day snowstorm of 18-19 February 1979: a subsynoptic-scale event. Mon. Wea. Rev., 109, 1542-1566.
- Bosart, L. F., and S. C. Lin, 1984: A diagnostic analysis of the Presidents' day storm of February, 1979. Mon. Wea. Rev., 112, 2148-2177.
- Brody, L. R., P. A. Harr, and T. L. Tsui, 1984: Automated verification of numerical forecasts - a decision aid for the operational forecaster. Preprints, Tenth Conf. on Wea. Analysis/Forecasting., Tampa, FL, 46-52.
- Brown, J. A., 1969: A numerical investigation of hydrodynamic instability and energy conversions in the quasi-geostrophic atmosphere. J. Atmos. Sci., 26, 352-365.

- Bullock, B. R., and D. R. Johnson, 1971: The generation of available potential energy by heat release in a mid-latitude cyclone. Mon. Wea. Rev., 99, 1-14.
- Calland, W. E., 1983: A quasi-lagrangian diagnostics applied to an extratropical explosive cyclogenesis in the North Pacific. M. S. Thesis, Naval Postgraduate School, Monterey, CA, 104 pp.
- Charney, J. G., 1947: The dynamics of long waves in a baroclinic westerly current. J. Meteor., 4, 135-162.
- Conant, P. R., 1982: A study of east-coast cyclogenesis employing quasi-Lagrangian diagnostics. M. S. Thesis, Naval Postgraduate School, Monterey, CA, 102 pp.
- Duncan, C. N., 1977: A numerical investigation of polar lows. Quart. J. Roy. Meteor. Soc., 103, 255-257.
- Eady, E. T., 1949: Long waves and cyclone waves. Tellus, 1, 33-52.
- Gall, R. L., 1976a: A comparison of linear baroclinic instability theory with the eddy statistics of a general circulation model. J. Atmos. Sci., 33, 349-373.
- Gall, R. L., 1976b: Structural changes of growing baroclinic waves. J. Atmos. Sci., 33, 374-390.
- Gall, R. L., 1976c: The effects of released latent heat on growing baroclinic waves. J. Atmos. Sci., 33, 1686-1701.
- Gall, R. L., R. Blakeslee, and R. C. J. Somerville, 1979: Baroclinic instability and the selection of the zonal scale of the transient eddies of middle latitudes. J. Atmos. Sci., 36, 767-784.

- Gent, P. R., 1974: Baroclinic instability of a slowly varying zonal flow. J. Atmos. Sci., 31, 1983-1994.
- Godske, C. L., Bergeron, T., Bjerknes, J., and R. C. Bundgaard, 1957: Dynamic meteorology and weather forecasting. Amer. Meteor. Soc., Boston, MA, 536 pp.
- Guo, X.-R., and J. E. Hoke, 1985: The impact of sensible and latent heat on the prediction of an intense extratropical cyclone - some experiments with the nested grid model on the Presidents' day snowstorm of 18-19 February 1979. U.S. Department of Commerce, Office note 314, 8 pp.
- Gyakum, J. R., 1983a: On the evolution of the QEII storm. Part I: synoptic aspects. Mon. Wea. Rev., 111, 1137-1155.
- Gyakum, J. R., 1983b: On the evolution of the QEII storm. Part II: dynamic and thermodynamic structure. Mon. Wea. Rev., 111, 1156-1173.
- Harr, P. A., and T. L. Tsui, 1985: Performance of the Navy Operational Global Atmospheric Prediction System as compiled by an automated verification system. Preprints, Seventh Conf. on Numerical Weather Prediction, Montreal, Canada, 190-195.
- Hillger, D. W., J. F. W. Purdom, and T. H. Vonder Haar, 1985: An analysis of various mesoscale air masses for 28 March 1984 using NOAA-7 TOVS. Preprints, Amer. Meteor. Soc. Severe Storms Conf., Indianapolis, Indiana.
- Hodur, R. M., 1982: Description and evaluation of NORAPS, the Navy Operational Regional Atmospheric Prediction System. Mon. Wea. Rev., 82, 1591-1602.

- Hodur, R. M., 1984: A numerical study of the Pacific polar low. Ph.D. Thesis, Naval Postgraduate School, Monterey, CA, 187 pp..
- Holton, J. R., 1979: In introduction to dynamic meteorology. Academic Press, 391 pp.
- Hoskins, B. J., and F. P. Bretherton, 1972: Atmospheric frontogenesis models: mathematical formulation and solution. J. Atmos. Sci., 29, 11-37.
- Kocin, P. J., and L. W. Uccellini, 1985: A survey of major east coast snowstorms, 1960-1983. Part 1: summary of surface and upper-level characteristics. NASA Technical Memorandum 86195, 102 pp.
- Kocin, P. J., L. W. Uccellini, J. W. Zack, and M. L. Kaplan, 1984: Recent examples of mesoscale numerical forecasts of severe weather events along the east coast. NASA Technical Memorandum 86172, 57 pp.
- Kuo, H. L., 1949: Dynamic instability of two-dimensional non-divergent flow in a barotropic atmosphere. J. Meteor., 6, 105-122.
- Liou, C.-S., and R. L. Elsberry, 1985: Physical processes in prediction of explosive maritime cyclogenesis. Preprints, Seventh Conf. on Numerical Weather Prediction, Montreal, Canada, 212-218.
- Lorenz, E. N., 1969: The nature of the global circulation of the atmosphere. G. A. Corby, Ed., Roy. Meteor. Soc., London, England, 23 pp.
- Maddox, R. A., 1980: Mesoscale convective complexes. Bull. Amer. Meteor. Soc., 61, 1374-1387.
- Mansfield, D. A., 1974: Polar lows; the development of baroclinic disturbances in cold air outbreaks. Quart. J. Roy. Meteor. Soc., 100, 541-554.

- Mullen, S. L., 1979: An investigation of small synoptic-scaled cyclones in polar air streams. Mon. Wea. Rev., 107, 1636-1647.
- Orlanski, I., 1968: Instability of frontal waves. J. Atmos. Sci., 25, 178-200.
- Palmen, E. and C. W. Newton, 1969: Atmospheric circulation systems. Academic Press, 603 pp.
- Pedlosky, J., 1982: Geophysical Fluid Dynamics. Springer-Verlag New York Inc., 624 pp.
- Petterssen, S., 1956: Weather analysis and forecasting. Vol. I: motion and motion systems. McGraw-Hill, New York, 428 pp.
- Richwien, B. A., 1980: The damming effect of the southern Appalachians. Nat. Wea. Dig., 5, 2-12.
- Rosmond, T. E., 1981: Navy Operational Global Atmospheric Prediction System. Preprints, Fifth Conf. on Numerical Weather Prediction, Monterey, CA, 74-79.
- Saltzman, B., 1957: Equations governing the energetics of the larger scales of atmospheric turbulence in the domain of wave number. J. Meteor., 11, 513-523.
- Sanders, F., 1971: Analytic solutions of the non-linear omega and vorticity equation for a structurally simple model of disturbances in the baroclinic westerlies. Mon. Wea. Rev., 99, 393-407.
- Sanders, F., and J. R. Gyakum, 1980: Synoptic-dynamic climatology of the "bomb". Mon. Wea. Rev., 108, 1589-1606.
- Shapiro, M. A., 1982: Mesoscale weather systems of the central United States. Cooperative Institute for Research in Environmental Sciences (CIRES) Boulder, Co., August, 1982, 78 pp.

- Song, R. T., 1971: A numerical study of the three-dimensional structure and energetics of unstable disturbances in zonal currents: Part II. J. Atmos. Sci., 28, 565-586.
- Staley, D. O., and R. L. Gall, 1977: On the wavelength of maximum baroclinic instability. J. Atmos. Sci., 34, 1679-1688.
- Thorpe, A. J., and K. A. Emanuel, 1985: Frontogenesis in the presence of small stability to slantwise convection. Submitted to Mon. Wea. Rev.
- Toll, R. F., and W. M. Clune, 1985: An operational evaluation of the Navy Operational Global Atmospheric Prediction System (NOGAPS): 48-hour surface pressure forecasts. Mon. Wea. Rev., 113, 1433-1440.
- Tracton, M. S., 1973: The role of cumulus convection in the development of the extratropical cyclone. Mon. Wea. Rev., 101, 537-592.
- Uccellini, L. W., and D. R. Johnson, 1979: The coupling of upper and lower tropospheric jet streaks and implications for the development of severe convective storms. Mon. Wea. Rev., 107, 682-703.
- Uccellini, L. W., P. Kocin, and C. Wash, 1981: An analysis of the LFM-II simulations of the Presidents' day cyclone, February 18-19, 1979. Preprints, Fifth Conf. on Numerical Weather Prediction, Monterey, CA, 255-262.
- Uccellini, L. W., P. Kocin, R. Petersen, C. Wash, and K. Brill, 1984: The Presidents' day cyclone of 18-19 February 1979: Synoptic overview and analysis of the subtropical jet streak influencing the pre-cyclogenetic period. Mon. Wea. Rev., 112, 31-55.

Uccellini, L. W., D. Keyser, C. Wash, and K. Brill, 1985: The Presidents' day cyclone of 18-19 February 1979: Influence of upstream trough amplification and associated tropopause folding on rapid cyclogenesis. Mon. Wea. Rev., 113, 962-988.

Wash, C., and W. Cook, 1985: A quasi-Lagrangian diagnostic investigation of rapid cyclogenesis in polar air streams. Conditionally accepted for publication in Mon. Wea. Rev.

Whittaker, T. M., and R. A. Petersen, 1975: Objective cross-section analysis incorporating thermal enhancement of the observed winds. Meteorological Applications of Satellite Indirect Soundings. University of Wisconsin, Madison, WI.

Williamson, D. L., 1981: Storm track representation and verification. Tellus, 33, 513-530.

INITIAL DISTRIBUTION LIST

| | No. | Copies |
|--|-----|--------|
| 1. Defense Technical Information Center Cameron Station Alexandria, VA 22304-6145 | | 2 |
| 2. Library, Code 0142 Naval Postgraduate School Monterey, CA 93943-5002 | | 2 |
| 3. Chairman (Code 63Rd) Department of Meteorology Naval Postgraduate School Monterey, CA 93943-5000 | | 1 |
| 4. Chairman (Code 68Mr) Department of Meteorology Naval Postgraduate School Monterey, CA 93943-5000 | | 1 |
| 5. Professor J. Chan (Code 63Cd) Department of Meteorology Naval Postgraduate School Monterey, CA 93943-5000 | | 3 |
| 6. Professor C. Wash (Code 63Wx) Department of Meteorology Naval Postgraduate School Monterey, CA 93943-5000 | | 5 |
| 7. Director Naval Oceanography Division Naval Observatory 34th and Massachusetts Avenue NW Washington, DC 20390 | | 1 |
| 8. Commander Naval Oceanography Command NSTL Station Bay St. Louis, MS 39522 | | 1 |
| 9. Commanding Officer Naval Oceanographic Office NSTL Station Bay St. Louis, MS 39522 | | 1 |
| 10. Commanding Officer Fleet Numerical Oceanography Center Monterey, CA 93943-5005 | | 1 |
| 11. Commanding Officer Naval Ocean Research and Development Activity NSTL Station Bay St. Louis, MS 39522 | | 1 |
| 12. Commanding Officer Naval Environmental Prediction Research Facility Monterey, CA 93940 | | 1 |
| 13. Chairman, Oceanography Department U.S. Naval Academy Annapolis, MD 21402 | | 1 |

14. Chief of Naval Research 1
 Naval Ocean Research and Development Activity
 800 N. Quincy Street
 Arlington, VA 22217
15. Office of Naval Research (Code 420) 1
 Naval Ocean Research and Development Activity
 800 N. Quincy Street
 Arlington, VA 22217
16. Scientific Liason Office 1
 Office of Naval Research
 Scripps Institution of Oceanography
 La Jolla, CA 92037
17. Library 1
 Scripps Institution of Oceanography
 P.O. Box 2367
 La Jolla, CA 92037
18. Library 1
 Department of Oceanography
 University of Washington
 Seattle, WA 98105
19. Library 1
 CICESE
 P.O. Box 4803
 San Ysidro, CA 92073
20. Library 1
 School of Oceanography
 Oregon State University
 Corvallis, OR 97331
21. Commander 1
 Oceanographic Systems Pacific
 Box 1390
 Pearl Harbor, HI 96860
22. Commanding Officer 1
 Naval Eastern Oceanography Center
 Naval Air Station
 Norfolk, VA 23511
23. Commanding Officer 1
 Naval Western Oceanography Center
 Box 113
 Pearl Harbor, HI 96860
24. Commanding Officer 1
 Naval Oceanography Command Center, Rota
 Box 31
 FPO San Francisco, CA 09540
25. Commanding Officer 1
 Naval Oceanography Command Center, Guam
 Box 12
 FPO San Francisco, CA 96630
26. Professor Robert Gall 1
 Department of Atmospheric Sciences
 University of Arizona
 Tucson, Arizona 85721
27. Lynn K. Shay (Code 63Sh) 1
 Department of Meteorology
 Monterey, Ca. 93943-5000

28. William Clune 1
Quality Control Division
Fleet Numerical Oceanography Center
Monterey, Ca. 93943-5005
29. Professor R. T. Williams (Code 63Wu) 1
Department of Meteorology
Naval Postgraduate School
Monterey, Ca. 93943-5000
30. Professor C. S. Liou (Code 63Lq) 1
Department of Meteorology
Naval Postgraduate School
Monterey, Ca. 93943-5000
31. Professor R. L. Elsberry (Code 63Es) 1
Department of Meteorology
Naval Postgraduate School
Monterey, Ca. 93943-5000
32. LCDR L. Warrenfeltz 1
Department of Meteorology
Naval Postgraduate School
Monterey, Ca. 93943-5000
33. LT R. Rau 1
Department of Meteorology
Naval Postgraduate School
Monterey, Ca. 93943-5000
34. Mr. Raymond F. Toll Sr. 1
1086 Plainfield Rd.
South Euclid, Ohio 44121
35. LT. Raymond F. Toll Jr. 2
Submarine Group Nine
Bremerton, WA. 98315-5100
36. Ms. Stacey Heikkinen 1
Department of Meteorology
Monterey, Ca. 93943-5000

217613

Thesis

T711

Toll

c.1

A linear stability
analysis of the rapid
development of an ex-
tratropical cyclone.

217613

Thesis

T711

Toll

c.1

A linear stability
analysis of the rapid
development of an ex-
tratropical cyclone.



thesT711

A linear stability analysis of the rapid



3 2768 000 66078 1

DUDLEY KNOX LIBRARY